

CEREBRAL VASCULAR HEALTH AND ACCELERATED LEUKOCYTE TELOMERE SHORTENING IN TYPE II DIABETES

by

Samira Tajbakhsh

Supervisor: Dr. Elke Sokoya

Department of Human Physiology

Co-Supervisor: Dr Karen Lower

Department of Haematology

*Thesis
Submitted to Flinders University
for the degree of*

Master of Biotechnology Studies

Faculty of Health Sciences

July 2017

DECLARATION

ACKNOWLEDGEMENTS

LIST OF ABBREVIATIONS

1. ABSTRACT	10
2. INTRODUCTION	12
2.1. Significance of Type 2 diabetes	12
2.1.1 Statistics	12
2.1.2 Economic Cost of T2D	13
2.2. Glucose Metabolism	14
2.3. Pathogenesis of T2D	14
2.3.1 Normal Endothelial Function	14
2.3.3 Endothelial dysfunction in diabetes	15
2.4. The vasculature and reactive oxygen species	15
2.4.1 Antioxidant defence mechanism	17
2.4.2 Effect of hyperglycaemia on the vasculature	18
2.4.3 Effect of lipotoxicity on the vasculature	19
2.5. Nitric oxide	20
2.5.1 Vascular oxidative stress and NO in T2D	20
2.6 Sirtuin 1	22
2.6.1 SIRT1 in T2D	23
2.7 Telomeres	24
2.7.1 Telomeres and T2D	26
3. Objectives and significance	27
4. MATERIALS AND METHODS	28
4.1 Animal model	28
4.2 Blood pressure and heart rate measurements	29
4.3 Blood collection and biochemical analysis	29
4.3.1 Serum insulin measurements	29
4.3.2 Serum free fatty acid measurements	30
4.3.3 Serum C reactive protein measurements	31
4.3.4 Plasma cholesterol, high density lipoprotein and triglyceride measurements	31

4.3.5	Serum leptin measurements	31
4.4	Quantitative real time qPCR	33
4.4.1	Extraction of genomic DNA from blood and femoral arteries	33
4.4.2	DNA Quality and Quantification	34
4.4.3	Primer design and preparation	34
4.4.4	Telomere data analysis	39
4.4.5	Nondenaturing Nucleic Acid Polyacrylamide Gel Electrophoresis (PAGE)	40
4.5	Protein analysis	40
4.5.1	Vessel harvesting and protein extraction from rodent cerebral arteries	40
4.5.2	Protein Quantification	41
4.5.3	Western Blotting	41
4.5.4	Statistical analysis and power	43
5.	RESULTS	44
5.1	Phenotype of T2D animal model	44
5.2	qPCR results: Pilot Studies	45
5.2.1	DNA Quantification	45
5.2.2	Single-copy gene qPCR using O'Callaghan cycling conditions and rat colon DNA	46
5.2.3	Single-copy gene qPCR using O'Callaghan cycling conditions and rat blood DNA	48
5.2.4	Telomere qPCR using O'Callaghan cycling conditions and rat blood DNA	52
5.2.5	Single-copy gene qPCR using Cawthon cycling conditions and rat blood DNA	54
5.2.6	Telomere qPCR using Cawthon cycling conditions and rat blood DNA	56
5.3	qPCR Results: Experimental Samples	58
5.3.1	Single-copy gene qPCR using O'Callaghan cycling conditions and rat experimental samples	58
5.3.3	Blood leukocyte mean telomere length	71
5.3.4	Visualisation of PCR Products using Gel Electrophoresis	72
5.4	Protein Expression Results	73
5.4.1	eNOS protein expression results	73
5.4.2	SIRT1 protein expression results	74
5.4.3	MnSOD protein expression results	75
5.4.4	Nox2 protein expression results	75

5.4.5 p66Shc protein expression results	76
5.4.6 3NT protein expression results	77
6. DISCUSSION	78
6.1 Weight Changes	78
6.2 Changes in circulating insulin and glucose	78
6.3 Changes in circulating leptin	79
6.4 Changes in circulating FFA	79
6.5 Changes in circulating CRP levels	80
6.6 Leukocyte and vascular telomere length	80
6.7 Vascular eNOS protein expression	82
6.8 Vascular SIRT1 protein expression	83
6.9 Vascular antioxidant protein expression	84
6.10 Vascular oxidative stress	84
6.11 Vascular nitrosative stress	85
7. CONCLUSION	86
8. REFERENCES	87
APPENDICES	102

DECLARATION

I hereby certify that this thesis entitles “Cerebral Vascular Health and Accelerated Leukocyte Telomere Shortening in Type II Diabetes” does not contain material which has been accepted for the award of any degree or diploma; and to the best of my knowledge and belief it does not contain any material previously published or written by another person except where due reference is made in the text of this thesis.

Samira Tajbakhsh

September 29th, 2016

ACKNOWLEDGEMENTS

My special thanks go to my very talented, patient and supportive supervisor **Dr. Elke Sokoya** who has been a tremendous help in completing this very interesting project. Her continuous support and understanding as I was transitioning into parenthood not once but twice (!) whilst undertaking this thesis, meant that I could finally finish this project with satisfactory result; and I am very grateful to her for that reason. I would also like to acknowledge my co-supervisor **Dr. Karen Lower** for generously extending her advice and sharing her valuable experiences with me during the course of this project.

This work could not have been possible without the generosity of so many fabulous individuals in sharing their knowledge and expertise with me through this process; I would like to especially thank **Ms. Michelle Pasman** for assisting through qPCR technique, **Dr. Damian Hussey** for his generous support and advice throughout the qPCR study. **Dr. Tim Chataway** for the use of his lab and sharing his vast knowledge in the field of proteomics, **Professor David Wilson** in University of Adelaide for the use of pulse transducer/pressure cuff and controller, **Mr. Lee Travis** for assistance with the tail cuff recordings, **Mr. Josua Dwinovan** for harvesting and freezing the femoral arteries, and **Mr. Brad Rumbelow** in SA Pathology for running the plasma samples on the automatic analyser.

I would like to also say Thank You to my lovely sister, **Negara Tajbakhsh** and my friends **Nusha Chegini, Kamelya Aliakbari, Fariba Chegini, Mahnaz Ramezanpour, Shahrbanoo Javadian** for being there to cheer me up, giving invaluable comments and guidance and creating a very friendly atmosphere that I enjoyed every moment of.

From half way around the world, I would like to also send my love and gratitude to my parents **Zohreh** and **Ezzatollah** for their love, devotion and support giving me the confidence to follow and achieve my goals.

My deepest thanks to my husband, **Armin** whose unlimited support, encouragement and love has enabled me to withstand the tough times and motivated me to complete this very long journey. Last but not least, thank you to my two lovely bundles of joy, **Ariana** and **Soren** for giving up so much from the very first days of their lives to help me finish my work, they both have come to the lab with me many times during my pregnancies when I was doing the experiments; I wouldn't be surprised to see them having an interest in science one day!

LIST OF ABBREVIATIONS

Abbreviation	Definition
Ach	acetylcholine
ADP	adenosine diphosphate ribose
AGEs	advanced glycation end-products
Akt	protein kinase B
BH2	Bcl2- homology domain 2
BH3	Bcl-2 homology domain 3
BH4	Bcl-2 homology domain 4 or Tetrahydrobiopterin
Bpm	beats per minute
cGMP	cyclic guanosine monophosphate
CoA	coenzyme A
CRP	C reactive protein
Cu-Zn SOD	copper-zinc superoxide dismutase
DAG	diacylglycerol
DNA	deoxyribonucleic acid
dNTP	deoxyribose nucleoside triphosphate
DTT	dithiothreitol
EDH	endothelium dependent hyperpolarisation
EDTA	ethylene Diamine Triacetic Acid
ELISA	enzyme-linked immunosorbent assay
eNOS	endothelial nitric oxide synthase
ERK ½	extracellular signal–regulated kinase ½
ET-1	endothelin-1
FFA	free fatty acid
FOXO1	forkhead box class O1
FOXO3a	forkhead box class O3a
FOXO4	forkhead box class O4
G	Gram
G proteins	guanine nucleotide-binding proteins
GAPDH	glyceraldehyde 3-phosphate dehydrogenase
GLUT 1	glucose transporter type 1
GLUT 2	glucose transporter type 2
GLUT 4	glucose transporter type 4
GPx	glutathione peroxidase
GTP	guanosine triphosphate
H ₂ O ₂	hydrogen peroxide
HDL	high-density lipoprotein
HFD	high fat diet
IKKB	inhibitory κB kinase
IL-6	interleukin-6
IRS	insulin receptor substrate

JNK	jun N-terminal kinase
kDa	kilodalton
LXR	liver X receptor
MAPK	mitogen activated protein kinase
MEK 1	MAP kinase kinase
2-MeSATP	2-methylthio-ATP
mmHg	millimeters of mercury
mmol/L	millimoles per liter
MnSOD	manganese superoxide dismutase
NAD ⁺	nicotinamide adenine dinucleotide
NADH	nicotinamide adenine dinucleotide
NADPH	nicotinamide adenine dinucleotide phosphate
NADPH oxidase	nicotinamide adenine dinucleotide phosphate oxidase
NF- κ B	nuclear factor-kappaB
ng/ml	nanograms per millilitre
3NT	3-nitrotyrosine
nM	Nanomolar
NO	nitric oxide
Nox	NADPH oxidase
Nox 1	NADPH oxidase 1
Nox 2	NADPH oxidase 2
Nox 4	NADPH oxidase 4
Nrf2	NF-E2-related factor 2
NTC	non-template control
O ₂	Oxygen
O ₂ ⁻	superoxide radical
•OH	hydroxyl radical
ONOO ⁻	Peroxynitrite
P22 phox	human neutrophil cytochrome b light chain
P47 phox	neutrophil cytosol factor 1
P67 phox	neutrophil cytosol factor 2
PARP	poly adenosine diphosphate ribose polymerase
PBS	phosphate buffered saline
PCR	polymerase chain reaction
PGC-1 α	peroxisome proliferator-activated receptor gamma coactivator 1-alpha
pH	power of Hydrogen
PI3 Kinase	phosphatidylinositol 3 kinase
PKC	protein kinase C
POT1	protection of telomeres protein 1
PPAR- γ	peroxisome proliferator-activated receptor gamma
PVDF	polyvinylidene fluoride
qPCR	quantitative polymerase chain reaction

Rac	rho family of GTPase
Rap1	Ras-proximate-1
RelA/p65	Transcription factor p65 encoded by RelA gene (Retroviral homologue) in humans
RIPA	radioimmunoprecipitation assay
ROS	reactive oxygen species
SCG	single-copy gene
SIRT1	sirtuin 1
SOD	superoxide dismutase
STZ	streptozotocin
T2D	type 2 diabetes
TIN2	TRF1-interacting protein 2
TNF- α	tumor necrosis factor- α
TPP1	tripeptidyl peptidase I
TRF1	telomeric restriction fragment 1
TRF2	telomeric restriction fragment 2
USA	United States of America
WBC	white blood cell
WHO	World Health Organization

1. ABSTRACT

Background: Hyperglycaemia and insulin resistance are the main causes of type 2 diabetes (T2D). The prevalence of T2D is rapidly growing with 257 million people worldwide having the disease in 2010. T2D increases the risk of emergent cardiovascular disease in patients.

Within the vasculature, the endothelium becomes dysfunctional and the cells develop a senescence-like phenotype. Senescent cells can no longer replicate and, more importantly, release destructive factors that promote other diseases such as cardiovascular disease. Preventing cellular senescence could therefore curtail the onset of T2D-related diseases. Cells can become senescent through disruption of their telomeres; protective DNA-protein caps at the end of the chromosome. Damaged telomeres predisposes the cell to chromosomal instability, DNA damage and disease risk. Despite the profound effects of inflammation and oxidative stress (key events in T2D) on telomeres, there is virtually nothing known regarding telomere integrity in the T2D vasculature. Therefore the objective of this project is to assess DNA telomeric length in an established animal model of T2D. We will test the hypothesis that T2D causes both vascular cell and leukocyte telomere shortening.

Methods: Male Hooded Wistar rats were split into two groups, control and T2D and were fed either a normal diet or high-fat diet, followed by an injection of a low dose of vehicle or streptozotocin. Blood parameters were measured and SIRT1, eNOS, and immunoblotting in cerebral artery lysates was used to assess the markers of oxidative stress including manganese superoxide dismutase (MnSOD), p66Shc, 3-nitrotyrosine (3-NT) and Nox2. DNA was extracted from whole blood DNA and femoral artery and telomere length (T/S ratio) measured using qPCR.

Results: Fasting blood glucose, free fatty acids and C-reactive protein were significantly higher in T2D rats in comparison with control rats. Plasma insulin and leptin were significantly lower in T2D rats. Cerebral artery protein expression of SIRT1, eNOS, MnSOD and p66Shc were significantly reduced in T2D rats compared with control rats. However, 3-NT and Nox2 protein expression were comparable between groups. Arterial telomere length was comparable while leukocyte telomere length was significantly shorter in T2D rats compared with their control counterparts.

Conclusions: Our results suggest that telomere length was shortened in leukocytes but not in arteries, in T2D compared with control rats. T2D was associated with reduced vascular SIRT1, eNOS and MnSOD protein expression. We have demonstrated that hyperglycaemia and down regulation of vascular SIRT1 are not sufficient to prematurely shorten vascular telomeres.

2. INTRODUCTION

2.1. Significance of Type 2 diabetes

Type 2 diabetes (T2D) is one of the major causes of premature death mainly due to vascular complications. More than 65% of diabetes-related mortality is due to cardiovascular disease (Barrett-Connor & Khaw 1988). T2D affects either the small vessels (microvasculature) or the large vessels (macrovasculature). Microvascular complications are mostly associated with damage to the small blood vessels of the retina and kidney, leading to blindness and renal insufficiency, respectively (Paneni et al. 2013). Macrovascular complications are associated with atherosclerosis involving arteries that supply the heart, brain and lower limbs, thereby escalating the risk of heart attack, stroke and diabetic foot disease, respectively (Muniyappa et al. 2007; Preis et al. 2009; Winer & Sowers 2004). Understanding the aetiology of vascular complications is of critical importance in reducing the mortality associated with T2D.

2.1.1 Statistics

Type 1 diabetes (T1D) is characterised by deficient insulin production. It is usually caused by an auto-immune reaction where the body's defence system attacks the cells that produce insulin. Symptoms include excessive excretion of urine, thirst, constant hunger, weight loss, vision changes and fatigue (International Diabetes Association 2017; WHO 2015). T1D patients require daily insulin injections.

Type 2 diabetes (T2D) accounts for at least 90% of all cases of diabetes. It results from the body's ineffective use of insulin. T2D is largely the result of excess body weight and physical inactivity. Symptoms may be similar to those of T1D, but are often less marked. As a result, the disease may be diagnosed several years after onset, once complications have already arisen (International Diabetes Association 2017; WHO 2015).

The global prevalence of T2D is rapidly growing. Since 1980, the number of people with diabetes has nearly doubled. In 2014, 422 million people worldwide were living with the disease (Roglic 2016). It has been estimated that this will increase to 366 million in 2030 (Wild et al. 2004). In Australia, there were just over one million known cases of diabetes in 2015 (NDSS 2015). On average, there are 180 Australians diagnosed with the disease every day (NDSS 2015). By 2030, the World Health Organisation (WHO) forecasts that there will be over 1.6 million cases of diabetes in Australia (OECD/WHO 2014). The majority of patients (68%) are older than 60 years of age, 28% are between 40-59 years old and fewer than 4% are under the age of 39 years (NDSS 2015). However a substantial proportion of the population has diabetes that remains undiagnosed, further highlighting the seriousness of the disease. T2D places patients at risk of developing other diseases including stroke and is the seventh leading cause of death (WHO 2015).

2.1.2 Economic Cost of T2D

Diabetes is a major burden to the healthcare system worldwide. In Australia, the annual healthcare cost for a person with T2D is \$4000. This cost can increase to over \$9,500 for a diabetic with vascular complications (Shaw 2012). In the US, diabetics pay close to \$8000 annually for their healthcare costs, which is 2.3 times higher than non-diabetics (Herman 2013). This equates to 14% of the total health expenditure of the US (Zhang et al. 2010). The economic burden associated with diabetes however is even greater as it includes financial costs not only associated with direct medical costs but also loss of productivity and carer expenses.

2.2. Glucose Metabolism

In non diabetics, plasma glucose levels remain tightly controlled between 4 and 7mM. Following food consumption, insulin secretion from the pancreatic beta cells is stimulated by the rise in plasma glucose concentration. The released insulin stimulates the translocation of the glucose transporter, GLUT4, from intracellular sites to the plasma membrane and promotes glucose uptake in cells within the liver, gut, muscle and adipose tissues. At the same time, insulin inhibits hepatic glucose production and supports the storage of substrates in fat, liver and muscle by promoting free fatty acid (FFA), glycogen and protein synthesis (DeFronzo 2004).

2.3. Pathogenesis of T2D

T2D is defined by hyperglycaemia, driven by the dysfunction of pancreatic beta cells and insulin resistance. Increased food intake in conjunction with low levels of physical activity promotes excessive fat storage, leading to increased breakdown of lipids into glycerol and FFAs. Chronic elevations in circulating FFAs lead to insulin resistance and a compensatory increase in insulin secretion (Boden & Shulman 2002). The high insulin levels ultimately cause downregulation of insulin receptors in target tissues and a decrease in glucose uptake, resulting in hyperglycaemia. Over time, hyperglycaemia and lipotoxicity (from elevated FFAs and triglycerides) promotes apoptosis of pancreatic beta cells thereby impairing insulin secretion (Lebovitz & Banerji 2004).

2.3.1 Normal Endothelial Function

The inner surface of all blood vessels is covered by the endothelium - a monolayer of endothelial cells. It plays an important role in the regulation of immune and inflammatory responses, thrombosis, adhesion, angiogenesis and permeability (Chrissobolis et al. 2011;

Zhang et al. 2008). The endothelium also modulates the contractile state of the underlying smooth muscle by releasing several vasodilating agents, including nitric oxide (NO), prostacyclin and a mechanism involving non-NO/prostacyclin endothelium-dependent hyperpolarisation (EDH) (Baron 2002; Faraci 1992; Zhang et al. 2008). On the other hand, the ROS, hydrogen peroxide (H₂O₂), has a physiological role as an endothelium-derived vasodilator (Lucchesi, Belmadani & Matrougui 2005). In addition to vasodilators, the vascular endothelium also releases contractile agents such as endothelin (Baron 2002).

2.3.3 Endothelial dysfunction in diabetes

Due to the direct exposure of endothelial cells to the circulating blood, it follows that changes within the blood has a potential impact on the endothelium and vascular function. Endothelial dysfunction is characterised by the reduction of endothelial-mediated vasodilation, a proinflammatory state, and prothrombic properties. Endothelial dysfunction is a hallmark of T2D in both humans (Faraci & Heistad 1998; Johnstone et al. 1993; O'Driscoll et al. 1999) and animal models of T2D (Faraci & Heistad 1998; Hattori et al. 1991; Pieper et al. 1992). This predisposes the vasculature to developing secondary complications. Indeed, loss of endothelium-dependent vasodilation is an independent predictor of cardiovascular disease (Schächinger, Britten & Zeiher 2000) and is a risk factor for dementia, particularly Alzheimer's disease. Understanding the mechanisms leading to vascular damage is extremely important with regards to developing therapeutic targets and lowering T2D-related mortality.

2.4. The vasculature and reactive oxygen species

The vasculature is prone to damage mediated by reactive oxygen species (ROS). ROS are molecules containing unpaired electrons and are therefore very unstable. They include superoxide radical (O₂⁻), hydroxyl radical (•OH) and hydrogen peroxide (H₂O₂) (Chrissobolis & Faraci 2008). Low levels of ROS are made endogenously and are critical for normal

cellular function (Trachootham et al. 2008). However, high levels of ROS can be produced in some diseases leading to DNA and cellular damage.

Hyperglycaemia and increased FFA in the blood can increase ROS levels by enhanced mitochondrial respiration (Guzik et al. 2002). In the electron-transport chain, the terminal oxidase enzyme which is the cytochrome oxidase, transfers electrons to O_2 , which causes O_2^- generation (Le Bras et al. 2005) (see **Fig. 2.1**).

Another source of ROS is nicotinamide adenine dinucleotide phosphate (NADPH) oxidase. NADPH oxidase comprises cytosolic p47phox and p67phox subunits, membrane bound Nox and p22phox subunits and a small G-protein Rac (Paravicini & Touyz 2008). Seven Nox isoforms have been identified, namely Nox1-Nox5, Duox1 and 2 (Paravicini & Touyz 2008). NADPH oxidase is expressed in neutrophils and phagocytes as part of the “respiratory burst”, a process whereby the cells use NADPH oxidase to reduce O_2 to form O_2^- . NADPH oxidase is also expressed within the vasculature (Drummond & Sobey 2014; Lassègue, San Martín & Griendling 2012) where it serves as one of the key sources of ROS. Nox1, Nox2 and Nox4 are expressed in cerebral arteries (Miller et al. 2009). Nox1 and Nox4 are mostly expressed in smooth muscle while Nox2 and Nox4 are found in endothelium (Li, Horke & Förstermann 2014).

ROS are also formed from uncoupled endothelial nitric oxide synthase (eNOS) where eNOS is driven towards superoxide rather than NO production (Li, Horke & Förstermann 2014). Superoxide then combines with NO to form peroxynitrite ($ONOO^-$) (see **Fig 2.1**). Peroxynitrite mediates cellular injury and can amplify oxidative stress by inactivating SOD and promoting eNOS uncoupling (Guzik et al. 2002).

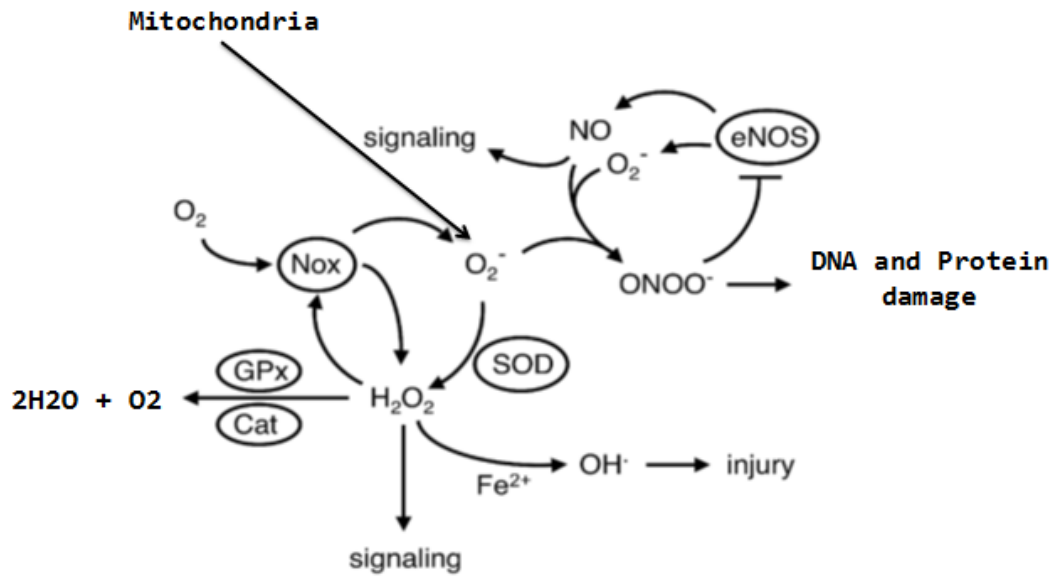


Fig. 2.1 Schematic of oxidative stress signalling and the interrelationships of various reactive oxygen species and nitric oxide. Adapted from (Chrissobolis & Faraci 2008).

2.4.1 Antioxidant defence mechanism

The production of ROS is counterbalanced by endogenous antioxidant enzymes, such as superoxide dismutase (SOD), glutathione peroxidase and catalase, which help to scavenge ROS. There are three isoforms of SOD, namely copper-zinc SOD (Cu-Zn SOD or SOD1), mitochondrial SOD (MnSOD or SOD2) and extracellular Cu-Zn SOD (SOD3). SOD catalyses the dismutation of O_2^- into H_2O_2 , which itself can form the hydroxyl radical leading to injury, or it can be eliminated by glutathione peroxidase and catalase.

Conditions whereby the antioxidant system cannot counteract the production of ROS, results in a condition called oxidative stress (De Vriese et al. 2000; Faraci 2005). Sustained high levels of ROS can affect DNA, proteins, lipids and carbohydrates, resulting in significant cellular damage (Le Bras et al. 2005).

2.4.2 Effect of hyperglycaemia on the vasculature

Endothelial cells are particularly sensitive to hyperglycaemia *in vivo*. Accumulating studies suggest that hyperglycaemia increases superoxide production by mitochondrial uncoupling (Brownlee 2001, 2005), activation of NADPH oxidase (Bakker et al. 2009; Dworakowski, Alom-Ruiz & Shah 2008) and eNOS uncoupling (Bakker et al. 2009; Wever et al. 1997). Increased superoxide results in the activation of PARP and inhibition of GAPDH leading to the accumulation of glycolysis intermediates. These intermediates can then promote four main pathways within the endothelial cell: (i) protein kinase C activation, (ii) generation of methylglyoxal and advanced glycation end-products (AGEs), (iii) hexosamine pathway activation and (iv) sorbitol pathway activation leading to a reduction in NADPH/NADP⁺ ratio (Bakker et al. 2009) (see **Fig 2.2**).

Figure has been removed due to copyright restrictions

Fig. 2.2 The effect of hyperglycaemia on endothelial activation. ROS is produced following eNOS and mitochondria uncoupling as well as NADPH oxidase activation. This leads to poly (ADP-ribose) polymerase (PARP) activation followed by inhibition of D-glyceraldehyde-3-phosphate dehydrogenase (GAPDH), a glycolysis enzyme. Thereby, hyperglycaemia leads to accumulation of glycolysis intermediates which changes a minimum of four chemical pathways in endothelial cells (Bakker et al. 2009).

2.4.3 Effect of lipotoxicity on the vasculature

As mentioned earlier, type 2 diabetics have an excessive mass of adipose tissue, resulting in increased lipolysis and elevated plasma free fatty acids (FFAs). FFAs from the bloodstream enter the endothelium, leading to enhanced FFA oxidation by the mitochondria and subsequent ROS production. There are a number of ways in which this is thought to occur.

First, there is evidence that suggests high FFAs increase intracellular levels of diacylglycerol (DAG), ceramide and long chain fatty acyl coenzyme A (CoA) which themselves activate serine kinases, PKC and inhibitory kappaB kinase (IKK β) that activates nuclear factor-kappaB (NF- κ B). Being a transcription factor, NF- κ B increases transcription of inflammatory cytokines IL-6 and TNF- α (Muniyappa et al. 2007; Paneni et al. 2013). Activation of PKC and IKK β also increases serine phosphorylation of insulin-receptor substrate-1(IRS-1) which itself downregulates insulin stimulated Akt and eNOS activities and simultaneously activates Jun N-terminal kinase (JNK). JNK results in serine phosphorylation of IRS-1 and decreases insulin-stimulated production of NO (Muniyappa et al. 2007).

Second, recent findings support the idea that elevated circulating FFAs activate toll-like receptors on the endothelium, resulting in phosphorylation of IRS-1 by JNK and PKC and activation of downstream targets, PI3-kinase and Akt. This inhibits the translocation of the glucose transporter GLUT-4 to the plasma membrane thereby promoting insulin resistance (Paneni et al. 2013). Moreover, downregulation of PI3-kinase and Akt leads to reduction of eNOS activity and NO production. Overall, reduced production of NO as well as intracellular oxidation of FFA generates ROS which leads to oxidative stress and vascular inflammation (Paneni et al. 2013).

2.5. Nitric oxide

Within the endothelium, arginine is converted to nitric oxide (NO) by the endothelial NO synthase (eNOS) enzyme (Bender et al. 2007). NO then diffuses to the vascular smooth muscle where it binds to soluble guanylate cyclase. This in turn causes increased production of guanosine 3',5'-cyclic monophosphate (cGMP) from GTP and vasodilation (Faraci 2011; Faraci & Heistad 1998).

In addition to its direct vasodilating effects, NO can also inhibit the expression of the vasoconstrictor, endothelin-1, either by its direct effect on vascular tone or by inhibiting endothelial production of ET-1 (Kourembanas et al. 1993). It can protect the vasculature by inhibiting platelet aggregation thereby providing an antithrombogenic surface for blood vessels (Faraci & Heistad 1998). Thus, when NO bioactivity is reduced, platelets can adhere to the endothelium and form a blood clot, thereby obstructing the flow of blood. NO also inhibits leukocyte adhesion to the endothelium, thereby preventing leukocytes from moving into the tissue and evoking an inflammatory response (Faraci & Heistad 1998). In addition, NO plays a key role in inhibiting vascular growth and hypertrophy (Baumbach, Sigmund & Faraci 2004) and non-specific host defence, helping to kill tumours and intracellular pathogens (Beckman & Koppenol 1996). Taken together, NO plays an important role in mediating vascular function, inflammation, coagulation and vascular growth.

2.5.1 Vascular oxidative stress and NO in T2D

Both human (Antonopoulos et al. 2015) and animal (Bagi, Koller & Kaley 2004) studies have shown that T2D leads to vascular oxidative stress. In addition to causing direct damage to proteins, lipids, proteoglycans and carbohydrates, ROS, and in particular superoxide, also reduce NO bioavailability. Oxidative stress decreases NO bioavailability through several mechanisms including (i) enhanced consumption of NO by high levels of superoxide to

generate peroxynitrite, (ii) inhibition of the enzyme dimethylarginine dimethylaminohydrolase, leading to an increase in asymmetric dimethylarginine, a competitive inhibitor of NO synthesis, (iii) oxidation and depletion of the endothelial NO synthase (eNOS) cofactor, tetrahydrobiopterin causing uncoupling of eNOS and (iv) activation of NADPH oxidase which in turn produces more superoxide. NADPH oxidase and uncoupling of eNOS are the main sources of reactive oxygen species in the vasculature (Cai & Harrison 2000). A reduction in NO bioavailability leads to impaired endothelium-dependent relaxation of blood vessels and to compound the problem, peroxynitrite often activates potent vasoconstriction. Mechanism of endothelium-derived NO-mediated dilation in cerebral vessels is demonstrated in **Fig. 2.3**.

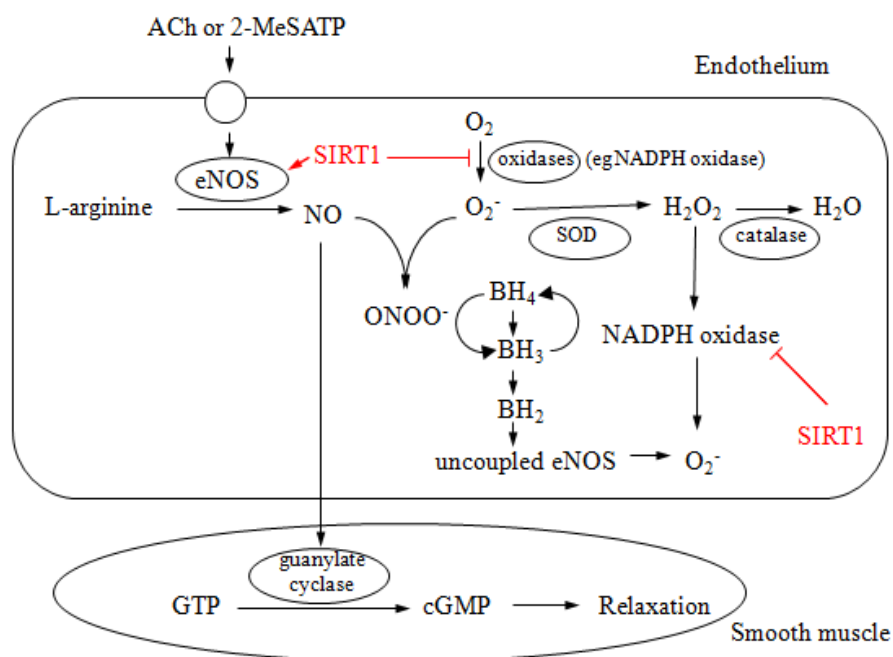


Fig 2.3 Mechanism of endothelium-derived NO-mediated dilation in cerebral vessels. Acetylcholine (ACh) or 2-methylthioATP (2-MeSATP) bind to receptors (muscarinic or P2Y1) on the endothelium increasing intracellular [Ca²⁺]. Elevations in intracellular [Ca²⁺] activate eNOS, leading to NO that diffuses to vascular smooth muscle, causing soluble guanylate cyclase activation, an increase in cGMP and relaxation. During pathological states, O₂⁻ production is enhanced (see text).

2.6 Sirtuin 1

The sirtuin family of proteins comprise adenosine diphosphate (ADP)-ribosylases and NAD⁺-dependent deacetylases. There are seven isoforms ranging from sirtuin 1 through to sirtuin 7. Sirtuin 1 (SIRT1) is mainly expressed in the nucleus but can shuttle into the cytoplasm. It has been detected in the heart (Winnik et al. 2015), brain (Ran et al. 2015), aorta (Zhang et al. 2008) and cerebral vessels (Michishita et al. 2005; Tajbakhsh & Sokoya 2012). SIRT1 deacetylates lysine residues on histones and nonhistone proteins, producing a deacetylated product and thereby either activating or inhibiting the target protein. Examples of nonhistone target proteins include transcription factors such as forkhead box class O (FOXO1, FOXO3a, FOXO4) (Brunet et al. 2004) and p53 (Vaziri et al. 2001), signalling molecules such as PPAR- γ (Han et al. 2010) and vasoactive molecules such as eNOS (Mattagajasingh et al. 2007; Ota et al. 2010) (see **Fig 2.4**). SIRT1 and eNOS have been shown to co-localise within endothelial cells (Mattagajasingh et al. 2007) and SIRT1 stimulates eNOS activity by deacetylation of eNOS at lysine residues 496 and 506, in the calmodulin-binding domain of eNOS (Yang et al. 2011). Importantly, evidence suggests that blunted SIRT1 is responsible for the reduced NO-dependent vasodilation (D'Onofrio et al. 2015; Donato et al. 2011). SIRT1 deacetylates and activates peroxisome proliferator-activated receptor γ coactivator- α (PGC-1 α), resulting in increased transcription of mitochondrial genes including MnSOD (Valle et al, 2005). PGC-1 α is also a coactivator of the PPAR nuclear receptor proteins that are involved in glucose uptake and glycolysis and fatty acid transport (Dominy et al. 2010; Picard et al. 2004; Rodgers et al. 2005). SIRT1 deacetylates and inhibits p53, thereby repressing apoptosis (Hori et al, 2013). SIRT1 also affects lipogenesis by deacetylating and activating mitochondrial acetyl-CoA synthetase (Hallows, Lee & Denu 2006), cholesterol and lipid homeostasis by deacetylating and activating LXR (Li, X et al. 2007) and fatty acid oxidation by PGC-1 α (Dominy et al. 2010). SIRT1 has an anti-inflammatory role by

deacetylating RelA/p65, thereby inhibiting NF- κ B transcription (Yeung et al. 2004). SIRT1 also enhances DNA repair and cell survival by deacetylating Ku70 which is a protein that binds to the end of DNA double-strand breaks and starts nonhomologous end-joining (Jeong et al. 2007).

There is evidence that SIRT1 increases NO bioavailability (Lovren et al. 2009; Mattagajasingh et al. 2007) and SIRT1 overexpression decreases superoxide production (Ungvari et al. 2009). This suggests that SIRT1 may have a protective role in the vasculature.

Figure has been removed due to copyright restrictions

Fig. 2.4 SIRT1 regulates acetylation and deacetylation of proteins by removing the acetyl group of lysine residues of proteins including FOXO3, p53, Nrf2, NF- κ B, PARP-1, Ku70 and Notch (Yao & Rahman 2012).

2.6.1 SIRT1 in T2D

SIRT1 has been shown to be blunted in adipose tissue, skeletal muscle (de Kreutzenberg et al. 2010), heart (Winnik et al. 2015), liver (Li, M et al. 2015) and cardiomyocytes (Dong & Ren 2007) of diabetic mice. Within the vasculature, SIRT1 protein expression was found to be blunted in the aorta of spontaneous type 2 diabetic rats (Zhang et al. 2008) and after six

months of high-fat feeding (Zhang et al. 2008). However it is still unclear whether SIRT1 is also downregulated in resistance-sized vessels, which control local blood flow, in T2D. Therefore, one of the aims of the present study was to assess SIRT1 protein expression within cerebral arteries in an animal model of T2D.

2.7 Telomeres

The repeating DNA sequences (TTAGGG) located at the end of chromosomes are called telomeres. They are bound to proteins to form a complex known as shelterin (see **Fig 2.5**). Shelterin inhibits DNA repair at the chromosome ends, thereby preventing chromosomal fusions and genome instability (O'Donnell et al. 2008). During cell division, DNA polymerase copies DNA. However DNA polymerase cannot replicate the telomeric DNA at the ends of the chromosome. Subsequently, the length of telomeres decrease with each round of cell division. Although an enzyme called telomerase can restore telomere length by addition of hexameric repeats to the telomeric ends of the chromosomes, its activity is low in somatic cells and therefore telomeres will gradually shorten as cells divide. Excessive telomere shortening induces cell-cycle arrest and cellular senescence (known as replicative senescence), where cells continue to have active metabolism but are incapable of replication. In this way, senescence protects cells from a cancerous phenotype by preventing replication of damaged DNA. Unfortunately senescent cells also secrete inflammatory cytokines, thereby increasing risk of secondary disease and promoting an aging phenotype. In addition to replicative senescence, cells can also be triggered to become senescent independent of telomere length, a condition called premature senescence. Oxidative stress, a common feature of T2D, can prematurely damage telomeric DNA by hydroxylation of the abundant guanine residues found within the telomeric regions (Khan, Chaturgoon & Naidoo 2012; Saliques et al. 2010; Sampson et al. 2006).

Figure has been removed due to copyright restrictions

Fig. 2.5 Telomere structure (Calado & Young 2008). Telomeres are placed at the end of DNA chromosomes and are capped by 6 proteins TRF1, TRF2, TIN2, POT1, TPP1 and Rap1 called shelterin proteins. Shelterin protects DNA as well as allowing discrimination of telomeres from double-stranded DNA breaks.

According to recent studies, overexpression of endothelial SIRT1 inhibits vascular cell senescence (Chen, H et al. 2012), suggesting an association between cellular senescence and reduced SIRT1 expression. There is also evidence to suggest that SIRT1 interacts with telomeric repeats and can attenuate telomere shortening (Chen, J et al. 2011; Palacios et al. 2010). Therefore, a correlation may exist between SIRT1 levels and cell viability (Chen, J et al. 2011).

Increased expression of SIRT1 improves telomere length maintenance *in vivo* and significantly increases recombination frequencies at telomeres, centromeres, and chromosome arms. These effects of increased SIRT1 expression are potentially beneficial to preserve genome integrity and stability and open new avenues to understand the known effects of increased SIRT1 expression on health span and protection from some age-associated diseases (Palacios et al. 2010).

SIRT1 has been shown to interact directly with telomeres and attenuate age-dependent telomere dysfunction *in vivo* by increasing homologous recombination events (Birch et al. 2016). Studies have also shown that SIRT1 is required for telomere maintenance (Palacios et al. 2010) and elongation in stem cells (De Bonis, Ortega & Blasco 2014).

2.7.1 Telomeres and T2D

Epidemiological studies have provided evidence of shorter leukocyte telomeres in obesity (Valdes et al. 2005) and T2D (Adaikalakoteswari, Balasubramanyam & Mohan 2005; Salpea et al. 2010; Testa et al. 2011). Circulating blood leukocytes are frequently used to measure telomere length. However, this assumption that the telomere content in circulating blood leukocytes is an accurate representative of the telomere content in the vascular wall has not yet been validated (Wilson et al. 2008b). Moreover, studying telomere content of human vascular tissues is impractical and therefore, circulating blood leukocytes have been used as an alternative source for quantification of telomere (Wilson et al. 2008b). Nevertheless, in many vascular diseases including hypertension, coronary heart disease and cerebrovascular disease, the telomere content in blood leukocytes have shown to be reduced comparing to the control group (Wilson et al. 2008b).

3. Objectives and significance

The overall objective of this investigation was to study whether T2D leads to reduced vascular SIRT1 protein expression, altered antioxidant defence capacity and accelerated leukocyte and vascular telomere shortening.

The specific aims of this project are:

- To measure cerebral artery SIRT1 and eNOS protein expression, along with markers of oxidative and nitrosative stress using an animal model of T2D.
- To assess mean telomere length in circulating leukocytes and the vasculature.

4. MATERIALS AND METHODS

4.1 Animal model

Animal studies were performed in agreement with the Australian Code for the Responsible Conduct of Research and were approved by Flinders University Animal Ethics Committee (Number 836/12). Male Hooded Wistar rats were bred and housed in the School of Medicine Animal Care Facility under conditions of controlled temperature (22°C) and light (12 hour light/12 hour dark cycle) with free access to water and chow. Rat chow was purchased from Gordon's speciality stockfeed.

Male rats were weaned at 3 weeks of age and categorised into two groups: type 2 diabetic (T2D; n=9) and control (n=8). A chronic model of high-fat feeding and low dose streptozotocin was used to simulate T2D. The high fat diet chow (D12451) contained 20% kcal protein, 45% kcal fat and 35% kcal carbohydrate. The normal chow (D12450H) contained 20% kcal protein, 70% kcal carbohydrate and 10% kcal fat.

At seven weeks before termination (18 weeks after diet initiation), rats on the high-fat diet were administered an intraperitoneal injection of low dose streptozotocin (Sigma, 30mg/kg) and the control counterparts were injected with vehicle (saline). Fresh streptozotocin stock solutions of 50 mg/ml were made in saline. Animals were continued on their prescribed diet for another seven weeks. Body weight was measured at the time of streptozotocin or vehicle injection and then again prior to termination.

Previous studies have shown that a high-fat feeding followed by a low dose of streptozotocin induces a mild impairment of insulin secretion, similar to that seen in late stage T2D (Srinivasan et al. 2005).

4.2 Blood pressure and heart rate measurements

Five days prior to termination, rats were anaesthetised with 3% isoflurane and their body temperature maintained on a heating pad at 37°C. Blood pressure was measured using an MLT125/R pulse transducer/pressure cuff and IN125 NIBP controller (AD Instruments, Australia) and recorded using PowerLab software (AD Instruments, Australia). Systolic pressure and heart rate were determined from the average of three consecutive readings obtained from each rat.

4.3 Blood collection and biochemical analysis

At the time of sacrifice, rats were anaesthetised with 3% isoflurane by inhalation. The weight of each animal was then measured and recorded. The tail vein was snipped with a scalpel blade to obtain a sample for fasting blood glucose measurement using a glucose meter (Accu-Chek Performa, Roche Diagnostics, Indianapolis, IN, USA). The animals were then decapitated using a rodent guillotine and trunk blood was acquired for DNA extraction. Plasma was obtained for total cholesterol, high-density lipoprotein (HDL) and triglycerides measurements and serum obtained for insulin, leptin, C-reactive protein (CRP) and FFA measurements.

4.3.1 Serum insulin measurements

Trunk blood was clotted for 30 minutes at room temperature followed by centrifugation at 2000g for 15 minutes at 4°C. 50µl aliquots were stored at -80°C for later insulin measurement. Serum insulin levels were measured in triplicate using an Ultra Sensitive Rat Insulin ELISA Kit for low range assay (Crystal Chem Inc, USA) by adding 5µl plasma sample or rat insulin standards to 95µl sample diluent in wells following 2 hours incubation at 4°C. 100µl of anti-insulin enzyme conjugate was added to each well and incubated for 30

minutes followed by adding 100µl enzyme substrate solution for 40 minutes at room temperature in dark (as per manufacturer's instructions). Absorbance was measured using BIOMECK-3000 microplate reader (Beckmann-Coulter, USA) and multimode detection software by subtracting absorbance readings at 630nm (background noise) from readings at 450nm (optimal absorbance wavelength of insulin). Subsequently, readings were compared with the slope of the standard curve constructed with insulin standards.

4.3.2 Serum free fatty acid measurements

Serum free fatty acid concentration of both T2D and control rats were measured in triplicate using a free fatty acid quantification kit (Abcam). In this fluorometric assay, fatty acids are converted to their CoA derivatives, that are subsequently oxidised along with the concomitant generation of fluorescence at Ex/Em of 535/590 nm. To obtain this, palmitic acid standard was diluted to 0.1nmol/µl by adding 10µl of the standard to 90µl of assay buffer. 0, 2, 4, 6, 8, 10 µl of this mix was added to each well of a microplate and the volume was subsequently adjusted to 50 µl/well according to the manufacturer's instructions.

2 µl acetyl-CoA synthesis reagent was added into all standard and sample wells which then were incubated for 30 minutes at 37°C. 50µl reaction mix containing assay buffer, fatty acid probe, enzyme mix and enhancer were added to each standard and sample, mixed and then incubated for 30 minutes at 37°C in the dark. Fluorescence was measured at 535nm excitation and 590nm emission using a BIOMECK-3000 microplate reader (Beckmann-Coulter, USA) and multimode detection software. The absorbance (Ex/Em 535/590 nm⁹⁰) was compared with the slope of the standard curve constructed with palmitic acid standards.

4.3.3 Serum C reactive protein measurements

CRP was measured in triplicate using a CRP (PTX1) rat ELISA kit (Abcam, USA). All reagents, samples and working standards were prepared as per manufacturer's instructions. 50µl of CRP standard or sample was added to each well and incubated for two hours at room temperature in the dark. Subsequently, 50µl of 1X biotinylated CRP antibody was added to each well followed by adding 50µl of 1X SP conjugate and 50µl of chromogen substrate and incubation for one hour, 30 minutes and 20 minutes (until appearance of blue colour) at room temperature in dark, respectively. Absorbance was measured at the time of changing colour to yellow using a BIOMECK-3000 microplate reader (Beckmann-Coulter, USA) and multimode detection software by subtracting 595nm readings from 450nm which then were compared with the slope of the standard curve constructed with CRP standards.

4.3.4 Plasma cholesterol, high density lipoprotein and triglyceride measurements

Trunk blood was added to 0.8ml MiniCollect lithium heparin tubes (Greiner) and was centrifuged at 2000g for 10 minutes at room temperature. The supernatant was collected and frozen at -20°C. The measurement was performed using an automatic analyser (SA Pathology Diagnostic Services).

4.3.5 Serum leptin measurements

Trunk blood was clotted at room temperature for 30 minutes followed by centrifugation at 2000g for 15 minutes at 4°C. 50µl aliquots were stored at -80°C for later leptin measurement. Serum leptin levels were measured in triplicate using a rat leptin ELISA kit (Crystal Chem Inc, USA, 90040) by preparing reagents including an antibody-coated microplate, rat leptin stock solution, sample diluents, guinea pig anti-leptin serum, anti-guinea pig IgG enzyme

conjugate, enzyme substrate solution, enzyme reaction stop solution and wash buffer according to the manufacturer's instructions (Crystal Chem Inc., USA, 90040).

Working rat leptin standards were prepared by pipetting 50 μ l of sample diluent and 50 μ l of rat leptin stock solution of 25.6 ng/mL into a microfuge tube to make 12.8 ng/mL leptin standard. 50 μ l of sample diluent was dispensed into seven microfuge tubes labelled 0, 0.2, 0.4, 0.8, 1.6, 3.2 and 6.4 ng/mL, respectively. Serial dilution of standards were made by adding 50 μ l of the 12.8 ng/mL standard to 6.4 ng/mL tube and mixed completely, 50 μ l of the 6.4 ng/mL standard to 3.2 ng/mL tube and repeating the same pattern for the rest of the tubes. Tube 0 contained only the sample diluent as the control.

The antibody-coated microplate was removed from the sealed pouch after being equilibrated to room temperature and was affixed to the supporting frame. The plate was washed twice by 300 μ l of wash buffer per well followed by dispensing 45 μ l of sample diluent and 50 μ l of guinea pig anti-leptin serum, respectively. 5 μ l of each of the working rat leptin standards plus the control were added to the wells followed by covering the microplate and overnight incubation at 4°C. On the second day, the microplate was washed five times using 300 μ l of wash buffer per well. 100 μ l of anti-guinea pig IgG enzyme conjugate was dispensed per well, covered and then incubated for three hours at 4°C. The microplate was washed seven times using 300 μ l of wash buffer per well followed by dispensing 100 μ l per well of enzyme substrate solution and reacting for 30 minutes at room temperature in the dark without covering. The enzyme reaction was terminated by adding 100 μ l per well of enzyme reaction stop solution.

Absorbance was measured using a BIOMECK-3000 microplate reader (Beckmann-Coulter, USA) and multimode detection software was used by subtracting absorbance readings at 630nm (background noise) from readings at 450nm (optimal absorbance wavelength of

leptin). Subsequently, readings were compared with the slope of the standard curve constructed with leptin standards.

4.4 Quantitative real time qPCR

4.4.1 Extraction of genomic DNA from blood and femoral arteries

Prior to extraction of genomic DNA, trunk blood was collected in MiniCollect 0.5ml EDTA tubes (Greiner) and stored at 20°C. The left and right femoral arteries were snap frozen in liquid nitrogen and stored at -80°C. DNA was extracted from whole blood using a DNeasy blood and tissue kit (Qiagen, Germany, 69504). DNA was extracted from femoral arteries using a QIAamp DNA micro kit (Qiagen, Germany, 56304). At the time of extraction, frozen trunk blood was thawed at room temperature. 20µl of proteinase K was pipetted into a 1.5ml microcentrifuge tube and 100µl of thawed blood was added to it followed by 100µl phosphate buffered saline (PBS) buffer. Subsequently, 200µl of buffer AL was added to the mix, vortexed and incubated in a water bath at 56°C for 10 minutes followed by addition of 200µl of 100% ethanol. The mix was pipetted into a DNeasy mini spin column and placed in a 2ml collection tube and centrifuged at 6000g for one minute using a microcentrifuge (GMC-360/361, LabTech). 500µl of buffer AW1 was added to the spin column and centrifuged at 6000g for one minute followed by addition of 500µl of buffer AW2 with 20,000g centrifugation for three minutes, each step in duplicate. The eluate (DNA) was washed twice by adding 100µl firstly, and secondly 20µl of buffer AE to the spin column and incubating for five minutes at room temperature followed by centrifugation at 6000g for one minute. DNA was stored in AE buffer at 4°C.

The frozen femoral arteries were added to 180µl buffer ATL and equilibrated to room temperature. 20µl of proteinase K was added and mixed by pulse-vortexing. This was incubated at 56°C overnight with mixing. 200µl buffer AL was added and then mixed by

pulse-vortexing. 200µl ethanol was added and pulse-vortexed followed by incubation for five minutes at room temperature. The entire lysate was transferred to a QIAamp MinElute column which was centrifuged at 6000g for one minute. The column was washed twice with 500µl Buffer AW1 and then 500µl Buffer AW2. 50µl Buffer AE was added to the column, followed by centrifugation at 20,000g and the eluate (DNA) was stored at 4°C.

4.4.2 DNA Quality and Quantification

DNA quality and concentration was assessed using a NanoDrop 2000 spectrophotometer (Thermo-Scientific). DNA concentration was measured by placing one µl of the sample on the NanoDrop. The concentration was measured three times for each sample and the mean value was used. DNA quality was assessed by gel electrophoresis.

4.4.3 Primer design and preparation

Two sets of telomere primers were used, both obtained from the literature (O’Callaghan and Fenech 2011, Cawthon, 2009). For the O’Callaghan method, the telomere primer sequences (written 5’→3’) were: Tel-F, CGG TTT GTT TGG GTT TGG GTT TGG GTT TGG GTT TGG GTT; Tel-R, GGC TTG CCT TAC CCT TAC CCT TAC CCT TAC CCT TAC CCT and used at a final concentration of 2µM or 0.1µM. For the Cawthon method, the telomere primer sequences (written 5’→3’) were: Tel-G, ACA CTA AG[GTTTGG]₄GTT AGT GT; Tel-C, TGT TAG G[TATCCC]₅ TA ACA and used at a final concentration of 0.9µM. For the single-copy gene, a β-actin primer was designed in-house using OligoAnalyzer (version 3.1). The rat β-actin single copy gene primers (written 5’→ 3’) were: β-actin-F, AGG TCA TCA CTA TCG GCA ATG A; β-actin-R, GAG ACT ACA ACT TAC CCA GGA AGG AA and used at a final concentration of 2µM. Power SYBR green PCR Mastermix (Life Technologies) was used. All primers were made by GeneWorks (Thebarton, SA, Australia).

The lyophilised primers were received as forward (F) and reverse (R) primers in microcentrifuge tubes which were first spun down for 10-15 seconds at 2000g. Water for injection (GlaxoSmithKline, AUST R 13051) was added to the forward and reverse primers. The amount of water added was calculated by multiplying nanomoles per tube of the primer by 10 (nmol x 10) (as per manufacturer's protocol) to make 100 μ M forward or reverse stock solution. Both tubes were vortexed briefly and flick mixed and let to sit at room temperature for more than 30 minutes to let primers dissolve completely in water. The primer stocks were then stored at -20°C.

4.4.3.1 O'Callaghan & Fenech telomere qPCR method

Absolute telomere length was assessed using a qPCR method as described by O'Callaghan and Fenech (O'Callaghan & Fenech, 2011). This method is based on introducing an oligomer standard to generate absolute telomere length values.

The telomere and single-copy gene (β -actin) were amplified in separate singleplex reactions because the efficiency of each amplicon was optimal in different master mixes (assessed in pilot studies). The method for the single-copy gene amplification is described in **Section 4.4.3.3.**

At the time of the experiment, 10 μ M telomere primer working solutions were made by thawing the 100 μ M frozen primer stocks on ice. 160 μ l of DNase-RNase free water (Sigma) was added to a microcentrifuge tube. 20 μ l of thawed 100 μ M F primer stock and 20 μ l of thawed 100 μ M R primer stock were added to the water to make 200 μ l stock of 10 μ M F and R primer mix. The solution was flick mixed and kept on ice.

Using the primer mix working solution that was prepared above, the master mix plus primer working solution was made. To have 20 μ l of PCR reaction volume in each well, master mix

plus primer working solution and rat blood/colon DNA working solutions were made separately. Starting DNA amount for rat colon was 83.8ng for rat colon using 0.1 μ M telomere primer and starting DNA amount for rat blood was 40.8ng using 2 μ M telomere primer. To have either 2 μ M or 0.1 μ M telomere primer concentrations in the PCR well, 10 μ l of commercial 2X power SYBR[®] Green PCR MasterMix (Life Technologies- 4367659) was added to a 2 μ l microfuge tube followed by adding either 4 μ l of the 10 μ M primer mix (for 2 μ M telomere primer concentration) or 2 μ l of the 10 μ M primer mix (for 0.1 μ M telomere primer concentration) working solution for each PCR well. The rat blood DNA working solution was made by making five tubes of 10-fold serial dilutions of DNA followed by adding 2 μ l per PCR well of each of the serial dilutions to either 4 μ l of DNase-RNase free water (for 2 μ M telomere primer concentration) or 6 μ l of Sigma water (for 0.1 μ M telomere primer concentration). The standard curve was performed in triplicate.

PCR reactions were set up by aliquoting either 14 μ l of the master mix stock (for 2 μ M telomere primer concentration) or 12 μ l of the master mix stock (for 0.1 μ M telomere primer concentration) and primer working solution into each reaction well of a 384-well plate (Life Technologies, 4309849) compatible with the ViiA[™] 7 detection system (Applied Biosystems). 6 μ l (for 2 μ M telomere primer concentration) or 8 μ l (for 0.1 μ M telomere primer concentration) of each dilution of the DNA working solution was added to reach a final volume of 20 μ l per reaction. A negative control (H₂O) was included on each PCR plate.

The thermal cycling profile (O'Callaghan & Fenech 2011) was Stage 1: 2 mins at 50°C; Stage 2: 10 mins at 95°C; Stage 3: 40 cycles of 15s at 95°C, 1 min at 60°C with signal acquisition followed by a dissociation (melt) curve. At the end of the experiment, the cycle threshold (Ct) values were exported and PCR products were analysed using polyacrylamide gel electrophoresis (see **Section 4.4.5**).

4.4.3.2 Cawthon telomere qPCR method

Mean telomere length was measured using a singleplex assay, adapted from Cawthon (Cawthon 2002). The telomere and single-copy gene (β -actin) were amplified in separate singleplex reactions because the efficiency of each amplicon was optimal in different master mixes (assessed in pilot studies). The method for the single-copy gene amplification is described in **Section 4.4.3.3**.

The telomere primers were used at a final concentration of 900nM (Cawthon 2009). At the time of the experiment, 9 μ M telomere primer working solutions were made by thawing the 100 μ M frozen primer stocks on ice. 164 μ l of DNase-RNase free water (Sigma) was added to a microcentrifuge tube. 18 μ l of thawed 100 μ M F primer stock and 18 μ l of thawed 100 μ M R primer stock were added to the water to make 200 μ l stock of 10 μ M F and R primer mix. The solution was flick mixed and kept on ice.

Each qPCR reaction was conducted in a total volume of 20 μ l using 384-well plates and performed on a ViiA 7 real-time PCR instrument (Life Technologies, Foster City, CA). A custom-made master mix adapted from Cawthon was used (Cawthon 2002). The final concentration of reagents in the PCR were 0.625 units in 25 μ l reaction volume of 5U/ μ l AmplitaqGold DNA polymerase (Life Technologies), 0.75 X SYBR Green I (Life Technologies), 10mM Tris-HCl pH 8.3 (Life Technologies), 50mM KCl (Life Technologies), 3mM MgCl₂ (Sigma), 0.2mM each dNTP (GeneSearch), 1mM DTT (Sigma) and 1M betaine (Sigma).

As described above, 9 μ M telomere primer working solution was made from the 100 μ M GC-Tel primer stock at the time of experiment. The solution was flick mixed and kept on ice.

To have 900nM telomere primer concentration in the PCR well with the highest concentration for a 20 μ l reaction volume, 8 μ l of the custom-made 2.5X SYBR Green PCR master mix was added to a microfuge tube followed by adding 2 μ l of the 9 μ M primer mix working solution for each PCR well. A standard curve was run alongside the experimental samples consisting of a calibrator DNA sample which was serially diluted by 5-fold to produce five DNA concentrations ranging from 515 to 0.824 ng/mL. To achieve this, three DNA batches were prepared: one with rat blood DNA (called the calibrator DNA), another with T2D rat DNA and the other with the control DNA. Rat blood DNA working solution was made by making 1:10 dilution for the first dilution and 4 tubes of 5 fold serial dilutions of DNA plus ultrapure H₂O (Invitrogen, 10977-015) out of the first dilution. T2D or control experimental rat DNA working solution was used either undiluted or a dilution. Consecutively, 2 μ l of each of the serial dilutions of rat blood DNA or experimental DNA samples was added to 8 μ l of ultrapure water. All DNA samples were assayed in quadruplicate. PCR reactions were set up by aliquoting 10 μ l of the stock of master mix and primer working solution into each reaction well of a 384-well plate (Life Technologies, 4309849) compatible with the ABI PRISM 7000 sequence detection system using 384-well reaction plates (Applied Biosystems). 10 μ l of each dilution of rat blood DNA or experimental DNA working solution was added to achieve a final volume of 20 μ l per reaction. The thermal cycling profile was Stage 1: 15 mins at 95°C; Stage 2: 36 cycles 2s at 98°C, 1min at 48°C; Stage 3: 15s at 74°C with signal acquisition followed by a dissociation (melt) curve.

4.4.3.3 Single copy gene qPCR assay

As the control for both telomere qPCR assays, the β -actin assay was amplified in Power SYBR green PCR Mastermix (Life Technologies). To make 10 μ M telomere primer working solution, a 1:10 dilution of the 100 μ M primer stock was made using ultrapure water. The solution was flick mixed and kept on ice. Using the primer mix working solution that was

prepared above, the master mix plus primer working solution was made. To have 20 μ l of PCR reaction volume in each well, master mix plus primer working solution and rat blood DNA/rat experimental DNA working solutions were made separately. To have 2 μ M primer concentration in the PCR well, 10 μ l of commercial 2X power SYBR Green PCR master mix (Life Technologies) was added to a microfuge tube followed by adding 4 μ l of the 10 μ M primer mix working solution to each PCR well.

The calibrator DNA (DNA extracted from whole rat blood) was diluted serially 5-fold to produce five DNA concentrations ranging from 5150 to 8.24ng/mL to produce a standard curve. T2D or control rat DNA working solution was used to achieve a final amount of 8-9ng DNA in the PCR well. All experimental DNA samples were assayed in triplicate. PCR reactions were set up by aliquoting 14 μ l of the stock of master mix and primer working solution into each reaction well of a 384-well plate (Life Technologies, 4309849) compatible with the ABI PRISM 7000 sequence detection system using 384-well reaction plates (Applied Biosystems). 6 μ l of each dilution of the calibrator DNA or experimental DNA was added to achieve a final volume of 20 μ l per reaction. The thermal cycling profile was Stage 1: 2 mins at 50°C; Stage 2: 10 mins at 95°C; Stage 3: 40 cycles of 15s at 95°C, 1 min at 60°C with signal acquisition followed by a dissociation (melt) curve.

4.4.4 Telomere data analysis

The amount of telomere was calculated as $T = E^{(Cq \text{ calibrator} - Cq \text{ sample})}$ where E was the efficiency of the telomere primer calculated from the standard curve, Cq calibrator was the Cq of the 1:5 dilution on the standard curve and Cq sample was the Cq of the experimental sample. The amount of β -actin (reference gene) was calculated as $S = E^{(Cq \text{ calibrator} - Cq \text{ sample})}$ where E was the efficiency of the β -actin primer calculated from the standard curve, Cq calibrator was the Cq of the 1:5 dilution on the standard curve and Cq

sample was the Cq of the experimental sample. Relative telomere length (T/S) was estimated as the ratio between the amount of telomere (T) and reference gene (S).

4.4.5 Nondenaturing Nucleic Acid Polyacrylamide Gel Electrophoresis (PAGE)

PCR amplification products were separated on a 15% TBE Criterion precast polyacrylamide gel (BioRad Laboratories - 3450057). The gel was placed in the gel tank and filled with 1X TBE buffer made from 10X stock TBE buffer (BioRad Laboratories - 1610733). A 50 bp DNA ladder (BioLabs - N3236S) was prepared as per the manufacturer's instructions. Samples were prepared by adding 10 µl of the PCR product to 2 µl of 6X DNA gel loading dye which was supplied with the ladder. 10 µl of PCR products and dye mix was loaded on the gel for each sample. Electrophoresis was conducted at 150V constant for 90 minutes. Consequently, the gel was stained for 40 minutes at room temperature using SYBR Green I Nucleic Acid Gel Stain (Invitrogen - S7563) diluted 1:10,000 in 0.5X TBE. The gel image was captured using a BioRad EZ-Doc Imager.

4.5 Protein analysis

4.5.1 Vessel harvesting and protein extraction from rodent cerebral arteries

On the day of termination, basilar and middle cerebral arteries were harvested from the brain and cleaned of connective tissue and were pooled in 180µl of protein extraction buffer (modified RIPA buffer). The buffer contained 50mM Tris, pH 7.8, 50mM NaCl, 1% Triton-X, 0.5% NP-40, 0.25% DOC and protease inhibitor tablet. All chemicals were supplied by Sigma Aldrich except protease inhibitor tablet which was purchased from Roche (Indianapolis, IN, USA). The arteries were homogenised on ice 3 times for 10 seconds with a rotor-stator homogeniser (IKA® ULTRA Turax®- T10 homogeniser). After centrifugation at 4°C at 12,000 g for 20 minutes, aliquots were immediately transferred to a -80°C freezer.

4.5.2 Protein Quantification

To determine the protein concentration of rat cerebral artery lysates, total protein content was quantified using the EZQ Protein Quantification Assay (Life Technology, R-33200). 2 mg/ml stock solution of ovalbumin standard (Life Technologies, R33200) was used to make serial dilutions of 1.0, 0.5, 0.2, 0.1, 0.05, and 0.02 mg/ml ovalbumin in water which formed the standard curve. All standards and samples were placed on the assay paper, fixed by methanol and stained with EZQ protein quantification reagent followed by destaining with EZQ destain (10% methanol and 7% acetic acid in H₂O). Assay results were read with a BioRad EZ-doc imager. Analysis was performed by using Carestream Molecular Imaging Software (Integrated Sciences) to determine the protein concentration of the artery lysate.

4.5.3 Western Blotting

Cerebral artery lysates were prepared by diluting them 1:2 with 2X Laemmli Sample Buffer (BioRad Laboratories) containing 10mM dithiothreitol (DTT) (BioRad Laboratories) followed by heating for 5 minutes at 95°C. Samples were then loaded onto each well of a 4-20% SDS-PAGE TGX-Mini-PROTEAN Stain-Free Precast Gel (BioRad Laboratories, 4568093) with Precision Plus Protein™ Standard Dual Colour (BioRad Laboratories) and were separated by electrophoresis at 100V for 1.1 hours. Proteins were transferred to an Immuno-Blot™ low fluorescence polyvinylidene fluoride (PVDF) membrane (Bio-Rad Laboratories, 1620264) for 1 hour at 4°C followed by blocking with buffer containing 5% blotting grade blocker (BioRad Laboratories, 1706404) and 0.1% Tween-20 (Sigma, P2287) for 1 hour at room temperature. The membrane was incubated overnight at 4°C with the desired antibody (**Table 4.1**).

Table 4.1. Primary antibodies that were used to probe proteins.

Primary Antibody	Dilution	Supplier/ Cat No.
SIRT1 (mouse monoclonal)	1:1000	Abcam, ab110304
eNOS (mouse monoclonal)	1:1000	BD Transduction Labs, 610296
MnSOD (rabbit polyclonal)	1:500	Millipore, 06-984
Nox2 (mouse monoclonal)	1:1000	BD Transduction Labs, 61141
Nitrotyrosine (mouse monoclonal)	1:250	Abcam, ab52309
p66Shc (rabbit polyclonal)	1:500	Millipore, 06-203

The membranes probed with p66Shc and MnSOD were washed and incubated the day after with goat anti-rabbit secondary antibody conjugated to horseradish peroxidase (Pierce-31460) at 1:5000 and the remaining membranes were washed and incubated with donkey anti-mouse secondary antibody conjugated to horseradish peroxidase (Jackson, 715-035-150) at 1:10,000 dilution for 1 hour at room temperature. The membranes were then washed and developed using either SuperSignal West Femto Maximum Sensitivity substrate (Thermo Scientific, 34095) for 1 minute or SuperSignal® West Pico Chemiluminescence substrate (Thermo Scientific, PIE34078) for 5 minutes followed by visualisation using a Fujifilm LAS-4000 digital imager. Carestream software was used to quantify the bands by densitometric analysis and the results were normalised according to the total protein loaded on the gel to neutralise variations in protein loading.

4.5.4 Statistical analysis and power

All data are expressed as mean \pm standard error of the mean. Statistical comparisons were performed using GraphPad InStat version 3 software (GraphPad software, La Jolla, CA, USA) using an unpaired *t*-test. Statistical significance was accepted at $P < 0.05$. The initial power analysis was performed based on previous telomere length studies in rodents (Raymond et al. 2013). The experiment was powered at 80% to detect a 20% change in telomere length, assuming a two-tailed alpha level of 5%.

5. RESULTS

5.1 Phenotype of T2D animal model

To simulate late stage T2D, animals were placed on a high-fat diet for a period of 18 weeks followed by a single injection of low dose streptozotocin (STZ). Animals were continued on the high-fat diet for another 8 weeks. Three T2D rats died; one just prior to STZ injection and the other two the following week after the injection. Animals in the control group were fed a normal diet followed by a single injection of vehicle (saline). The biochemistry characterisation is shown in Table 5.1.

Table 5.1. Comparison of clinical and biochemistry characteristics of T2D rats (n=6) with the control group (n=8). Values are mean \pm standard error of the mean. * indicates $P < 0.05$ between control and T2D rats. Cholesterol, triglyceride and HDL were measured from plasma samples and insulin, leptin, CRP and FFA were measured from serum samples.

Characterisation	Control rats	T2D rats	p value
Weight at injection (g)	387 \pm 5	413 \pm 9	0.029*
Final Weight (g)	432 \pm 7	358 \pm 12	0.0001*
Systolic pressure (mmHg)	105 \pm 5	113 \pm 5	0.15
Heart rate (bpm)	346 \pm 10	310 \pm 6	0.019*
Blood glucose (mM)	8.6 \pm 0.3	24.2 \pm 1.3	<0.0001*
Cholesterol	2.5 \pm 0.1	2.3 \pm 0.1	0.06
Triglycerides (mM)	1.4 \pm 0.1	2.0 \pm 0.4	0.14
HDL (mM)	2.4 \pm 0.1	1.9 \pm 0.2	0.07

Insulin (ng/ml)	2.8 ± 0.5	0.5 ± 0.1	0.0028*
Leptin (ng/ml)	8.8 ± 0.6	1.5 ± 0.2	<0.0001*
C-Reactive Protein (ng/ml)	16 ± 0.7	263 ± 23	<0.0001*
Free Fatty Acids (mmol/L)	0.34 ± 0.02	0.51 ± 0.06	0.012*

Animals gained significantly more weight after 18 weeks of high fat feeding (413±9g) compared with animals on a normal diet (387±5g). STZ injection reversed the weight gain such that at the conclusion of the experimental period, the weight of T2D rats was significantly less than the control rats (358±12 g compared with 432±7g).

As demonstrated in **Table 5.1**, fasting blood glucose, and free fatty acid levels were all significantly higher in T2D rats in comparison with the control rats. Serum insulin and leptin levels were significantly lower in T2D rats. Plasma CRP, a marker of systemic inflammation, was significantly higher in T2D rats in comparison with control rats. As demonstrated in **Table 5.1**, systolic blood pressure was comparable between the two groups; however heart rate was significantly lower in T2D rats compared with their control counterparts.

5.2 qPCR results: Pilot Studies

5.2.1 DNA Quantification

The quality of DNA extracted from rat colon, whole blood and femoral arteries was confirmed using a NanoDrop spectrophotometer and DNA concentrations are reported in Appendix 1.

5.2.2 Single-copy gene qPCR using O'Callaghan cycling conditions and rat colon DNA

In pilot studies, the O'Callaghan qPCR method was used to measure the single-copy gene (SCG), β -actin, using their published cycling conditions (O'Callaghan & Fenech, 2011). As can be seen from Fig 5.2, this produced exponential amplification curves and a single peak in the melt-curve. The efficiency was 105% (within the acceptable efficiency range of 95-105%) and the R^2 value was 0.999. The exponential curves in the amplification plot together with the single sharp peak in the melt curve and the R^2 and efficiency values, suggest that this is an optimal SCG assay using rat colon DNA.

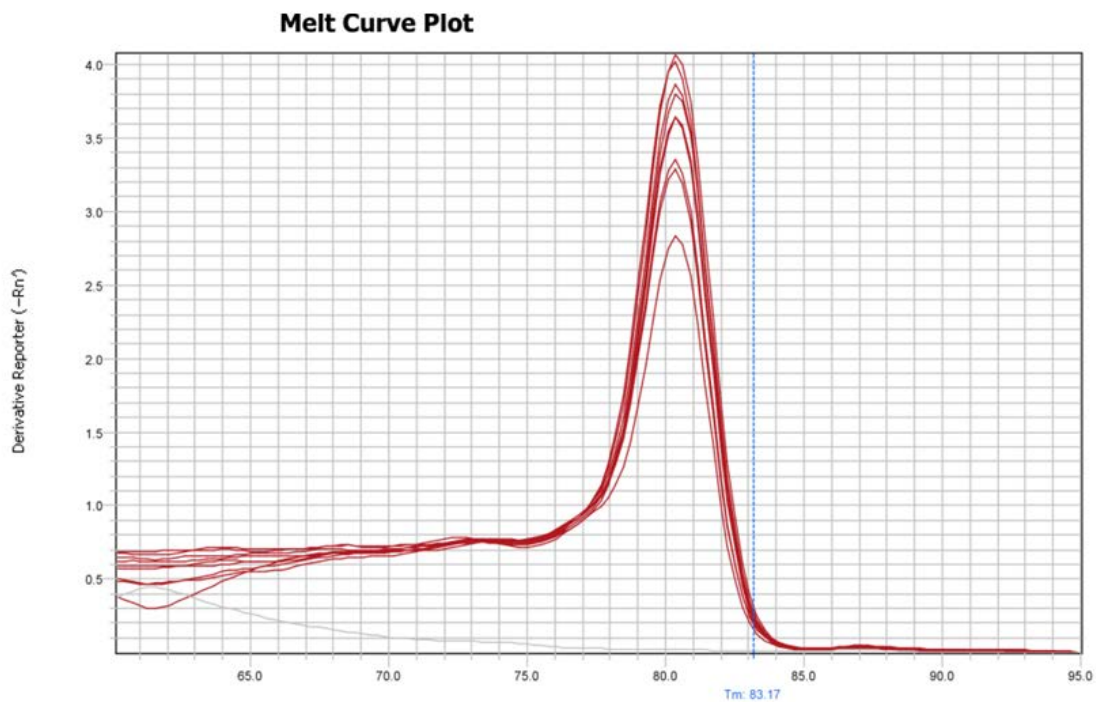
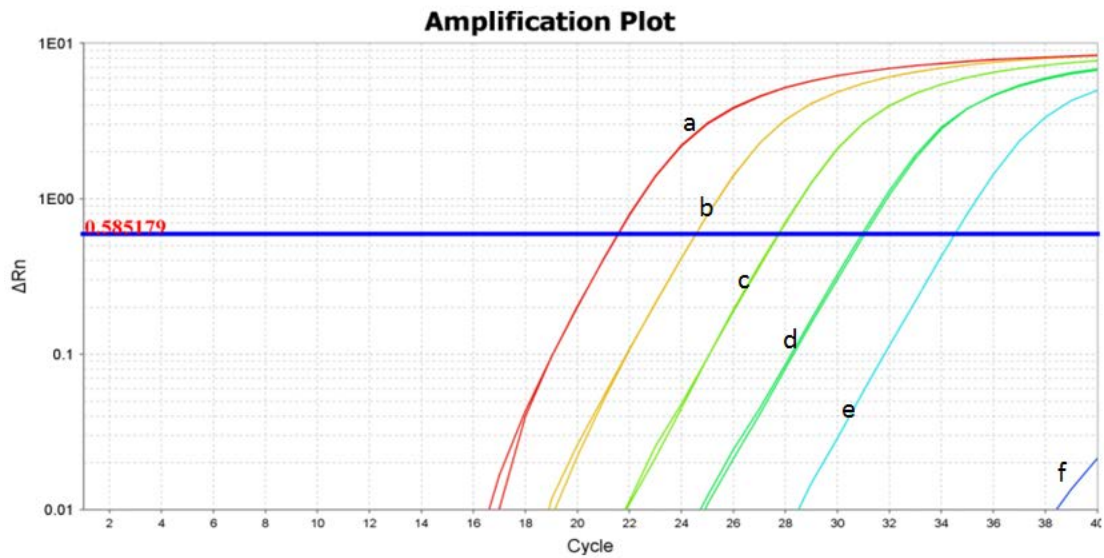


Fig. 5.2. The qPCR amplification plot and melt curve plot using rat colon DNA and rat β actin SCG primer. Starting DNA amount in the undiluted well was 95.4 ng. The primer concentration in each well was 2 μ M. Amplification plot- a: undiluted; b: 1:10 dilution; c: 1:100 dilution; d: 1:1000 dilution; e: 1:10,000 dilution; f: water.

5.2.3 Single-copy gene qPCR using O'Callaghan cycling conditions and rat blood

DNA

Our previous results showed that the O'Callaghan assay was optimal using our SCG primers and rat colon DNA. We therefore wanted to confirm the efficiency of the assay using DNA extracted from rat blood. In the previous experiment using rat colon DNA, we had used 95.4ng DNA in the undiluted well. Therefore, for this experiment we used approximately the same amount of rat blood DNA (103ng) in the undiluted well. The amplification plots and melt-curve are shown in **Fig. 5.3**. Here we observed an efficiency of 97.2% which is within the optimal efficiency range and an R^2 value of 0.999 which confirms reproducibility. The sharp single melt curve plot confirms that there was a single product (see **Fig. 5.3**). Running the PCR product on a gel confirmed that there was one product and it was the expected size of 81 base pairs (see **Fig. 5.17**).

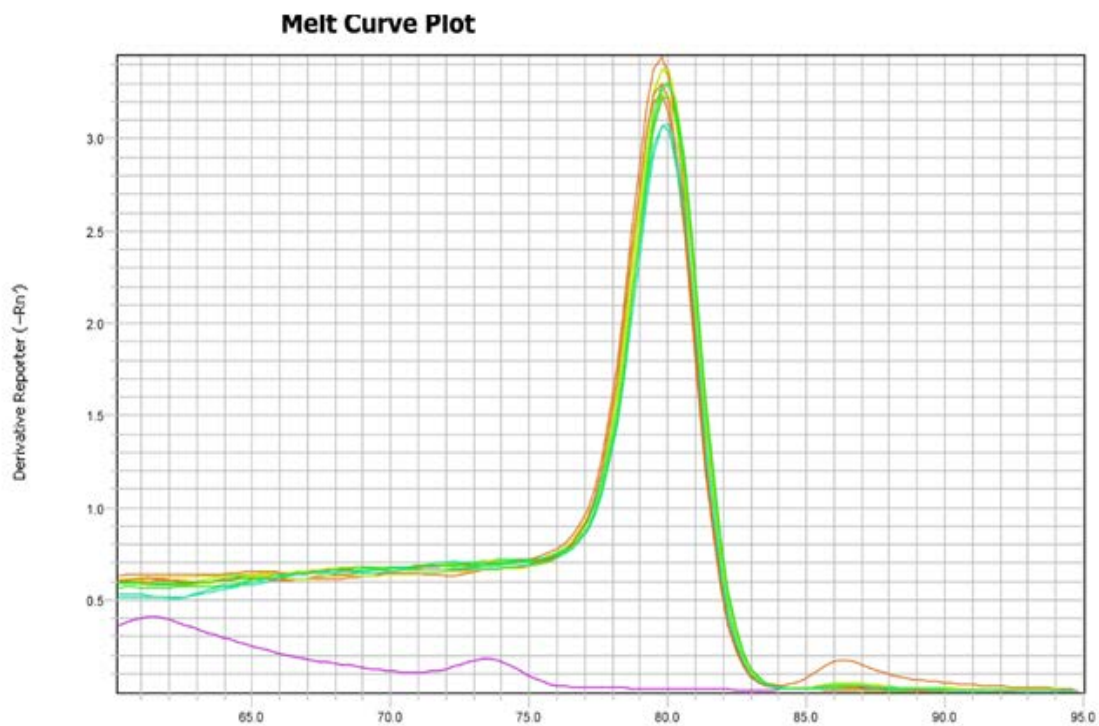
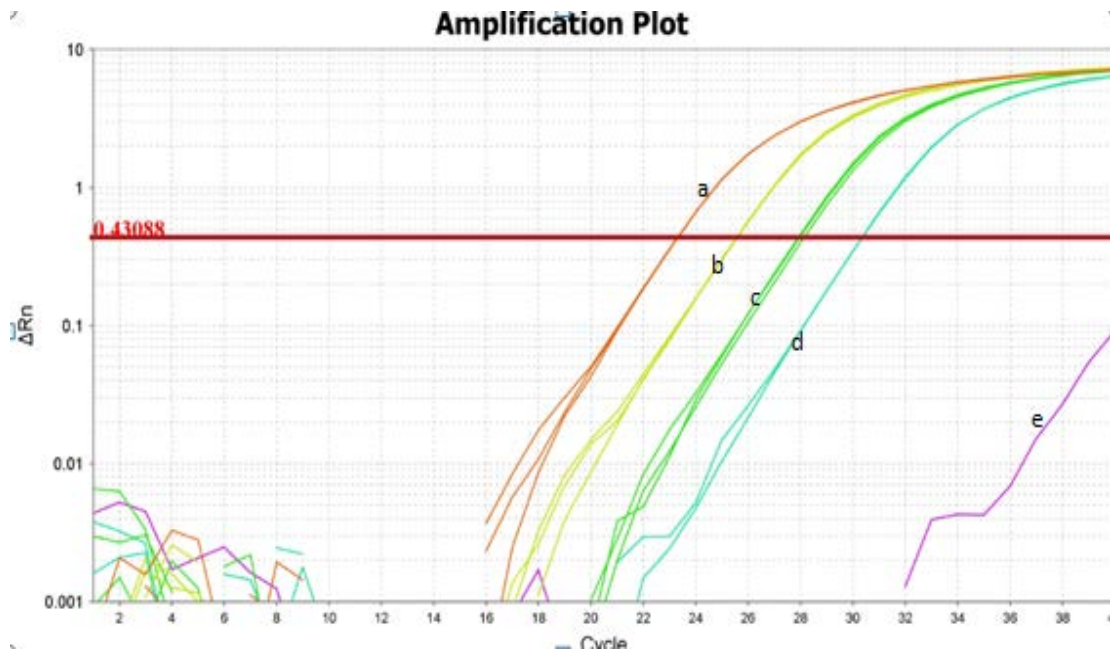


Fig. 5.3. The qPCR amplification plot and melt curve plot using rat blood DNA and rat β -actin SCG primer. The starting DNA amount in the undiluted well was 103 ng DNA (orange line). Primer concentration in each well was 2 μ M. Amplification plot - a: undiluted; b: 1:5 dilution; c: 1:10 dilution; d: 1:15; e: Water.

Telomere qPCR using O'Callaghan cycling conditions and rat colon DNA

The O'Callaghan qPCR method was then used to measure mean telomere length using their published telomere primers and cycling conditions (O'Callaghan & Fenech, 2011). As can be seen in **Fig. 5.4**, the telomere qPCR produced non-exponential curves; especially at the higher DNA concentrations and the curves were not equidistant. Although the initial starting amount of DNA could have been changed in further experiments to optimise these curves, several peaks in the melt-curve were observed, suggesting that multiple products were produced. Therefore, optimising the DNA concentration would not have been beneficial and we concluded that this method is not optimal for amplification of telomere primers.

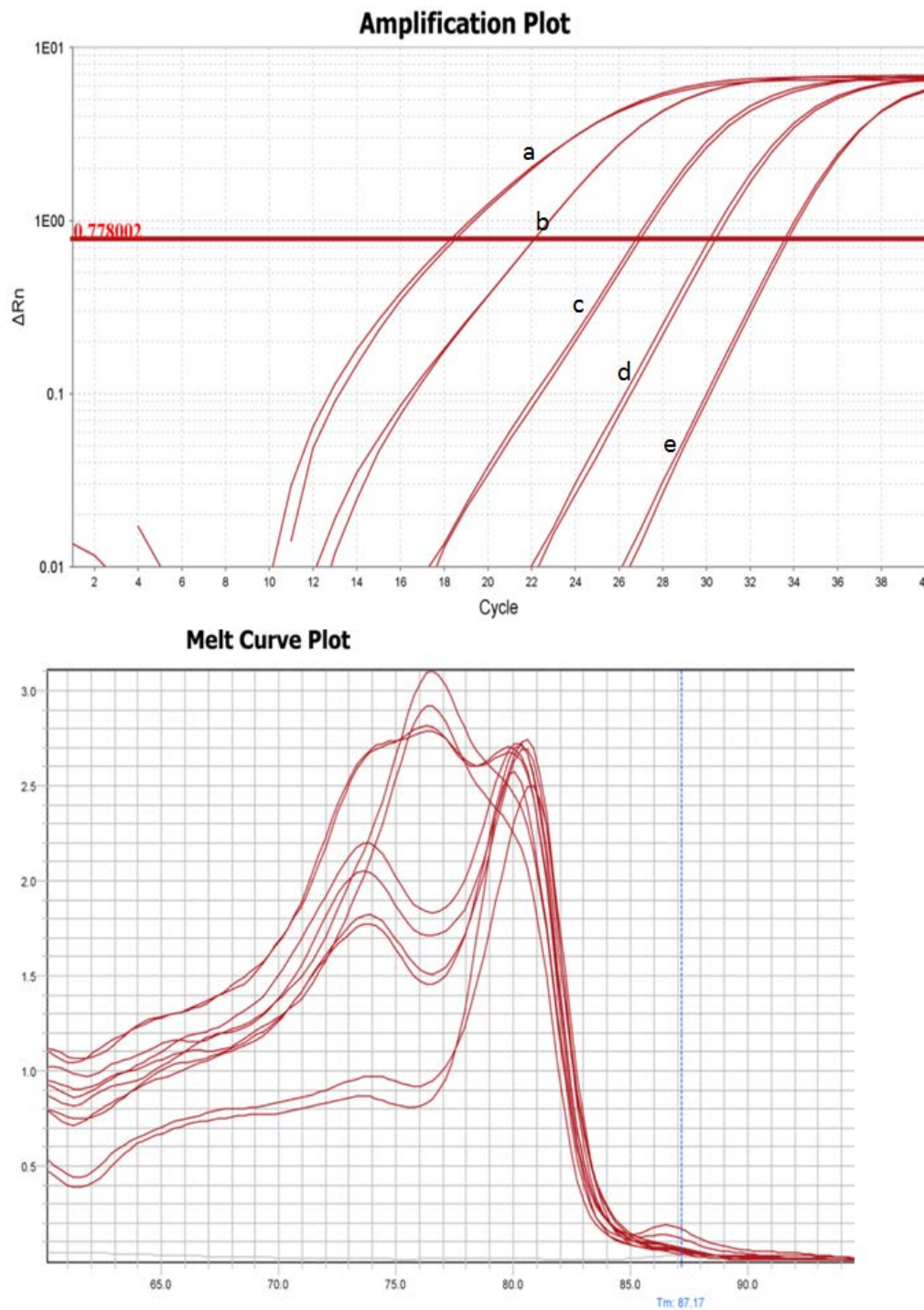


Fig. 5.4. The qPCR amplification plot and melt curve plot using rat colon DNA and telomere primers. Starting DNA amount in the undiluted well was 40.8 ng. Primer concentration in each well was 0.1 μ M. Amplification plot- a: undiluted; b: 1:10 dilution; c: 1:100 dilution; d: 1:1000 dilution; e: 1:10,000 dilution.

5.2.4 Telomere qPCR using O'Callaghan cycling conditions and rat blood DNA

As the telomere qPCR assay using rat colon DNA was not optimal, we tested rat blood DNA because this was the DNA obtained from our experimental animals. As can be seen from **Fig. 5.5**, the telomere qPCR results from DNA extracted from both rat colon and rat blood were similar. Therefore, our findings suggest that the O'Callaghan method was not an optimal method to amplify telomere primers in our experimental samples.

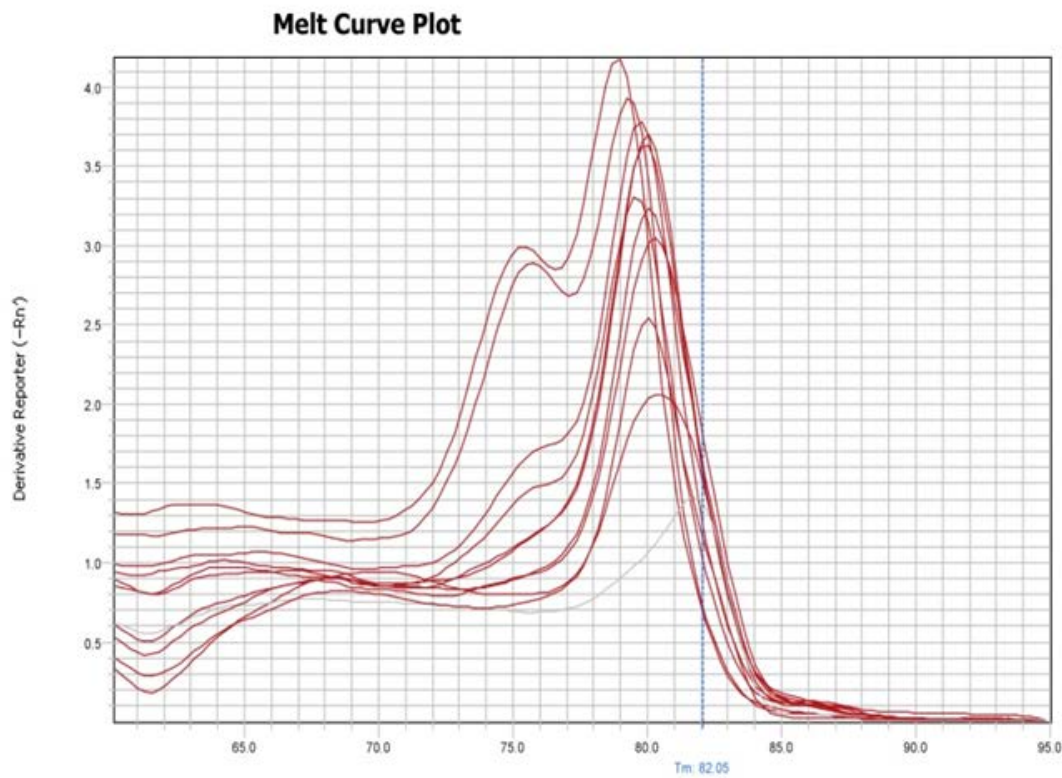
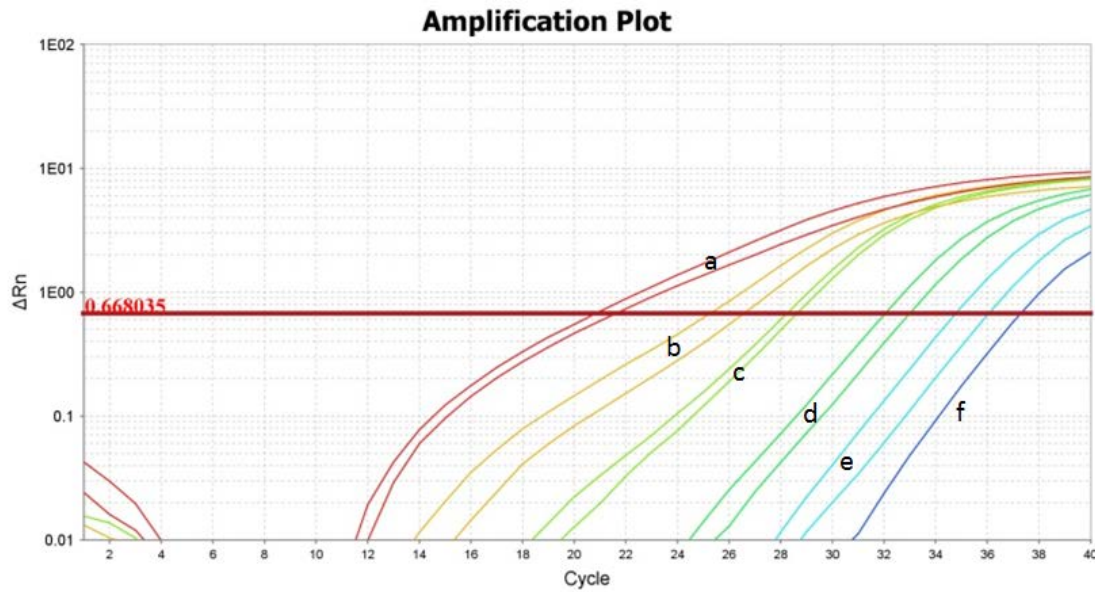


Fig. 5.5. The qPCR amplification plot and melt curve plot using rat blood DNA and telomere primers. Starting DNA amount in the undiluted well was 83.8 ng. The primer concentration in each well was 2 μ M. Amplification plot- a: undiluted; b: 1:10 dilution; c: 1:100 dilution; d: 1:1000 dilution; e: 1:10,000 dilution; f: water.

5.2.5 Single-copy gene qPCR using Cawthon cycling conditions and rat blood DNA

Since the O'Callaghan telomere assay was unsuccessful, the Cawthon qPCR method was then evaluated using their published cycling conditions (Cawthon, 2002). The β -actin SCG primer produced scattered amplification curves with multiple peaks in the melt-curve (see **Fig. 5.6**) suggesting that the Cawthon thermal cycling conditions did not produce optimal results with the β -actin SCG primer.

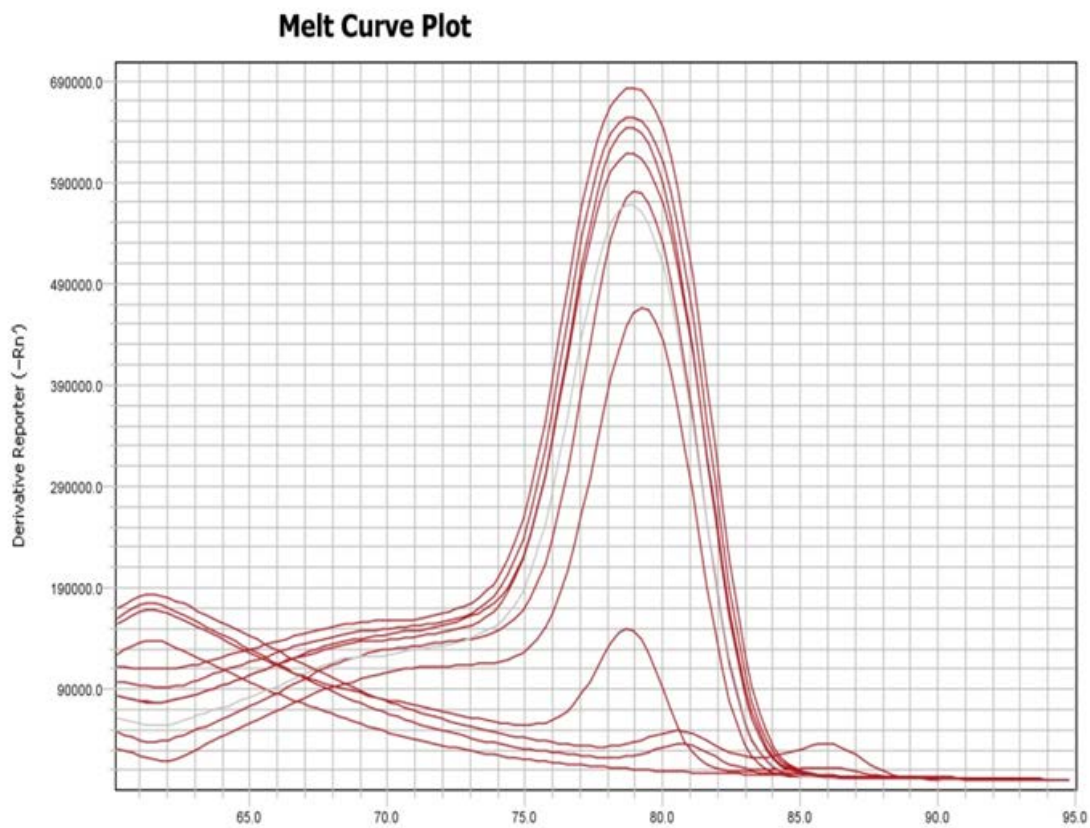
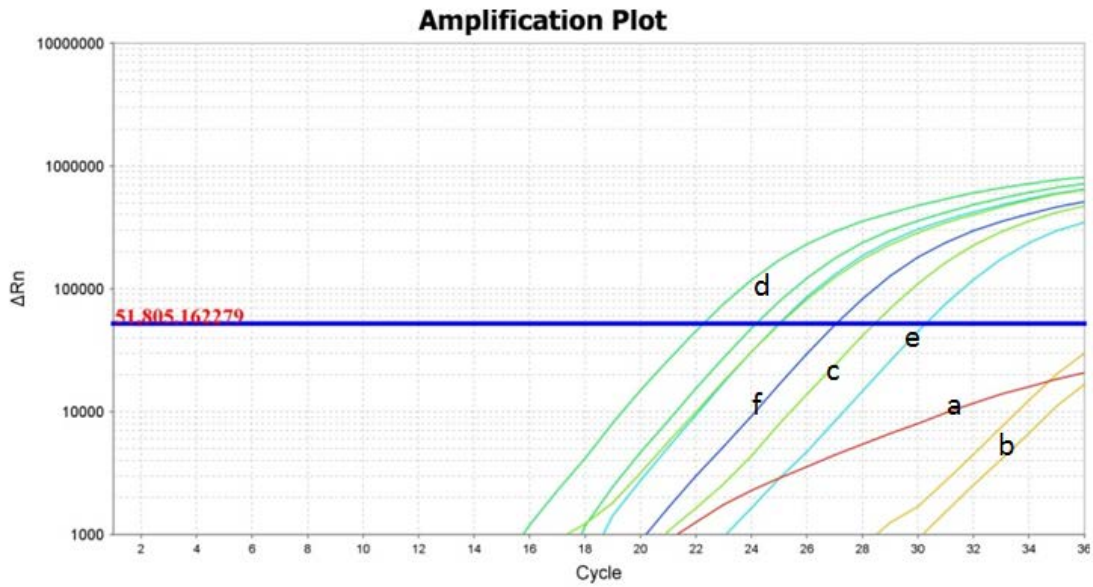


Fig. 5.6. The qPCR amplification plot and melt curve plot using rat blood DNA and rat β -actin SCG primer with Cawthon thermal cycling conditions. Starting DNA amount in the undiluted well was 87.6 ng. The primer concentration in each well was $2\mu\text{M}$. Amplification plot- a: undiluted; b: 1:10 dilution; c: 1:100 dilution; d: 1:1000 dilution; e: 1:10,000 dilution; f: water.

5.2.6 Telomere qPCR using Cawthon cycling conditions and rat blood DNA

The telomere qPCR assay was then tested using Cawthon's published telomere primers and thermal cycling conditions (Cawthon, 2009) with rat blood DNA. The amplification plot in Fig. 5.7 shows exponential curves with the most concentrated DNA (curve a) being shifted to the right. This suggests that too much DNA was present in the undiluted sample thereby inhibiting the PCR reaction. The negative control (water, curve f) appeared within 2 cycles from the most diluted DNA sample (curve e) which has been explained in the discussion. The efficiency was 104% which is within the optimal efficiency range (95-110%). R^2 was 0.996 which proves high reproducibility (low standard deviation between replicates). The single peak in the melt curve plot suggests that there is one main product which has been further confirmed by running the product out on an agarose gel (see **Fig. 5.17**). The telomere PCR product showed a main product at 82 base pairs (the sum of the length of the two telomere primers). Therefore we concluded that the Cawthon thermal cycling conditions and telomere primer set were optimal for assessing telomere length in our rat blood samples.

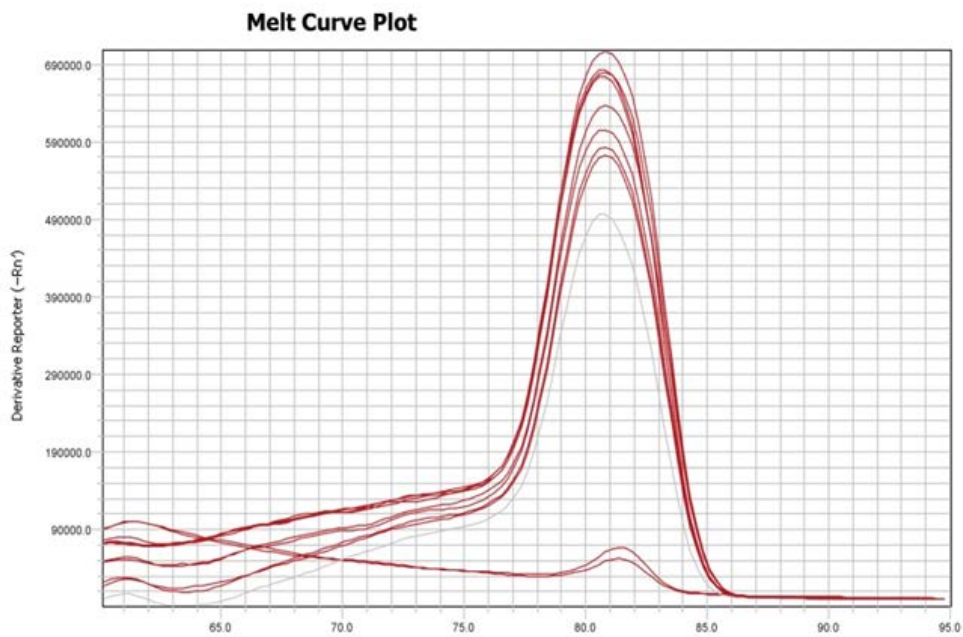
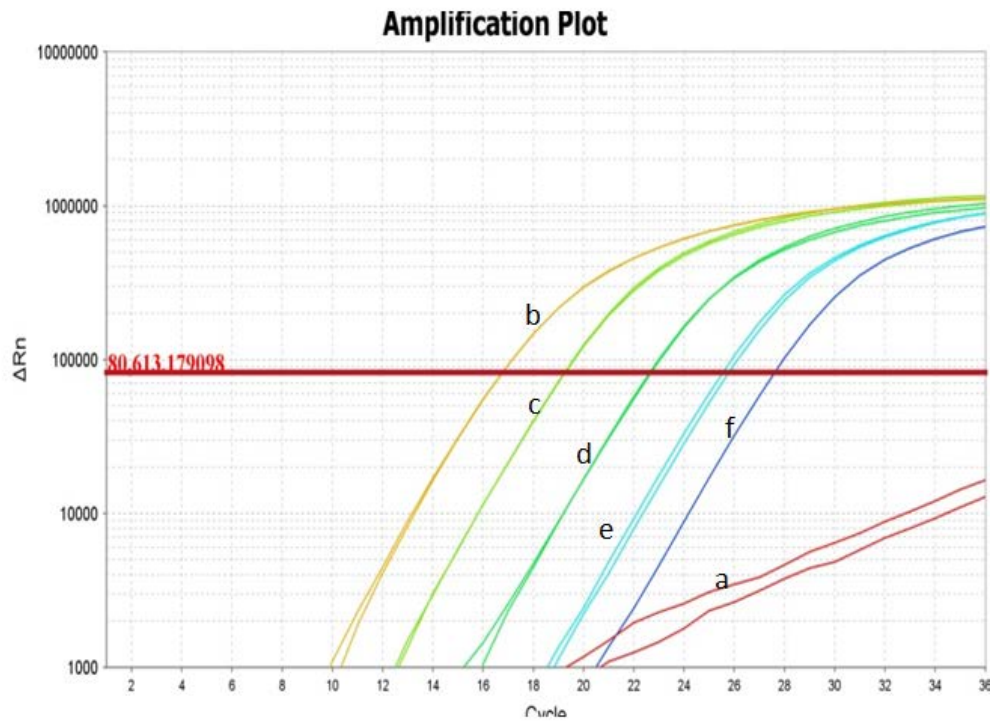


Fig. 5.7. The qPCR amplification plot and melt curve plot using rat blood DNA and telomere primers. The starting DNA amount in the undiluted well was 87.6 ng. Primer concentration in each well was 0.9 μ M. Amplification plot- a: undiluted; b: 1:10 dilution; c: 1:100 dilution; d: 1:1000 dilution; e: 1:10,000 dilution; f: water.

The conclusion from our pilot studies was that a multiplex assay, using the SCG and

telomere primers under the same cycling conditions, could not be used. Rather, a singleplex qPCR assay was developed, based on the O'Callaghan thermal cycling conditions for the SCG primer and the Cawthon thermal cycling conditions for the telomere primer.

5.3 qPCR Results: Experimental Samples

Singleplex qPCR assays can be run as long as a consistent DNA sample, known as the “calibrator”, is used in all assays (Olsen et al. 2012). The experimental samples are then normalised to this calibrator. DNA extracted from male Hooded Wistar rat blood was used as the calibrator in our experiments.

5.3.1 Single-copy gene qPCR using O'Callaghan cycling conditions and rat experimental samples

In this assay, we ran the calibrator DNA alongside the experimental samples, control rat blood (Rat 10 – Rat 17) and one T2D rat blood (Rat 4). The calibrator DNA was diluted serially by 5-fold to produce five DNA concentrations ranging from 5150 to 8.24 ng/ml and the qPCR results are shown in **Fig. 5.8**.

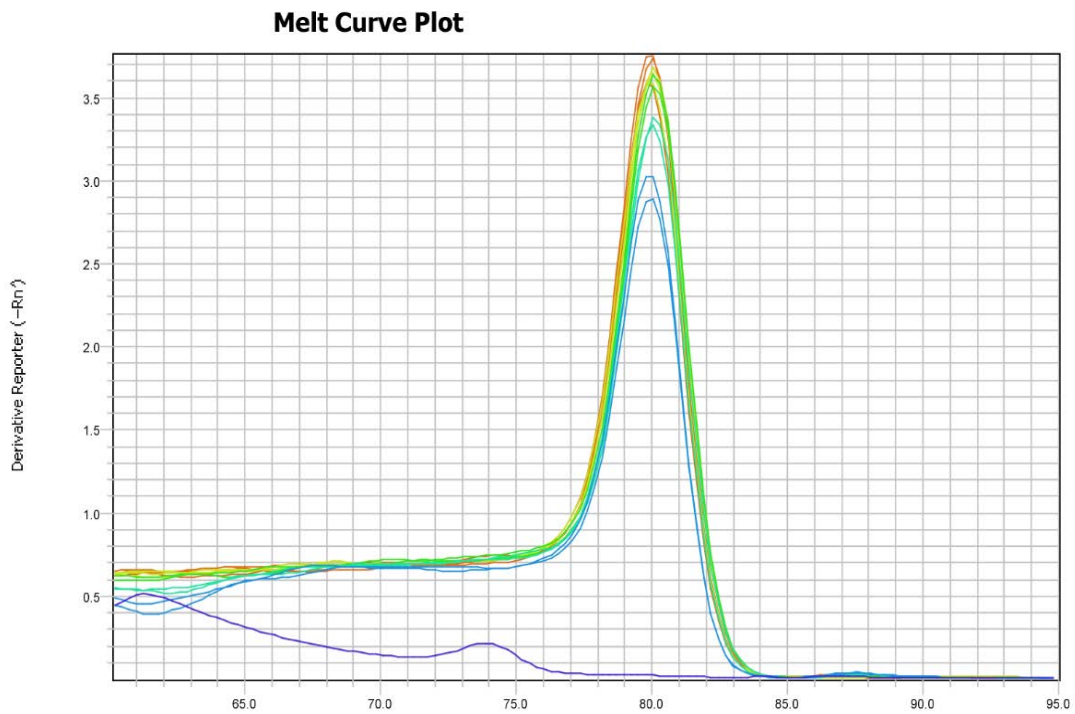
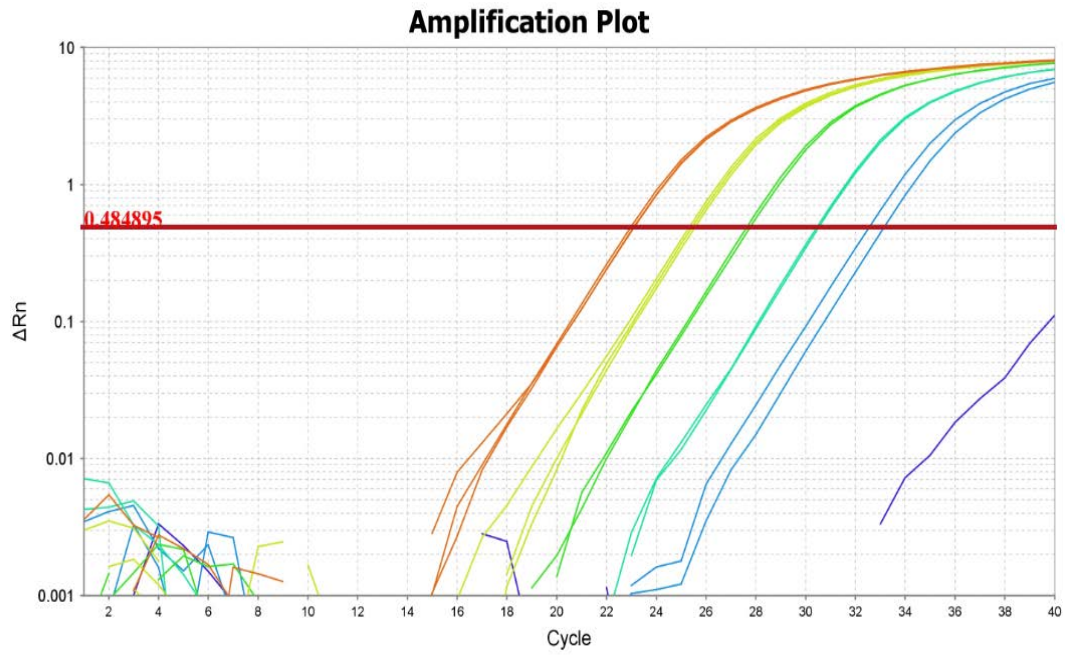


Fig. 5.8. The qPCR amplification plot and melt curve plot using calibrator DNA and rat β -actin SCG primer. The starting DNA amount in the undiluted well was 103 ng DNA (orange line). Primer concentration in each well was 2 μ M. Amplification plot - a: undiluted; b: 1:5 dilution; c: 1:10 dilution; d: 1:15; e: 1:20; f: Water.

Here we observed an efficiency of 92.1% which is within the optimal efficiency range and an R^2 value of 0.999 which confirms reproducibility. The single sharp peak in the melt-curve plot confirms that there was a single product (see **Fig. 5.8**). On the same PCR plate, all the experimental control rat blood samples (Rat 10 – Rat 17) and one T2D rat blood sample (Rat 4) were run.

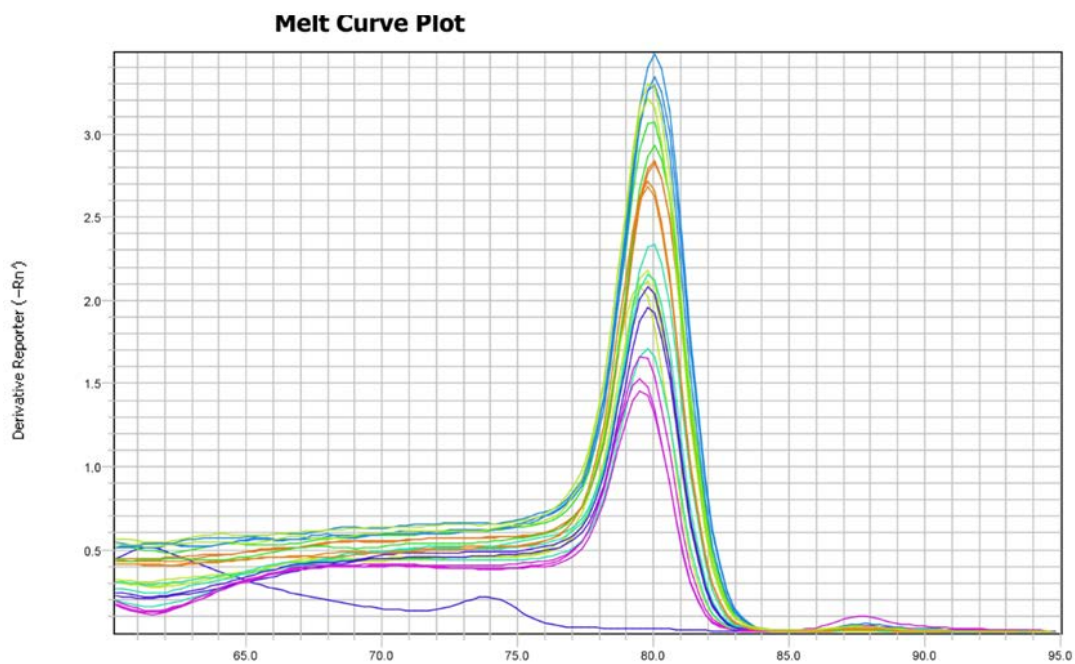
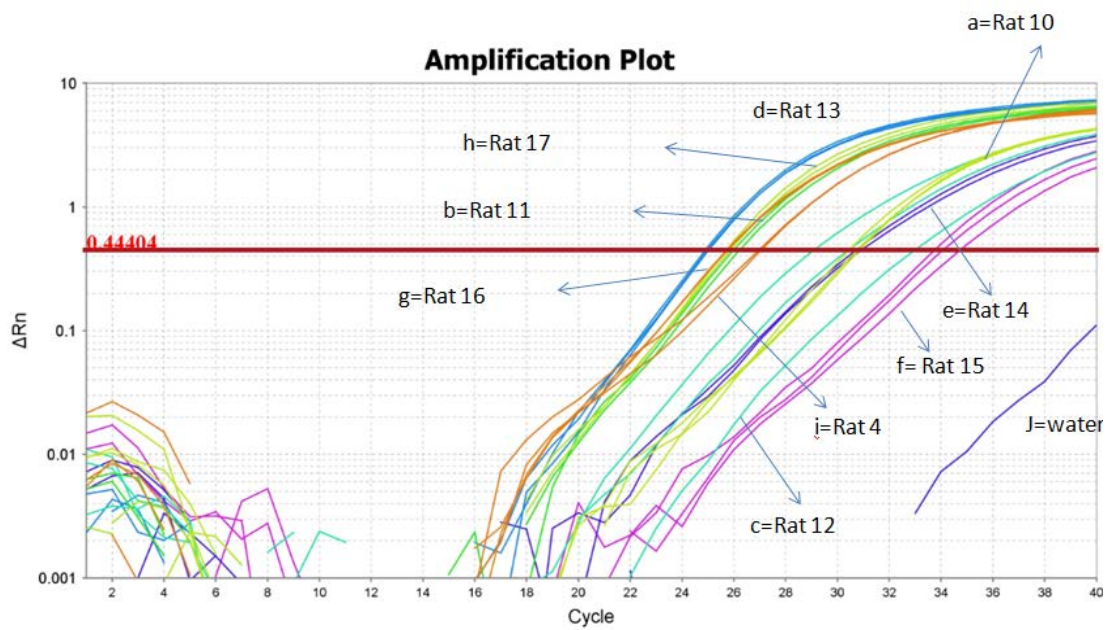


Fig. 5.9. The qPCR amplification plot and melt curve plot using experimental rat blood DNA and rat β -actin SCG primer. Primer concentration in wells was 2 μ M. Amplification plot – a (light green): Rat 10; b (dark green): Rat 11; c (aqua): Rat 12; d (blue): Rat 13; e (purple): Rat 14; f (pink): Rat 15; g (orange): Rat 16; h (light green): Rat 17; i (orange): Rat 4; j: Water.

As can be seen from **Fig. 5.9**, the Ct values from the majority of the experimental lean DNA samples was less than 32, however some of the replicates were not consistent. In addition, Rat 12 and Rat 15 produced replicates that were variable and Rat 15 gave a Ct value >32. Therefore the control rat blood samples (Rat 11-Rat 17) and one T2D rat blood sample (Rat 3) were run again using rat β -actin primers and the O'Callaghan thermal cycling conditions.

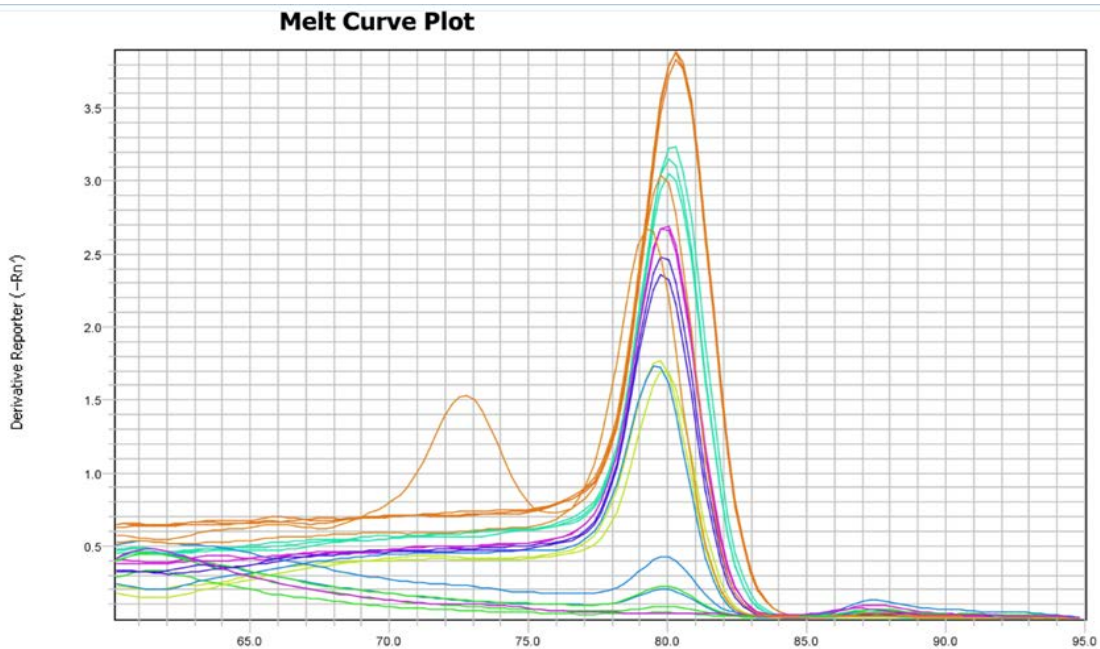
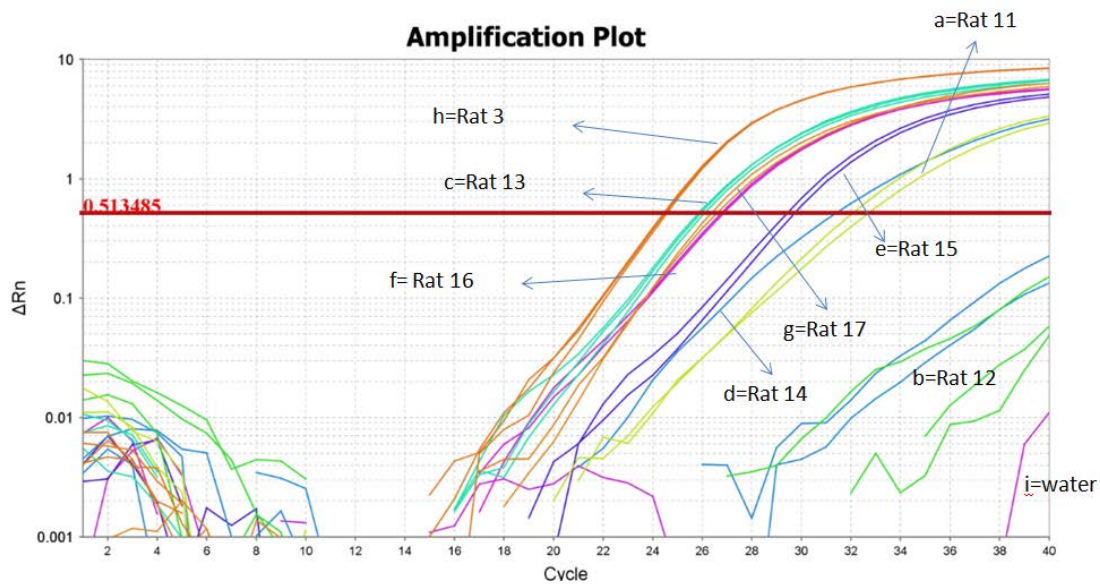


Fig. 5.10. Real time PCR amplification plot and melt curve plot using experimental rat blood DNA and rat β -actin SCG primer. Primer concentration in wells was 2 μ M. Amplification plot – a (light green): Rat 11; b (green): Rat 12; c (aqua): Rat 13; d (blue): Rat 14; e (purple): Rat 15; f (pink): Rat 16; g (orange): Rat 17; h (orange): Rat 3; i: Water.

As can be seen in Figure 5.10, the Ct values of Rat 11, Rat 12 and Rat 14 are very high which may be due to degradation of DNA. A single sharp peak was observed in the melt-curve which confirms the production of a specific product. The melt-curve correlating to the DNA sample from Rat 17 had an extra peak in one replicate. It was concluded that this was due to localised contamination in that well, because the other replicates did not show this peak. We repeated the SCG assay using control rat blood from Rats 11, 12 and 14 (see **Fig. 5.10**).

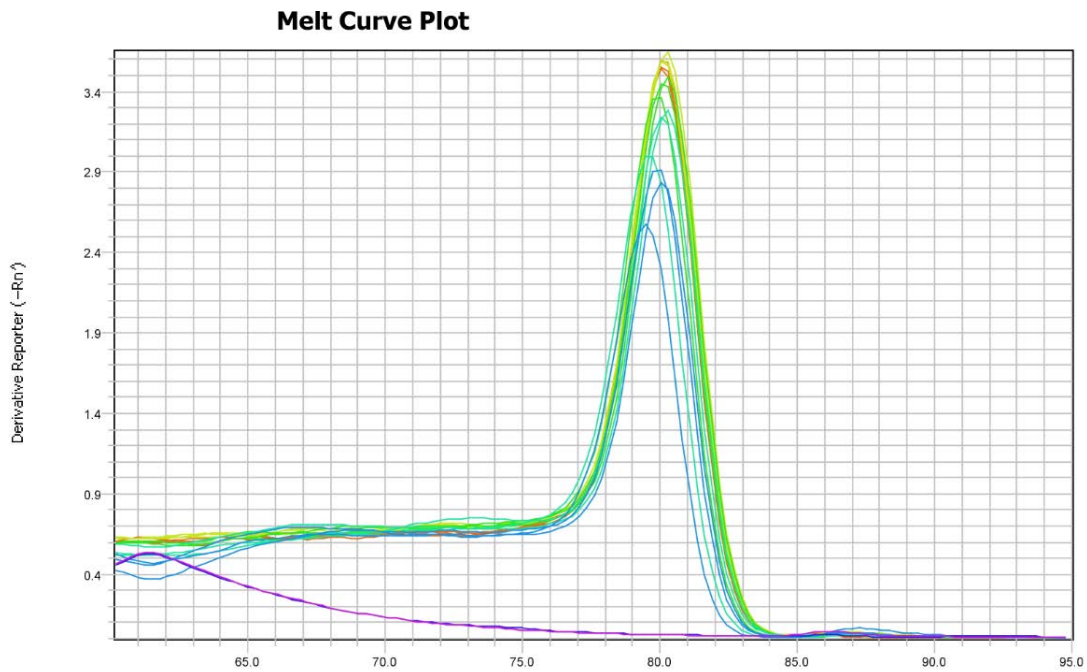
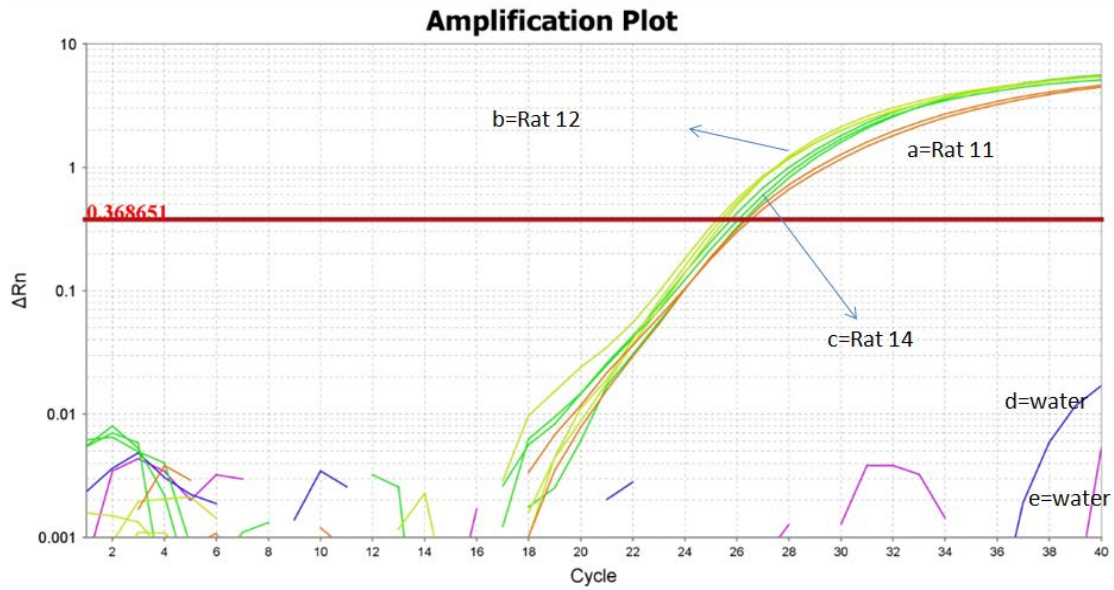


Fig. 5.11. The qPCR amplification plot and melt curve plot using control rat blood DNA and rat β actin SCG primer. Primer concentration in wells was 2 μ M. Amplification plot – a (orange): Rat 11; b (lime green): Rat 12; c (green): Rat 14; d (purple): Water; e (pink): Water.

In a final experiment, the rat experimental T2D rat blood samples (Rat 2-Rat 9) were run using rat β -actin primers and the O'Callaghan thermal cycling conditions.

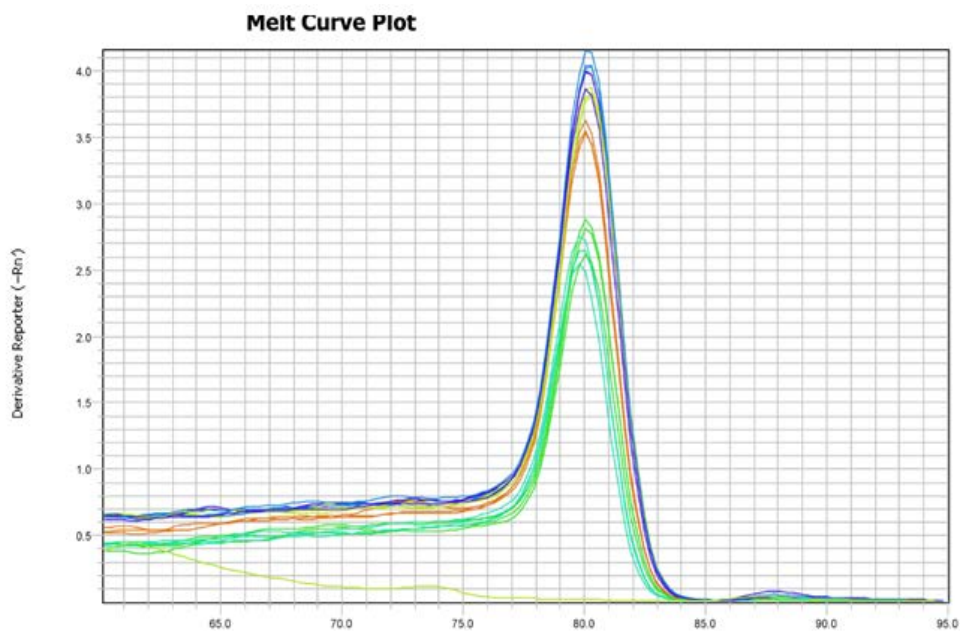
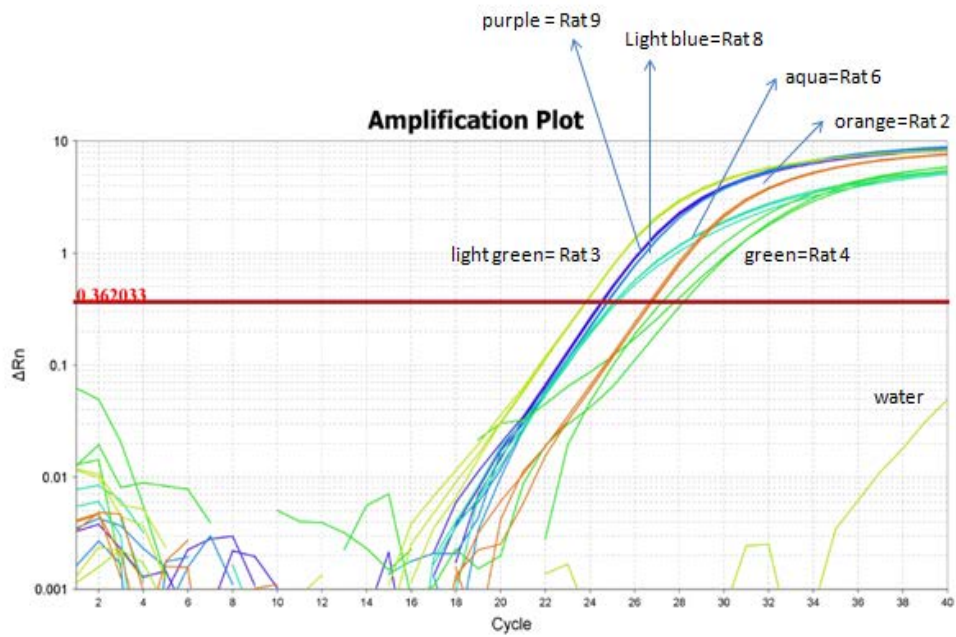


Fig. 5.12. The qPCR amplification plot and melt curve plot using T2D rat blood DNA as the experimental sample and rat β actin SCG primer. Primer concentration in wells was 2 μ M. Amplification plot – a (orange): Rat 2; b (light green): Rat 3; c (green): Rat 4; d (aqua): Rat 6; e (light blue): Rat 8; f (purple): Rat 9; g (light green): Water.

As can be seen in **Fig. 5.12**, all the Ct values are within the normal range. A sharp peak was observed in the melt-curve which confirms the production of a specific product.

5.3.2 Telomere qPCR using Cawthon cycling conditions and rat experimental samples

Similar to the design of our SCG qPCR plate, a standard curve was run on the same plate as the experimental DNA samples. The same calibrator DNA sample was diluted serially by 5-fold to give concentrations of DNA ranging from 515 to 0.824ng/ml. However in order to avoid the first DNA sample being shifted to the right, the starting amount of DNA was decreased from 87.6ng to 10.3 ng. As can be seen from **Fig. 5.13**, the Ct values of this sample were now between 16 and 28. Efficiency was 101% which is within the optimal efficiency range and R^2 was 0.992 which confirms reproducibility. The single sharp peak in the melt-curve plot confirms specificity.

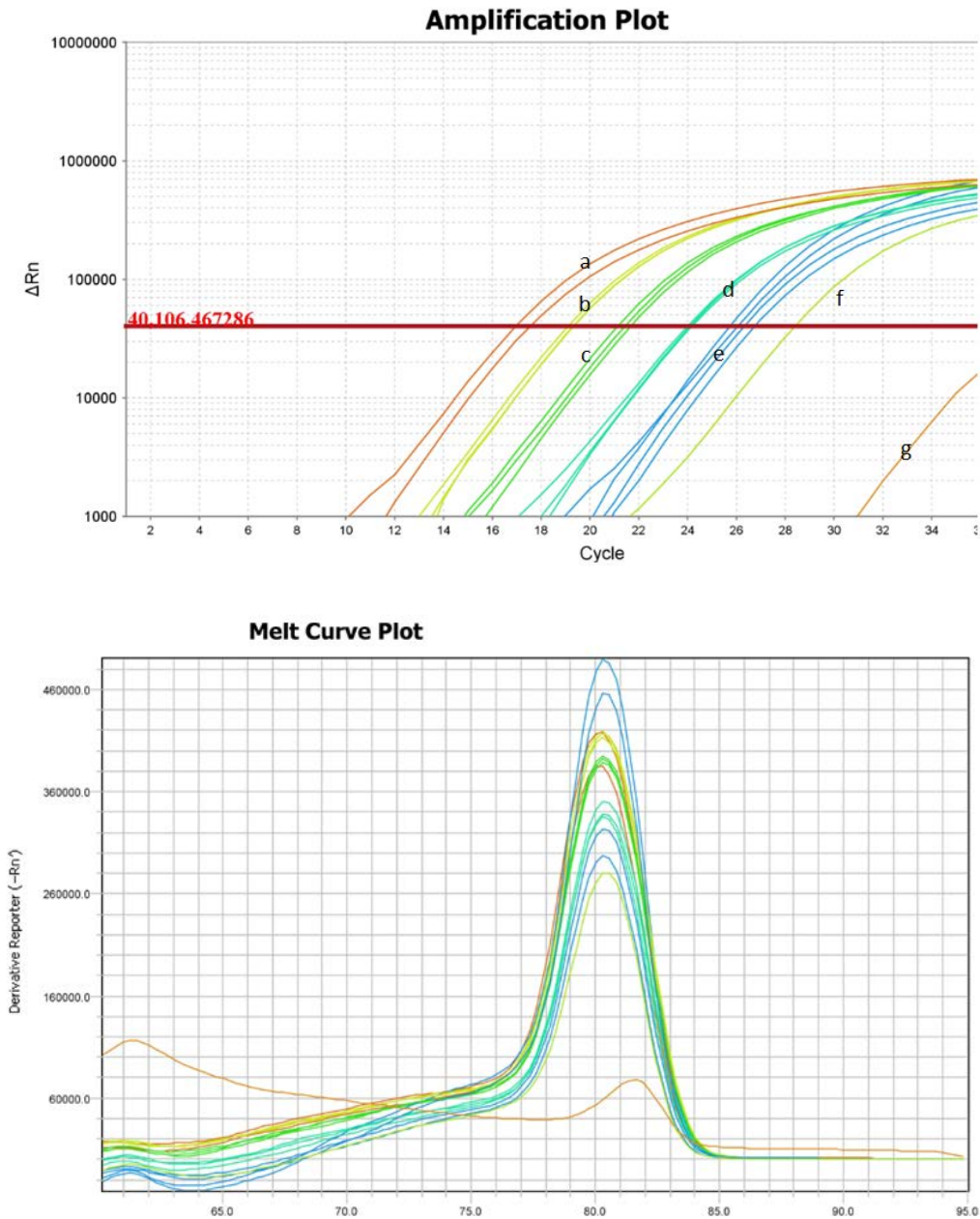


Fig. 5.13. The qPCR amplification plot and melt curve plot using calibrator DNA and telomere primers. 10.3 ng DNA was the starting DNA amount. Primer concentration in wells was 900 nM. Amplification plot - a: undiluted; b: 1:5 dilution; c: 1:10 dilution; d: 1:15; e: 1:20; f: water; g: water.

On the same PCR plate, all the control rat blood samples (Rat 10 – Rat 17) were run using the rat telomere primers and Cawthon thermal cycling conditions. As can be seen in **Fig. 5.13**, Ct

values were between about 16 and 26 which are within the optimal range. A single sharp peak in the melt-curve was observed which confirms the production of a specific product.

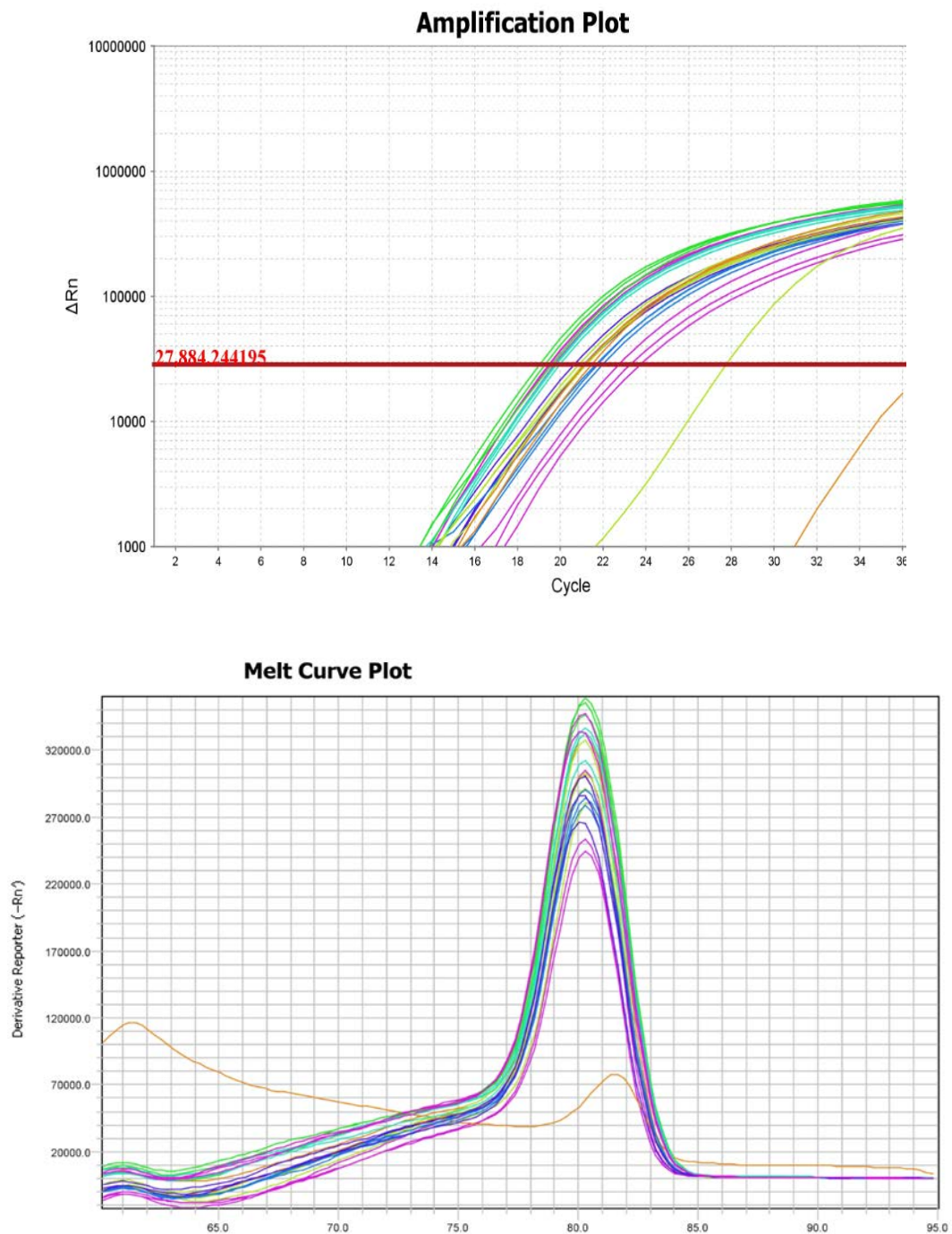


Fig. 5.14. The qPCR amplification plot and melt curve plot using control rat blood DNA and telomere primers. Primer concentration in wells was 900 nM.

All the T2D rat blood samples were then tested using the rat telomere primers and the Cawthon thermal cycling conditions. As demonstrated in **Fig. 5.14**, Ct values were between about 16 and 26 that are within the optimal range. A single sharp peak in the melt-curve was observed which confirms the formation of a specific product.

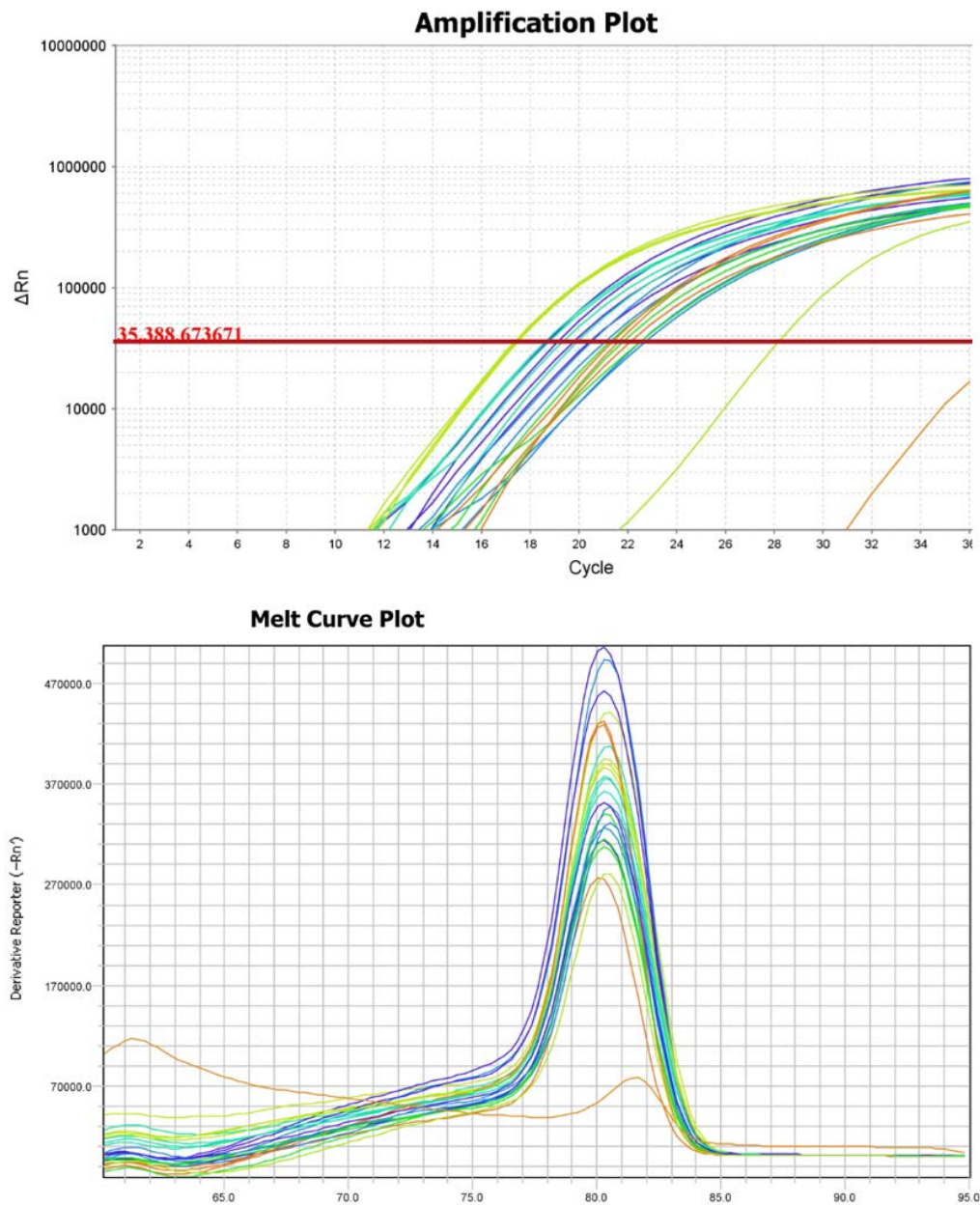


Fig. 5.15. The qPCR amplification plot and melt curve plot using T2D rat blood DNA and telomere primers. Primer concentration in wells was 900 nM.

5.3.3 Blood leukocyte mean telomere length

The leukocyte T/S ratio was calculated using the Ct values of the experimental samples and the Ct value of the calibrator DNA (see Section 4.4.4 in Materials and Methods). As shown in Fig. 5.16, the T/S ratio was significantly less in the T2D group (0.52 ± 0.31) compared to the control group (1.09 ± 0.5). The percent efficiency of β actin and telomere primers ranged between 92 and 102%.

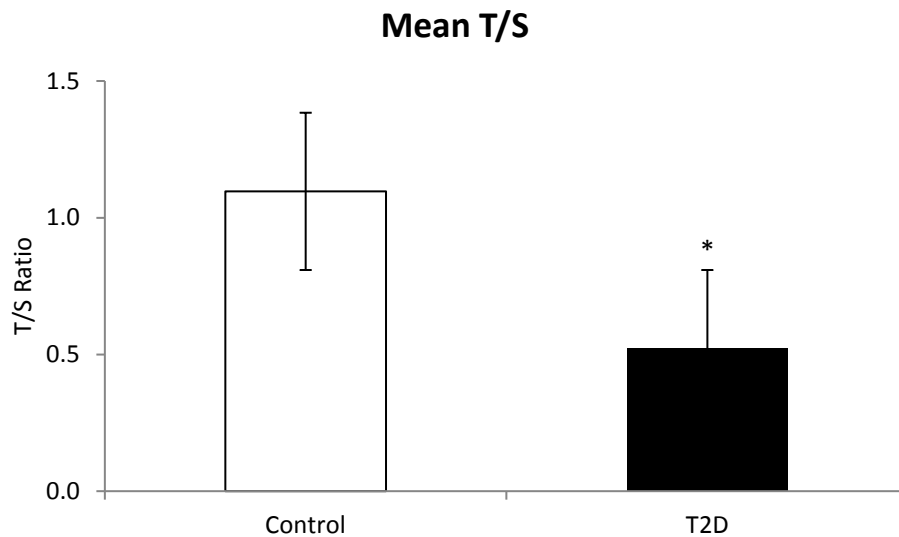


Fig. 5.16. Blood leukocyte T/S ratio was significantly lower in T2D rats compared with control rats (n=3; $P < 0.05$; t-test).

In contrast to the leukocyte T/S ratio, the femoral artery T/S ratio was comparable between T2D (0.92 ± 0.04) and control (0.81 ± 0.08) groups (see **Fig. 5.17**).

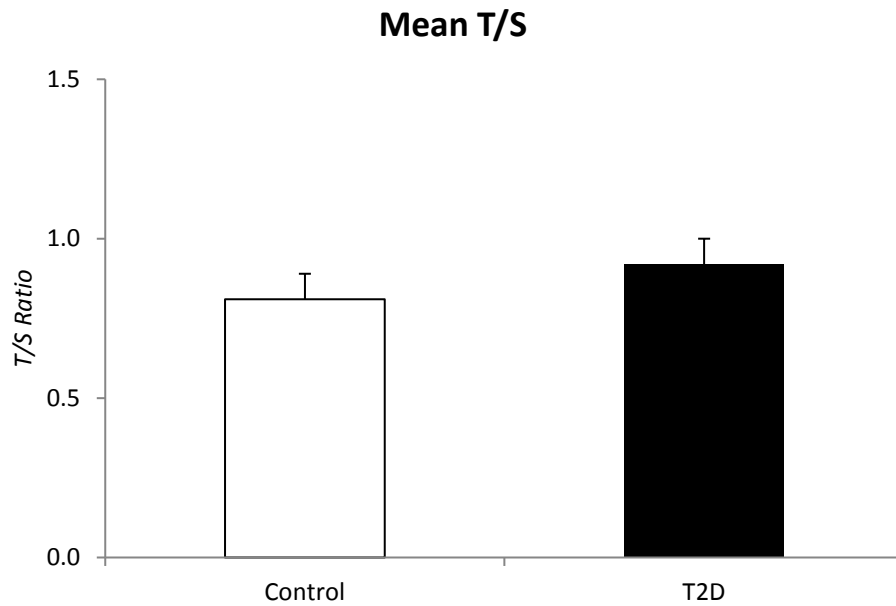


Fig. 5.17. Femoral artery T/S ratio was comparable between T2D and control rats (n=3; P>0.05; t-test).

5.3.4 Visualisation of PCR Products using Gel Electrophoresis

The PCR amplification products were visualised by polyacrylamide gel electrophoresis, ethidium bromide staining and UV transillumination. The β actin PCR product had a main product at the expected size of 81 base pairs whereas the telomere PCR product was observed as a main product at 82 base pairs, which is the sum of the length of the two telomere primers, with a smear up to 150bp. The smear reflecting longer PCR products is due to staggered annealing of the primers and is consistent with other reports in the literature (Cawthon 2002; Lee et al. 2005).

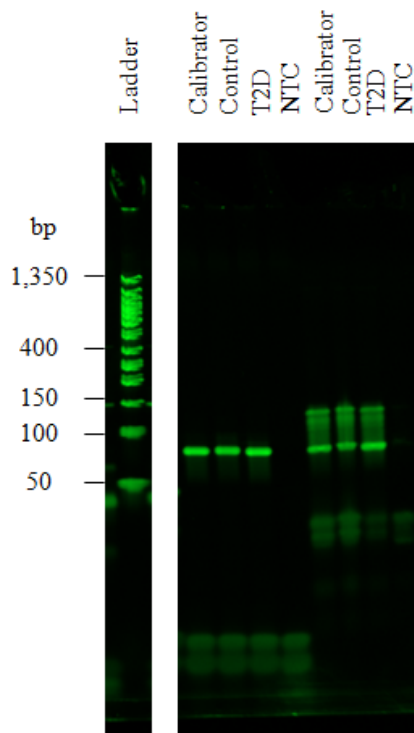


Figure 5.18. Visualisation of rat β actin and telomere primers qPCR products on polyacrylamide gel electrophoresis. Lane 1: DNA ladder; lanes 2 and 6: rat leukocyte calibrator DNA; lanes 3 and 7: control rat leukocyte DNA; lanes 4 and 8: T2D rat leukocyte DNA; lanes 5 and 9: no template control (H₂O).

5.4 Protein Expression Results

5.4.1 eNOS protein expression results

Western blotting revealed the presence of a single band at the expected molecular weight of 140 kDa. In T2D mice, cerebral artery eNOS protein expression was significantly less compared to non-diabetic mice ($P= 0.011$) (see **Fig. 5.19**).

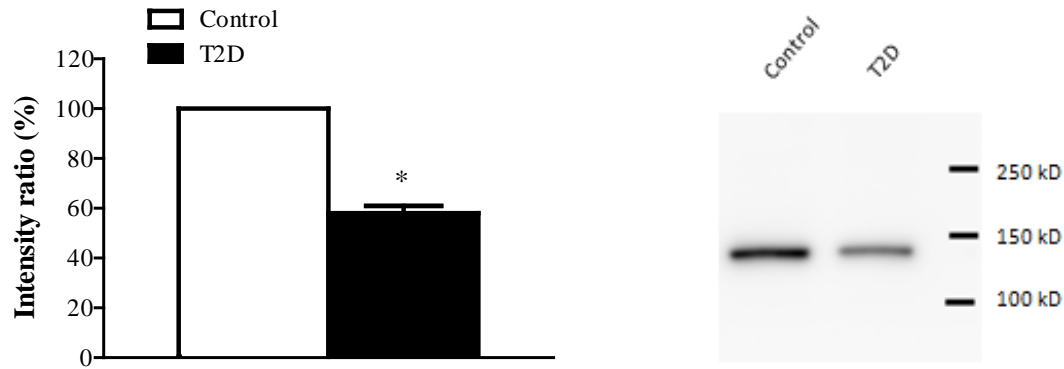


Figure 5.19. eNOS protein expression in T2D versus control rat cerebral artery. Arterial protein expression levels of eNOS was decreased in T2D rats compared with control rats ($n=3$; $P = 0.011$; t -test). A representative immunoblot is shown beside the bar graph. A single band was observed at the expected 140kD.

5.4.2 SIRT1 protein expression results

Western blotting revealed the presence of a single band at the expected molecular weight of 110 kDa. Cerebral artery SIRT1 protein expression was significantly lower in T2D rats compared with their control counterparts ($P = 0.0082$) (see **Fig. 5.20**).

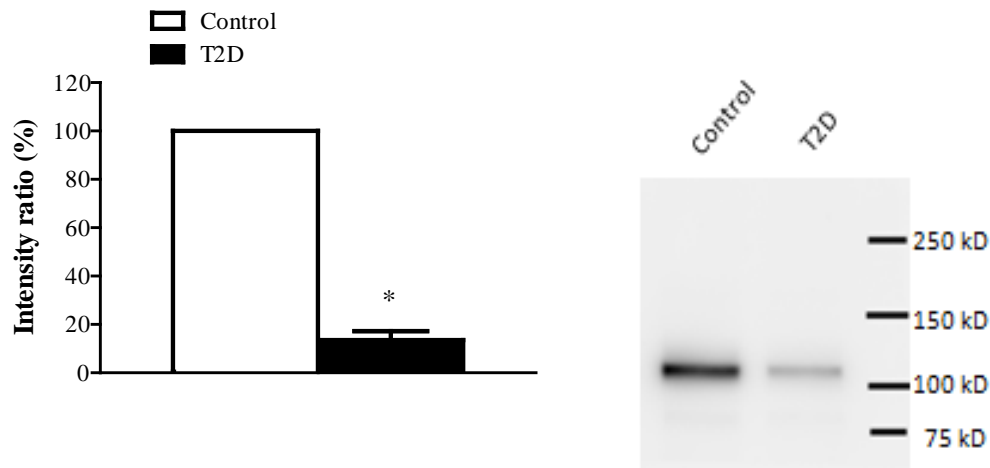


Figure 5.20. SIRT1 protein expression in T2D versus control rat cerebral artery. Arterial protein expression levels of SIRT1 was decreased in T2D rats compared with control rats ($n=3$; $P= 0.0082$; t -test). A representative immunoblot is shown beside the bar graph. A single band was observed at the expected 110kD.

5.4.3 MnSOD protein expression results

Western blotting revealed the presence of a single band at the expected molecular weight of 24 kDa. MnSOD protein levels were significantly lower in T2D rats compared with control littermates ($P = 0.039$) (see Fig. 5.21).

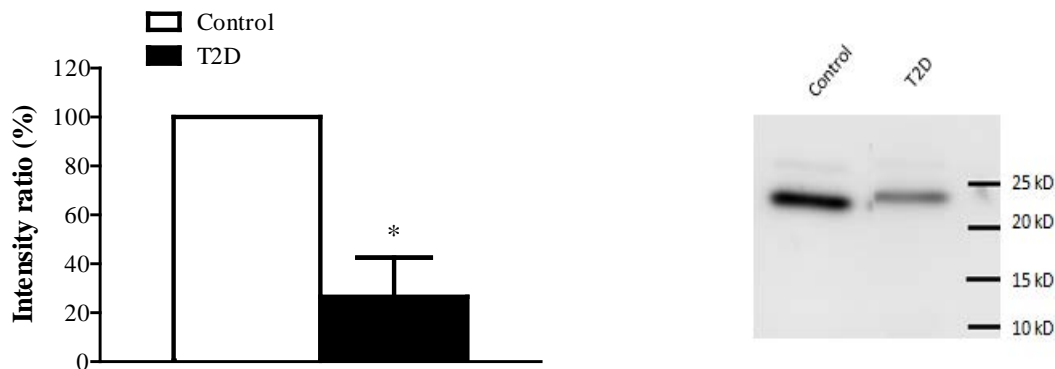


Figure 5.21. MnSOD protein expression in T2D versus control rat cerebral artery. Arterial protein expression levels of MnSOD was decreased in T2D rats compared with control rats ($n=3$; $P = 0.039$; t-test). A representative immunoblot is shown beside the bar graph. A single band was observed at the expected 24kD.

5.4.4 Nox2 protein expression results

A single band at the expected molecular weight of around 58 kDa was observed using Western blotting. Nox2 protein expression levels in cerebral arteries were not significantly different in T2D rats compared with control rats (see **Fig. 5.22**).

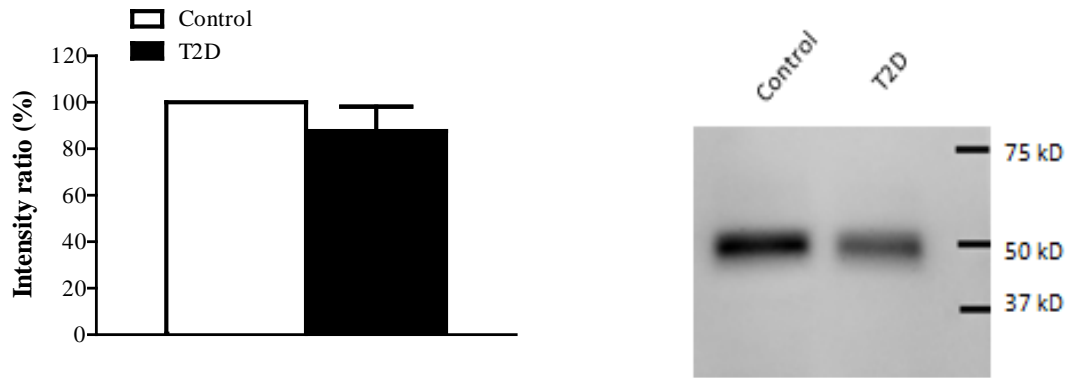


Figure 5.22. Nox2 protein expression in T2D versus control rat cerebral artery. Arterial protein expression levels of Nox2 was comparable between the two T2D and Control rats ($n=3$; $P>0.05$; t -test). A representative immunoblot is shown beside the bar graph. A single band was observed at expected 58kD.

5.4.5 p66Shc protein expression results

Three bands were seen as expected at 46kD, 52kD and 66kD using western blotting. p66Shc protein levels were significantly lower in T2D rats compared with control rats ($P = 0.028$) (see **Fig. 5.23**).



Figure 5.23. p66Shc protein expression in T2D versus control rat cerebral artery. Arterial protein expression levels of p66Shc was significantly decreased in T2D rats compared with control rats ($n=3$; $P = 0.028$; t -test). A representative immunoblot is shown beside the bar graph. Three bands were observed at expected 46kD, 52kD and 66kD. The bar chart represents the densitometry analysis of all three bands.

5.4.6 3NT protein expression results

Western blotting demonstrated multiple bands throughout the blot revealing nitrosylated proteins. Nitrotyrosine protein levels were comparable between T2D and control rat groups (see Fig. 5.24).

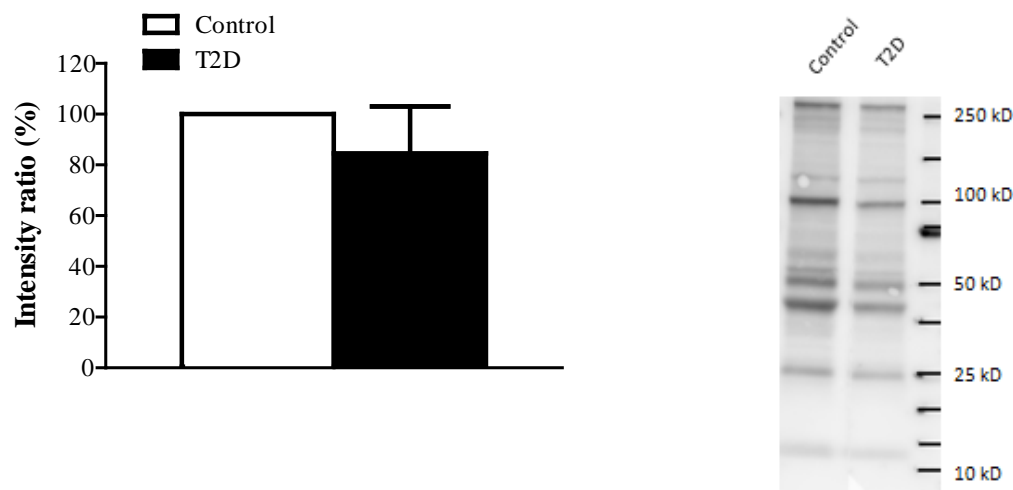


Figure 5.24. Nitrotyrosine protein expression in T2D versus control rat cerebral artery. Arterial 3NT protein expression levels were comparable between T2D and control rats ($n=3$; $P>0.05$; t -test). A representative immunoblot is shown beside the bar graph. Multiple bands throughout the blot reveal the nitrosylated proteins detected by the 3NT antibody. The bar chart represents the densitometry analysis of all bands in the entire lane.

6. DISCUSSION

6.1 Weight Changes

In this study, the HFD/low dose STZ animal model was chosen to mimic the natural characteristics of human T2D. We showed that 18 weeks of a high fat diet leads to a significant weight increase in rats. The weight gain that was observed in our study is consistent with other reports using the same high-fat diet (Davidson et al. 2010; Davidson et al. 2012). In our animals, a single injection of STZ caused a significant decrease in weight, suggesting that STZ was leading to pancreatic beta cell damage and loss of insulin release. Similar weight changes have been reported with STZ (Davidson et al. 2011; Mansor et al. 2013).

STZ is preferentially taken up by pancreatic beta cells through a low affinity GLUT2 transporter. Once in the cell, STZ leads to DNA methylation, nitric oxide production and free radical production, thereby causing cell death and reduced release of insulin (Qinna & Badwan 2015). The lack of insulin prevents the uptake of glucose in muscle and liver cells. The body resorts to burning fat and muscle as its energy source, thereby resulting in a reduction in body weight (Howarth et al. 2005).

6.2 Changes in circulating insulin and glucose

HFD/STZ rats had significantly higher levels of blood glucose and lower levels of insulin compared to the control rats. This is in line with other studies using a similar animal model of T2D (Reed et al, 2000). Insulin resistance was demonstrated by Reed et al. using the same animal model (Reed et al. 2000).

These findings reveal that there was STZ-mediated pancreatic beta cell damage that caused a decrease in insulin secretion, thereby leading to high levels of circulating glucose. This has been shown to be a feature of clinical late stage T2D (Lebovitz & Banerji 2004). Previous studies have shown that rats fed a HFD alone, do not develop hyperglycaemia perhaps due to compensatory hyperinsulinemia (Reed et al. 2000). Therefore, based on previous reports, we used HFD along with a low dose of STZ to ensure the development of hyperglycaemia (Reed et al. 2000).

6.3 Changes in circulating leptin

Leptin levels were also significantly lower in T2D rats which is again supportive of a loss of pancreatic beta-cell function. Similar findings have been reported in STZ-induced diabetes (Sivitz et al. 1998). As glucose cannot enter cells, the body uses the stored fat as an energy source which is the key driver of weight loss. Since leptin is also produced by adipocytes, fewer adipocytes lead to reduced circulating levels (Fernández-Sánchez et al. 2011; Havel et al. 1998).

6.4 Changes in circulating FFA

Circulating free fatty acid levels were significantly elevated in T2D rats which has been observed in other animal models (Bellinger, Merricks & Nichols 2006; Srinivasan & Ramarao 2007) and is also observed clinically (Reaven et al. 1988).

Type 2 diabetics typically have an excessive mass of adipose tissue, resulting in increased lipolysis and elevated plasma FFAs. Elevated levels of lipids can impair pancreatic β -cell function in T2D (Briaud et al. 2001). As a result of lipolysis, circulating levels of FFAs are increased and transported to the liver and skeletal muscle (Arner 2002). In the liver, high FFA levels impair hepatocyte insulin function and may lead to excessive endogenous glucose

production (Pankow et al. 2004; Reaven et al. 1988). In skeletal muscle, FFAs and glucose compete to act as a substrate for energy. Increased levels of FFAs causes FFA oxidation rather than glucose oxidation when muscles require energy. In this way, FFAs are used as an energy source in muscle when FFA levels are elevated (Arner 2002).

6.5 Changes in circulating CRP levels

The T2D rats in our study had significantly elevated levels of CRP compared with the control group. This is also mirrored in human T2D (Donath & Shoelson 2011). CRP is synthesised and released by hepatocytes under the control of cytokines (Dongway et al. 2015) and is therefore used as a marker of systemic inflammation (Dongway et al. 2015). Similar changes in CRP have been observed in rats (Ferreira et al. 2010) as well as in humans (Mugabo, Li & Renier 2010) and mice (Sandu et al. 2005; You et al. 2016).

6.6 Leukocyte and vascular telomere length

Blood is composed of fluid (plasma) and cellular elements, including erythrocytes, leukocytes and platelets. Erythrocytes and platelets both lack a nucleus and therefore DNA. Leukocytes, on the other hand, contain a nucleus that carries DNA. Therefore assessing telomere length of whole blood is a specific reflection of leukocyte telomere length.

We found that T2D rats had shorter leukocyte telomere length compared with control rats. Our findings in rats are in line with clinical studies that have shown a correlation between T2D and shortened telomeres (Adaikalakoteswari, Balasubramanyam & Mohan 2005; Salpea et al. 2010; Zee et al. 2010). In contrast, vascular telomere length was comparable in T2D and control rats. Shortened vascular telomere length has been previously documented in pathological tissue such as human coronary and aortic heart disease (Minamino & Komuro 2007; Wilson et al. 2008a), atherosclerosis (Matthews et al. 2006; Minamino & Komuro

2007), and abdominal aortic aneurysms (Wilson et al. 2008a). Because vascular biopsies cannot be taken from T2D patients, leukocyte telomere measurements have been used as a surrogate to predict vascular disease risk (Wilson et al. 2008a). Importantly, our data suggest that leukocyte telomere assessment may not be an ideal predictor of vascular telomere length. However it is worth noting that a change in telomere length less than 20% would not have been detected in our study due to the sample size. Therefore we cannot rule out the possibility that T2D results in more subtle changes in telomere length.

One possible explanation for the shorter leukocyte telomere length in T2D animals could be increased leukocyte turnover due to systemic inflammation. However clinical studies have failed to show that leukocyte telomere length and markers of inflammation have a significant inverse correlation (Olivieri et al. 2009; Salpea et al. 2010; Testa et al. 2011). A second possible explanation for the shorter leukocyte telomere length is oxidative stress (Tentolouris et al. 2007). Increased oxidative stress has been shown to be strongly related to enhanced telomere attrition in WBCs (Demissie et al. 2006; Samani et al. 2001; Sampson et al. 2006), vascular smooth muscle cells (Matthews et al. 2006), and endothelial cells (Kurz et al. 2004). Another possible reason responsible for shorter leukocyte telomere length is nitrosative stress (Tentolouris et al. 2007). Since we have evidence of oxidative stress, but not nitrosative stress, in the vasculature of our T2D animals, we speculate that the observed leukocyte telomere attrition may be due, at least in part, to nitrosative stress which is absent within the vasculature in this animal model of T2D.

Several methods were used in this study to measure mean telomere length (O'Callaghan & Fenech 2011; Cawthon 2002). Our results suggest that the O'Callaghan method was not optimal to amplify the telomere primers in our experimental samples because a lower than 90% efficiency was obtained. On the other hand, the melt-curve had multiple peaks, suggesting that multiple products were produced. A number of reasons could lead to

efficiency below 90% including the formation of secondary structures, GC content of the amplicon, enzyme quality and non-optimal reagent concentrations.

The Cawthon method was successful in amplifying the telomere primers in our experimental samples. Cawthon specifically designed primers with built-in mismatches to prevent amplification of primer dimers (Cawthon 2002, 2009). However, Cawthon (2002) had performed multiplexing with both the telomere and SCG primers in each reaction well. Unfortunately our PCR machine was unable to perform multiplexing with a single fluorophore and therefore we amplified our products in separate singleplex reactions.

We observed that the NTC was fewer than 10 cycles away from the most diluted experimental DNA sample. This has been confirmed by Olsen and colleagues (Olsen et al. 2012) and is due to the repeating nature of telomeres.

We need to note that the qPCR assay used in the current study measures mean telomere length. There is evidence that a cell may go through apoptosis and senescence by a single critically short telomere (Hemann et al. 2001). Therefore it is possible that a small number of critically short telomeres trigger telomere dysfunction within the T2D vasculature. High-throughput quantitative fluorescence in situ hybridisation can be used in future studies to resolve this issue (Canela et al. 2007).

6.7 Vascular eNOS protein expression

Compared with control rats, T2D cerebral arteries had significantly blunted eNOS protein expression (see **Fig. 5.17**). This is consistent with previous studies showing a reduction in eNOS expression within the vasculature (Davidson et al. 2011). The observed decline in eNOS protein expression may have been caused by a number of factors. First, hyperglycaemia promotes eNOS glycosylation thereby reducing the active form of NO

(Federici et al. 2002). Second, CRP directly decreases eNOS protein expression and activity (Venugopal et al. 2002). A reduction in total eNOS production suggests that NO bioavailability may be reduced, potentially leading to blunted endothelial-mediated relaxations, which have previously been shown in this model (Davidson et al. 2011).

6.8 Vascular SIRT1 protein expression

SIRT1 protein expression was significantly blunted in T2D compared with control cerebral arteries. According to previous studies, cultured cells exposed to elevated levels of glucose result in blunted SIRT1 levels (Balestrieri et al. 2008; Orimo et al. 2009). Other studies have shown a similar decline in SIRT1 protein expression in the macrovasculature (aorta) after six months of high-fat feeding (Potente et al. 2007; Zhang et al. 2008). Our findings in resistance-sized vessels, however, are important because these data suggest that these changes in SIRT1 may ultimately impact blood flow.

Both nutritional status and oxidative stress have been shown to affect SIRT1. SIRT1 is dependent on NAD^+ to maintain its enzymatic activity. In an environment of excess nutrients, the NAD^+/NADH ratio is blunted thereby leading to a decrease in SIRT1 activity (Zhang et al. 2008). As discussed previously, SIRT1 needs NAD^+ as its cofactor for enzymatic activity. Therefore SIRT1 activity is upregulated in caloric restriction or exercise where energy levels are low (Winnik et al. 2015). Calorie restriction and fasting has been shown to increase SIRT1 levels in muscle, brain, liver and fat of rodents (Metoyer & Pruitt 2008). This means that in a nutrient rich environment, NAD^+ is reduced to NADH, leading to a decrease in SIRT1 activity (Zhang et al. 2008). On the other hand, it has been shown that endothelial progenitor cells (Balestrieri et al. 2008), human umbilical vein endothelial cells (Orimo et al. 2009), and mouse brain endothelial cells (Sokoya et al., unpublished findings) cultured in high glucose have lower levels of SIRT1 protein expression.

Oxidative post-translational modifications such as phosphorylation, carbonylation and S-nitrosylation have also been shown to attenuate SIRT1 activity (Shao et al. 2014). Therefore in our model of T2D, both a reduction in cellular energy status and an increase in oxidative stress may account for the reduced SIRT1 expression.

6.9 Vascular antioxidant protein expression

Protein expression of both MnSOD and p66Shc was significantly blunted in T2D compared with control cerebral arteries (see **Fig. 5.19** and **5.21**). Low levels of MnSOD suggest that this antioxidant pathway is blunted. This could be the consequence of excess production of ROS within the vasculature and is in line with other studies (Faraci 2005; Giacco & Brownlee 2010; Green, Brand & Murphy 2004; Morrison et al. 2010; Roberts et al. 2006; Sadi & Güray 2009).

Our finding of blunted vascular p66Shc protein levels in T2D is in accordance with other reports (Pagnin et al. 2005; Xu et al. 2016). Moreover, a study in mice on a high-fat diet has also shown blunted cerebral p66Shc expression (Morrison et al. 2010). p66Shc, which is part of the mammalian Shc family (Miyazawa & Tsuji 2014), is a redox enzyme that produces mitochondrial ROS (hydrogen peroxide) (Giorgio et al. 2005). Recent studies have shown that this enzyme also functions as an antioxidant in the cytoplasm where it is regulated by the redox sensitive transcription factor, NFE2-related factor2 (Nrf2) (Miyazawa & Tsuji 2014).

6.10 Vascular oxidative stress

Nox2 levels were comparable between T2D and control groups. Nox2, one of the subunits of NADPH oxidase, is one of the major generators of superoxide in cerebral blood vessels during diabetes (Faraci 2005; Miller et al. 2010) and can lead to cerebral artery dysfunction (Miller et al. 2009). Nox2 has been shown to be elevated after high fat feeding including in

mouse aorta (Lynch et al. 2013) and mouse cerebral arteries (Miller et al. 2010). While we did not observe changes in Nox2, our findings do not rule out potential changes in the other subunits of NADPH oxidase including Nox1, Nox4 (Jiang et al. 2011) and Nox5. We also cannot rule out other sources of superoxide such as cyclooxygenase (Zhu et al. 2014) and xanthine oxidase (Inkster, Cotter & Cameron 2007). This can be assessed in future studies.

6.11 Vascular nitrosative stress

The levels of nitrosylated proteins were comparable in cerebral arteries of T2D and control rats. Our findings are in contrast to other T2D studies that have shown elevated nitrotyrosine levels in mouse aorta (Molnar et al. 2005), rat aorta (Davidson et al. 2007) and human blood (Al-Nimer, Al-Ani & Ali 2012).

Superoxide and nitric oxide are highly reactive, leading to the formation of peroxynitrite (Al-Nimer, Al-Ani & Ali 2012; Chrissobolis & Faraci 2008). Peroxynitrite is a strong oxidant and can directly modify proteins by nitration of tyrosine residues and formation of nitrotyrosine (Pacher, Beckman & Liaudet 2007). Even a moderate production of peroxynitrite over time, can lead to necrosis, apoptosis and cell death (Pacher, Beckman & Liaudet 2007). The effect of NO reacting with superoxide is a decrease in NO bioavailability and is a common cause of endothelial dysfunction in T2D (Al-Nimer, Al-Ani & Ali 2012).

We need to note that markers of oxidative and nitrosative stress were measured within the cerebral vasculature while telomere length was measured in DNA extracted from the peripheral vasculature. Ideally, telomere length would have been measured within cerebral arteries, but this was not possible due to the fact that we were limited with regards to the small size of rodent cerebral arteries.

7. CONCLUSION

In conclusion, this study reveals that T2D leads to shortened leukocyte telomere length. In contrast, vascular telomere length was not affected, even though there was concomitant blunted vascular SIRT1, eNOS and MnSOD protein expression. Importantly, our data suggest that leukocyte telomere assessment may not be an ideal predictor of vascular telomere length. We have further demonstrated that hyperglycaemia and downregulation of vascular SIRT1 are not sufficient to prematurely shorten vascular telomeres.

8. REFERENCES

Adaikalakoteswari, A, Balasubramanyam, M & Mohan, V 2005, 'Telomere shortening occurs in Asian Indian Type 2 diabetic patients', *Diabetic Medicine*, vol. 22, no. 9, pp. 1151-6.

Al-Nimer, MS, Al-Ani, FS & Ali, FS 2012, 'Role of nitrosative and oxidative stress in neuropathy in patients with type 2 diabetes mellitus', *Journal of Neurosciences in Rural Practice*, vol. 3, no. 1, pp. 41-44.

Antonopoulos, AS, Margaritis, M, Coutinho, P, Shirodaria, C, Psarros, C, Herdman, L, Sanna, F, De Silva, R, Petrou, M & Sayeed, R 2015, 'Adiponectin as a link between type 2 diabetes and vascular NADPH oxidase activity in the human arterial wall: the regulatory role of perivascular adipose tissue', *Diabetes*, vol. 64, no. 6, pp. 2207-19.

Arner, P 2002, 'Insulin resistance in type 2 diabetes: role of fatty acids', *Diabetes/Metabolism Research and Reviews*, vol. 18, no. S2, pp. S5-S9.

Bagi, Z, Koller, A & Kaley, G 2004, 'PPAR γ activation, by reducing oxidative stress, increases NO bioavailability in coronary arterioles of mice with Type 2 diabetes', *American Journal of Physiology-Heart and Circulatory Physiology*, vol. 286, no. 2, pp. H742-H8.

Bakker, W, Eringa, EC, Sipkema, P & van Hinsbergh, VW 2009, 'Endothelial dysfunction and diabetes: roles of hyperglycemia, impaired insulin signaling and obesity', *Cell and Tissue Research*, vol. 335, no. 1, pp. 165-89.

Balestrieri, ML, Rienzo, M, Felice, F, Rossiello, R, Grimaldi, V, Milone, L, Casamassimi, A, Servillo, L, Farzati, B & Giovane, A 2008, 'High glucose downregulates endothelial progenitor cell number via SIRT1', *Biochimica et Biophysica Acta (BBA)-Proteins and Proteomics*, vol. 1784, no. 6, pp. 936-45.

Baron, AD 2002, 'Insulin resistance and vascular function', *Journal of Diabetes and Its Complications*, vol. 16, no. 1, pp. 92-102.

Barrett-Connor, E & Khaw, K-T 1988, 'Diabetes mellitus: an independent risk factor for stroke?', *American Journal of Epidemiology*, vol. 128, no. 1, pp. 116-23.

Baumbach, GL, Sigmund, CD & Faraci, FM 2004, 'Structure of cerebral arterioles in mice deficient in expression of the gene for endothelial nitric oxide synthase', *Circulation Research*, vol. 95, no. 8, pp. 822-9.

Beckman, JS & Koppenol, WH 1996, 'Nitric oxide, superoxide, and peroxynitrite: the good, the bad, and ugly', *American Journal of Physiology-Cell Physiology*, vol. 271, no. 5, pp. C1424-C37.

Bellinger, DA, Merricks, EP & Nichols, TC 2006, 'Swine models of type 2 diabetes mellitus: insulin resistance, glucose tolerance, and cardiovascular complications', *ILAR Journal*, vol. 47, no. 3, pp. 243-58.

Bender, S, Herrick, E, Lott, N & Klabunde, R 2007, 'Diet-induced obesity and diabetes reduce coronary responses to nitric oxide due to reduced bioavailability in isolated mouse hearts', *Diabetes, Obesity and Metabolism*, vol. 9, no. 5, pp. 688-96.

Birch, J, Victorelli, S, Rahmatika, D, Anderson, RK, Jiwa, K, Moisey, E, Ward, C, Fisher, AJ, Soyza, AD & Passos, JF 2016, 'Telomere dysfunction and senescence-associated pathways in bronchiectasis', *American Journal of Respiratory and Critical Care Medicine*, vol. 193, no. 8, pp. 929-32.

Boden, G & Shulman, G 2002, 'Free fatty acids in obesity and type 2 diabetes: defining their role in the development of insulin resistance and β -cell dysfunction', *European Journal of Clinical Investigation*, vol. 32, no. s3, pp. 14-23.

Briaud, I, Harmon, JS, Kelpke, CL, Segu, VBG & Poitout, V 2001, 'Lipotoxicity of the pancreatic β -cell is associated with glucose-dependent esterification of fatty acids into neutral lipids', *Diabetes*, vol. 50, no. 2, pp. 315-21.

Brownlee, M 2001, 'Biochemistry and molecular cell biology of diabetic complications', *Nature*, vol. 414, no. 6865, pp. 813-20.

Brownlee, M 2005, 'The pathobiology of diabetic complications a unifying mechanism', *Diabetes*, vol. 54, no. 6, pp. 1615-25.

Brunet, A, Sweeney, LB, Sturgill, JF, Chua, KF, Greer, PL, Lin, Y, Tran, H, Ross, SE, Mostoslavsky, R & Cohen, HY 2004, 'Stress-dependent regulation of FOXO transcription factors by the SIRT1 deacetylase', *Science*, vol. 303, no. 5666, pp. 2011-5.

Cai, H & Harrison, DG 2000, 'Endothelial dysfunction in cardiovascular diseases: the role of oxidant stress', *Circulation Research*, vol. 87, no. 10, pp. 840-4.

Calado, RT & Young, NS 2008, 'Telomere maintenance and human bone marrow failure', *Blood*, vol. 111, no. 9, pp. 4446-55.

Canela, A, Vera, E, Klatt, P & Blasco, MA 2007, 'High-throughput telomere length quantification by FISH and its application to human population studies', *Proceedings of the National Academy of Sciences*, vol. 104, no. 13, pp. 5300-5.

Cawthon, RM 2002, 'Telomere measurement by quantitative PCR', *Nucleic Acids Research*, vol. 30, no. 10, p. e47.

Cawthon, RM 2009, 'Telomere length measurement by a novel monochrome multiplex quantitative PCR method', *Nucleic Acids Research*, vol. 37, no. 3, p. e21.

Chen, H, Wan, Y, Zhou, S, Lu, Y, Zhang, Z, Zhang, R, Chen, F, Hao, D, Zhao, X & Guo, Z 2012, 'Endothelium-specific SIRT1 overexpression inhibits hyperglycemia-induced upregulation of vascular cell senescence', *Science China Life Sciences*, vol. 55, no. 6, pp. 467-73.

Chen, J, Zhang, B, Wong, N, Lo, AW, To, K-F, Chan, AW, Ng, MH, Ho, CY, Cheng, S-H & Lai, PB 2011, 'Sirtuin 1 is upregulated in a subset of hepatocellular carcinomas where it is essential for telomere maintenance and tumor cell growth', *Cancer Research*, vol. 71, no. 12, pp. 4138-49.

Chrissobolis, S & Faraci, FM 2008, 'The role of oxidative stress and NADPH oxidase in cerebrovascular disease', *Trends in Molecular Medicine*, vol. 14, no. 11, pp. 495-502.

Chrissobolis, S, Miller, AA, Drummond, GR, Kemp-Harper, BK & Sobey, CG 2011, 'Oxidative stress and endothelial dysfunction in cerebrovascular disease', *Frontiers in bioscience: A Journal and Virtual Library*, vol. 16, pp. 1733-45.

D'Onofrio, N, Vitiello, M, Casale, R, Servillo, L, Giovane, A & Balestrieri, ML 2015, 'Sirtuins in vascular diseases: emerging roles and therapeutic potential', *Biochimica et Biophysica Acta (BBA)-Molecular Basis of Disease*, vol. 1852, no. 7, pp. 1311-22.

Davidson, EP, Coppey, LJ, Calcutt, NA, Oltman, CL & Yorek, MA 2010, 'Diet-induced obesity in Sprague–Dawley rats causes microvascular and neural dysfunction', *Diabetes/Metabolism Research and Reviews*, vol. 26, no. 4, pp. 306-18.

Davidson, EP, Coppey, LJ, Dake, B & Yorek, MA 2011, 'Treatment of streptozotocin-induced diabetic rats with alogliptin: effect on vascular and neural complications', *Experimental Diabetes Research*, doi: 10.1155/2011/810469.

Davidson, EP, Coppey, LJ, Holmes, A & Yorek, MA 2012, 'Changes in corneal innervation and sensitivity and acetylcholine-mediated vascular relaxation of the posterior ciliary artery in a type 2 diabetic rat', *Investigative Ophthalmology & Visual Science*, vol. 53, no. 3, pp. 1182-7.

Davidson, EP, Kleinschmidt, TL, Oltman, CL, Lund, DD & Yorek, MA 2007, 'Treatment of Streptozotocin-Induced Diabetic Rats With AVE7688, a Vasopeptidase Inhibitor Effect on Vascular and Neural Disease', *Diabetes*, vol. 56, no. 2, pp. 355-62.

De Bonis, ML, Ortega, S & Blasco, MA 2014, 'SIRT1 is necessary for proficient telomere elongation and genomic stability of induced pluripotent stem cells', *Stem Cell Reports*, vol. 2, no. 5, pp. 690-706.

de Kreutzenberg, SV, Ceolotto, G, Papparella, I, Bortoluzzi, A, Semplicini, A, Dalla Man, C, Cobelli, C, Fadini, GP & Avogaro, A 2010, 'Downregulation of the longevity-associated protein sirtuin 1 in insulin resistance and metabolic syndrome: potential biochemical mechanisms', *Diabetes*, vol. 59, no. 4, pp. 1006-15.

De Vriese, AS, Verbeuren, TJ, Van de Voorde, J, Lameire, NH & Vanhoutte, PM 2000, 'Endothelial dysfunction in diabetes', *British Journal of Pharmacology*, vol. 130, no. 5, pp. 963-74.

DeFronzo, RA 2004, 'Pathogenesis of type 2 diabetes mellitus', *Medical Clinics of North America*, vol. 88, no. 4, pp. 787-835.

Demissie, S, Levy, D, Benjamin, EJ, Cupples, LA, Gardner, JP, Herbert, A, Kimura, M, Larson, MG, Meigs, JB & Keaney, JF 2006, 'Insulin resistance, oxidative stress, hypertension, and leukocyte telomere length in men from the Framingham Heart Study', *Aging Cell*, vol. 5, no. 4, pp. 325-30.

Dominy, JE, Lee, Y, Gerhart-Hines, Z & Puigserver, P 2010, 'Nutrient-dependent regulation of PGC-1 α 's acetylation state and metabolic function through the enzymatic activities of Sirt1/GCN5', *Biochimica et Biophysica Acta (BBA)-Proteins and Proteomics*, vol. 1804, no. 8, pp. 1676-83.

Donath, MY & Shoelson, SE 2011, 'Type 2 diabetes as an inflammatory disease', *Nature Reviews Immunology*, vol. 11, no. 2, pp. 98-107.

Donato, AJ, Magerko, KA, Lawson, BR, Durrant, JR, Lesniewski, LA & Seals, DR 2011, 'SIRT-1 and vascular endothelial dysfunction with ageing in mice and humans', *The Journal of Physiology*, vol. 589, no. 18, pp. 4545-54.

Dong, F & Ren, J 2007, 'Fidarestat improves cardiomyocyte contractile function in db/db diabetic obese mice through a histone deacetylase Sir2-dependent mechanism', *Journal of Hypertension*, vol. 25, no. 10, pp. 2138-47.

Dongway, AC, Faggad, AS, Zaki, HY & Abdalla, BE 2015, 'C-reactive protein is associated with low-density lipoprotein cholesterol and obesity in type 2 diabetic Sudanese', *Diabetes, metabolic syndrome and obesity: targets and therapy*, vol. 8, pp. 427-35.

Drummond, GR & Sobey, CG 2014, 'Endothelial NADPH oxidases: which NOX to target in vascular disease?', *Trends in Endocrinology & Metabolism*, vol. 25, no. 9, pp. 452-63.

Dworakowski, R, Alom-Ruiz, SP & Shah, AM 2008, 'NADPH oxidase-derived reactive oxygen species in the regulation of endothelial phenotype', *Pharmacol Rep*, vol. 60, no. 1, pp. 21-8.

Faraci, FM 1992, 'Regulation of the cerebral circulation by endothelium', *Pharmacology & Therapeutics*, vol. 56, no. 1, pp. 1-22.

Faraci, FM 2005, 'Oxidative Stress The Curse That Underlies Cerebral Vascular Dysfunction?', *Stroke*, vol. 36, no. 2, pp. 186-8.

Faraci, FM 2011, 'Protecting against vascular disease in brain', *American Journal of Physiology-Heart and Circulatory Physiology*, vol. 300, no. 5, pp. H1566-H82.

Faraci, FM & Heistad, DD 1998, 'Regulation of the cerebral circulation: role of endothelium and potassium channels', *Physiological Reviews*, vol. 78, no. 1, pp. 53-97.

Federici, M, Menghini, R, Mauriello, A, Hribal, ML, Ferrelli, F, Lauro, D, Sbraccia, P, Spagnoli, LG, Sesti, G & Lauro, R 2002, 'Insulin-dependent activation of endothelial nitric oxide synthase is impaired by O-linked glycosylation modification of signaling proteins in human coronary endothelial cells', *Circulation*, vol. 106, no. 4, pp. 466-72.

Fernández-Sánchez, A, Madrigal-Santillán, E, Bautista, M, Esquivel-Soto, J, Morales-González, Á, Esquivel-Chirino, C, Durante-Montiel, I, Sánchez-Rivera, G, Valadez-Vega, C & Morales-González, JA 2011, 'Inflammation, oxidative stress, and obesity', *International Journal of Molecular Sciences*, vol. 12, no. 5, pp. 3117-32.

Ferreira, L, Teixeira-de-Lemos, E, Pinto, F, Parada, B, Mega, C, Vala, H, Pinto, R, Garrido, P, Sereno, J & Fernandes, R 2010, 'Effects of sitagliptin treatment on dysmetabolism, inflammation, and oxidative stress in an animal model of type 2 diabetes (ZDF rat)', *Mediators of Inflammation*, doi: 10.1155/2010/592760.

Giacco, F & Brownlee, M 2010, 'Oxidative stress and diabetic complications', *Circulation Research*, vol. 107, no. 9, pp. 1058-70.

Giorgio, M, Migliaccio, E, Orsini, F, Paolucci, D, Moroni, M, Contursi, C, Pelliccia, G, Luzi, L, Minucci, S & Marcaccio, M 2005, 'Electron transfer between cytochrome c and p66 Shc generates reactive oxygen species that trigger mitochondrial apoptosis', *Cell*, vol. 122, no. 2, pp. 221-33.

Green, K, Brand, MD & Murphy, MP 2004, 'Prevention of mitochondrial oxidative damage as a therapeutic strategy in diabetes', *Diabetes*, vol. 53, no. suppl 1, pp. S110-S8.

Guzik, TJ, Mussa, S, Gastaldi, D, Sadowski, J, Ratnatunga, C, Pillai, R & Channon, KM 2002, 'Mechanisms of increased vascular superoxide production in human diabetes mellitus Role of NAD (P) H oxidase and endothelial nitric oxide synthase', *Circulation*, vol. 105, no. 14, pp. 1656-62.

Hallows, WC, Lee, S & Denu, JM 2006, 'Sirtuins deacetylate and activate mammalian acetyl-CoA synthetases', *Proceedings of the National Academy of Sciences*, vol. 103, no. 27, pp. 10230-5.

Han, L, Zhou, R, Niu, J, McNutt, MA, Wang, P & Tong, T 2010, 'SIRT1 is regulated by a PPAR γ -SIRT1 negative feedback loop associated with senescence', *Nucleic Acids Research*, vol. 38, no. 21, pp. 7458-71.

Hattori, Y, Kawasaki, H, Abe, K & Kanno, M 1991, 'Superoxide dismutase recovers altered endothelium-dependent relaxation in diabetic rat aorta', *American Journal of Physiology-Heart and Circulatory Physiology*, vol. 261, no. 4, pp. H1086-H94.

Havel, PJ, Uriu-Hare, JY, Liu, T, Stanhope, KL, Stern, JS, Keen, CL & Ahrén, B 1998, 'Marked and rapid decreases of circulating leptin in streptozotocin diabetic rats: reversal by insulin', *American Journal of Physiology-Regulatory, Integrative and Comparative Physiology*, vol. 274, no. 5, pp. R1482-R91.

Hemann, MT, Strong, MA, Hao, L-Y & Greider, CW 2001, 'The shortest telomere, not average telomere length, is critical for cell viability and chromosome stability', *Cell*, vol. 107, no. 1, pp. 67-77.

Herman, WH 2013, 'The economic costs of diabetes: is it time for a new treatment paradigm?', *Diabetes Care*, vol. 36, no. 4, pp. 775-6.

Howarth, F, Jacobson, M, Shafiullah, M & Adeghate, E 2005, 'Long-term effects of streptozotocin-induced diabetes on the electrocardiogram, physical activity and body temperature in rats', *Experimental Physiology*, vol. 90, no. 6, pp. 827-35.

Inkster, ME, Cotter, MA & Cameron, NE 2007, 'Treatment with the xanthine oxidase inhibitor, allopurinol, improves nerve and vascular function in diabetic rats', *European Journal of Pharmacology*, vol. 561, no. 1, pp. 63-71.

International Diabetes Association 2017, 'About Diabetes', *International Diabetes Association*.

Jeong, J, Juhn, K, Lee, H, Kim, S, Min, B, Lee, K, Cho, M, Park, G & Lee, K 2007, 'SIRT1 promotes DNA repair activity and deacetylation of Ku70', *Experimental and Molecular Medicine*, vol. 39, no. 1, pp. 8-13.

Jiang, F, Lim, HK, Morris, MJ, Prior, L, Velkoska, E, Wu, X & Dusting, GJ 2011, 'Systemic upregulation of NADPH oxidase in diet-induced obesity in rats', *Redox Report*, vol. 16, no. 6, pp. 223-9.

Johnstone, MT, Creager, SJ, Scales, KM, Cusco, JA, Lee, BK & Creager, MA 1993, 'Impaired endothelium-dependent vasodilation in patients with insulin-dependent diabetes mellitus', *Circulation*, vol. 88, no. 6, pp. 2510-6.

Khan, S, Chuturgoon, A & Naidoo, D 2012, 'Telomeres and atherosclerosis', *Cardiovascular Journal of Africa*, vol. 23, no. 10, pp. 563-71.

Kourembanas, S, McQuillan, LP, Leung, GK & Faller, DV 1993, 'Nitric oxide regulates the expression of vasoconstrictors and growth factors by vascular endothelium under both normoxia and hypoxia', *Journal of Clinical Investigation*, vol. 92, no. 1, p. 99.

Kurz, DJ, Decary, S, Hong, Y, Trivier, E, Akhmedov, A & Erusalimsky, JD 2004, 'Chronic oxidative stress compromises telomere integrity and accelerates the onset of senescence in human endothelial cells', *Journal of Cell Science*, vol. 117, no. 11, pp. 2417-26.

Lassègue, B, San Martín, A & Griendling, KK 2012, 'Biochemistry, physiology, and pathophysiology of NADPH oxidases in the cardiovascular system', *Circulation Research*, vol. 110, no. 10, pp. 1364-90.

Le Bras, M, Clement, M, Pervaiz, S & Brenner, C 2005, 'Reactive oxygen species and the mitochondrial signaling pathway of cell death', *Histology and Histopathology*, vol. 20, no. 1, pp. 205-19.

Lebovitz, HE & Banerji, MA 2004, 'Treatment of insulin resistance in diabetes mellitus', *European Journal of Pharmacology*, vol. 490, no. 1, pp. 135-46.

Lee, D-C, Im, J-A, Kim, J-H, Lee, H-R & Shim, J-Y 2005, 'Effect of long-term hormone therapy on telomere length in postmenopausal women', *Yonsei Medical Journal*, vol. 46, no. 4, pp. 471-9.

Li, H, Horke, S & Förstermann, U 2014, 'Vascular oxidative stress, nitric oxide and atherosclerosis', *Atherosclerosis*, vol. 237, no. 1, pp. 208-19.

Li, M, Guo, K, Vanella, L, Taketani, S, Adachi, Y & Ikehara, S 2015, 'Stem Cell Transplantation Upregulates Sirt1 and Antioxidant Expression, Ameliorating Fatty Liver in Type 2 Diabetic Mice', *International Journal of Biological Sciences*, vol. 11, no. 4, pp. 472-81.

Li, X, Zhang, S, Blander, G, Jeanette, GT, Krieger, M & Guarente, L 2007, 'SIRT1 deacetylates and positively regulates the nuclear receptor LXR', *Molecular Cell*, vol. 28, no. 1, pp. 91-106.

Lovren, F, Pan, Y, Shukla, PC, Quan, A, Teoh, H, Szmitko, PE, Peterson, MD, Gupta, M, Al-Omran, M & Verma, S 2009, 'Visfatin activates eNOS via Akt and MAP kinases and improves endothelial cell function and angiogenesis in vitro and in vivo: translational implications for atherosclerosis', *American Journal of Physiology-Endocrinology and Metabolism*, vol. 296, no. 6, pp. E1440-E9.

Lucchesi, PA, Belmadani, S & Matrougui, K 2005, 'Hydrogen peroxide acts as both vasodilator and vasoconstrictor in the control of perfused mouse mesenteric resistance arteries', *Journal of Hypertension*, vol. 23, no. 3, pp. 571-9.

Lynch, CM, Kinzenbaw, DA, Chen, X, Zhan, S, Mezzetti, E, Filosa, J, Ergul, A, Faulkner, JL, Faraci, FM & Didion, SP 2013, 'Nox2-derived superoxide contributes to cerebral vascular dysfunction in diet-induced obesity', *Stroke*, vol. 44, no. 11, pp. 3195-201.

Mansor, LS, Gonzalez, ER, Cole, MA, Tyler, DJ, Beeson, JH, Clarke, K, Carr, CA & Heather, LC 2013, 'Cardiac metabolism in a new rat model of type 2 diabetes using high-fat diet with low dose streptozotocin', *Cardiovasc Diabetol*, vol. 12, no. 1, p. 136.

Mattagajasingh, I, Kim, C-S, Naqvi, A, Yamamori, T, Hoffman, TA, Jung, S-B, DeRicco, J, Kasuno, K & Irani, K 2007, 'SIRT1 promotes endothelium-dependent vascular relaxation by activating endothelial nitric oxide synthase', *Proceedings of the National Academy of Sciences*, vol. 104, no. 37, pp. 14855-60.

Matthews, C, Gorenne, I, Scott, S, Figg, N, Kirkpatrick, P, Ritchie, A, Goddard, M & Bennett, M 2006, 'Vascular smooth muscle cells undergo telomere-based senescence in human atherosclerosis effects of telomerase and oxidative stress', *Circulation Research*, vol. 99, no. 2, pp. 156-64.

Metoyer, CF & Pruitt, K 2008, 'The role of sirtuin proteins in obesity', *Pathophysiology*, vol. 15, no. 2, pp. 103-8.

Michishita, E, Park, JY, Burneskis, JM, Barrett, JC & Horikawa, I 2005, 'Evolutionarily conserved and nonconserved cellular localizations and functions of human SIRT proteins', *Molecular Biology of the Cell*, vol. 16, no. 10, pp. 4623-35.

Miller, AA, De Silva, TM, Judkins, CP, Diep, H, Drummond, GR & Sobey, CG 2010, 'Augmented superoxide production by Nox2-containing NADPH oxidase causes cerebral artery dysfunction during hypercholesterolemia', *Stroke*, vol. 41, no. 4, pp. 784-9.

Miller, AA, Drummond, GR, De Silva, TM, Mast, AE, Hickey, H, Williams, JP, Broughton, BR & Sobey, CG 2009, 'NADPH oxidase activity is higher in cerebral versus systemic arteries of four animal species: role of Nox2', *American Journal of Physiology-Heart and Circulatory Physiology*, vol. 296, no. 1, pp. H220-H5.

Minamino, T & Komuro, I 2007, 'Vascular cell senescence contribution to atherosclerosis', *Circulation Research*, vol. 100, no. 1, pp. 15-26.

Miyazawa, M & Tsuji, Y 2014, 'Evidence for a novel antioxidant function and isoform-specific regulation of the human p66Shc gene', *Molecular Biology of the Cell*, vol. 25, no. 13, pp. 2116-27.

Molnar, J, Yu, S, Mzhavia, N, Pau, C, Chereshev, I & Dansky, HM 2005, 'Diabetes induces endothelial dysfunction but does not increase neointimal formation in high-fat diet fed C57BL/6J mice', *Circulation Research*, vol. 96, no. 11, pp. 1178-84.

Morrison, CD, Pistell, PJ, Ingram, DK, Johnson, WD, Liu, Y, Fernandez-Kim, SO, White, CL, Purpera, MN, Uranga, RM & Bruce-Keller, AJ 2010, 'High fat diet increases hippocampal oxidative stress and cognitive impairment in aged mice: implications for decreased Nrf2 signaling', *Journal of Neurochemistry*, vol. 114, no. 6, pp. 1581-9.

Mugabo, Y, Li, L & Renier, G 2010, 'The connection between C-reactive protein (CRP) and diabetic vasculopathy. Focus on preclinical findings', *Current Diabetes Reviews*, vol. 6, no. 1, pp. 27-34.

Muniyappa, R, Montagnani, M, Koh, KK & Quon, MJ 2007, 'Cardiovascular actions of insulin', *Endocrine Reviews*, vol. 28, no. 5, pp. 463-91.

NDSS 2015, *NDSS National Diabetes Data Snapshot for Diabetes Type 2 at 31 March 2015*, National Diabetes Services Scheme (NDSS), viewed 26/06/2015 2015, <<http://www.ndss.com.au/Global/Data%20Snapshots/March%202015/SnapshotData-31March2015Final-T2.pdf>>.

O'Callaghan, NJ & Fenech, M 2011, 'A quantitative PCR method for measuring absolute telomere length', *Biological Procedures Online.*, vol. 13, p. 3.

O'Donnell, CJ, Demissie, S, Kimura, M, Levy, D, Gardner, JP, White, C, D'Agostino, RB, Wolf, PA, Polak, J & Cupples, LA 2008, 'Leukocyte telomere length and carotid artery

intimal medial thickness the Framingham heart study', *Arteriosclerosis, Thrombosis, and Vascular Biology*, vol. 28, no. 6, pp. 1165-71.

O'Driscoll, G, Green, D, Maiorana, A, Stanton, K, Colreavy, F & Taylor, R 1999, 'Improvement in endothelial function by angiotensin-converting enzyme inhibition in non-insulin-dependent diabetes mellitus', *Journal of the American College of Cardiology*, vol. 33, no. 6, pp. 1506-11.

OECD/WHO 2014, *Diabetes*, OECD Publishing, Paris.
<http://dx.doi.org/10.1787/health_glance_ap-2014-16-en/>.

Olivieri, F, Lorenzi, M, Antonicelli, R, Testa, R, Sirolla, C, Cardelli, M, Mariotti, S, Marchegiani, F, Marra, M & Spazzafumo, L 2009, 'Leukocyte telomere shortening in elderly Type2DM patients with previous myocardial infarction', *Atherosclerosis*, vol. 206, no. 2, pp. 588-93.

Olsen, MT, Bérubé, M, Robbins, J & Palsbøll, PJ 2012, 'Empirical evaluation of humpback whale telomere length estimates; quality control and factors causing variability in the singleplex and multiplex qPCR methods', *BMC Genetics*, vol. 13, p. 77.

Orimo, M, Minamino, T, Miyauchi, H, Tateno, K, Okada, S, Moriya, J & Komuro, I 2009, 'Protective role of SIRT1 in diabetic vascular dysfunction', *Arteriosclerosis, Thrombosis, and Vascular Biology*, vol. 29, no. 6, pp. 889-94.

Ota, H, Eto, M, Ogawa, S, Iijima, K, Akishita, M & Ouchi, Y 2010, 'SIRT1/eNOS axis as a potential target against vascular senescence, dysfunction and atherosclerosis', *Journal of Atherosclerosis and Thrombosis*, vol. 17, no. 5, pp. 431-5.

Pacher, P, Beckman, JS & Liaudet, L 2007, 'Nitric oxide and peroxynitrite in health and disease', *Physiological Reviews*, vol. 87, no. 1, pp. 315-424.

Pagnin, E, Fadini, G, de Toni, R, Tiengo, A, Calò, L & Avogaro, A 2005, 'Diabetes induces p66shc gene expression in human peripheral blood mononuclear cells: relationship to oxidative stress', *The Journal of Clinical Endocrinology & Metabolism*, vol. 90, no. 2, pp. 1130-6.

Palacios, JA, Herranz, D, De Bonis, ML, Velasco, S, Serrano, M & Blasco, MA 2010, 'SIRT1 contributes to telomere maintenance and augments global homologous recombination', *The Journal of Cell Biology*, vol. 191, no. 7, pp. 1299-313.

Paneni, F, Beckman, JA, Creager, MA & Cosentino, F 2013, 'Diabetes and vascular disease: pathophysiology, clinical consequences, and medical therapy: part I', *European Heart Journal*, pp. 2436-43.

Pankow, JS, Duncan, BB, Schmidt, MI, Ballantyne, CM, Couper, DJ, Hoogeveen, RC & Golden, SH 2004, 'Fasting Plasma Free Fatty Acids and Risk of Type 2 Diabetes The Atherosclerosis Risk in Communities study', *Diabetes Care*, vol. 27, no. 1, pp. 77-82.

Paravicini, TM & Touyz, RM 2008, 'NADPH Oxidases, Reactive Oxygen Species, and Hypertension Clinical implications and therapeutic possibilities', *Diabetes Care*, vol. 31, no. Supplement 2, pp. S170-S80.

Picard, F, Kurtev, M, Chung, N, Topark-Ngarm, A, Senawong, T, De Oliveira, RM, Leid, M, McBurney, MW & Guarente, L 2004, 'Sirt1 promotes fat mobilization in white adipocytes by repressing PPAR- γ ', *Nature*, vol. 429, no. 6993, pp. 771-6.

Pieper, GM, Mei, DA, Langenstroer, P & O'Rourke, ST 1992, 'Bioassay of endothelium-derived relaxing factor in diabetic rat aorta', *American Journal of Physiology-Heart and Circulatory Physiology*, vol. 263, no. 3, pp. H676-H80.

Potente, M, Ghaeni, L, Baldessari, D, Mostoslavsky, R, Rossig, L, Dequiedt, F, Haendeler, J, Mione, M, Dejana, E & Alt, FW 2007, 'SIRT1 controls endothelial angiogenic functions during vascular growth', *Genes & Development*, vol. 21, no. 20, pp. 2644-58.

Preis, SR, Pencina, MJ, Hwang, S-J, D'Agostino, RB, Savage, PJ, Levy, D & Fox, CS 2009, 'Trends in cardiovascular disease risk factors in individuals with and without diabetes mellitus in the Framingham Heart Study', *Circulation*, vol. 120, no. 3, pp. 212-20.

Qinna, NA & Badwan, AA 2015, 'Impact of streptozotocin on altering normal glucose homeostasis during insulin testing in diabetic rats compared to normoglycemic rats', *Drug Design, Development and Therapy*, vol. 9, p. 2515.

Ran, M, Li, Z, Yang, L, Tong, L, Zhang, L & Dong, H 2015, 'Calorie restriction attenuates cerebral ischemic injury via increasing SIRT1 synthesis in the rat', *Brain Research*, vol. 1610, pp. 61-8.

Raymond, AR, Hodson, B, Woodiwiss, AJ, Norton, GR & Brooksbank, RL 2013, 'Telomere length and adrenergic-induced left ventricular dilatation and systolic chamber dysfunction in rats', *European Journal of Applied Physiology*, vol. 113, no. 11, pp. 2803-11.

Reaven, GM, Hollenbeck, C, Jeng, C-Y, Wu, MS & Chen, Y-DI 1988, 'Measurement of plasma glucose, free fatty acid, lactate, and insulin for 24 h in patients with NIDDM', *Diabetes*, vol. 37, no. 8, pp. 1020-4.

Reed, M, Meszaros, K, Entes, L, Claypool, M, Pinkett, J, Gadbois, T & Reaven, G 2000, 'A new rat model of type 2 diabetes: the fat-fed, streptozotocin-treated rat', *Metabolism*, vol. 49, no. 11, pp. 1390-4.

Roberts, CK, Barnard, RJ, Sindhu, RK, Jurczak, M, Ehdaie, A & Vaziri, ND 2006, 'Oxidative stress and dysregulation of NAD (P) H oxidase and antioxidant enzymes in diet-induced metabolic syndrome', *Metabolism*, vol. 55, no. 7, pp. 928-34.

Rodgers, JT, Lerin, C, Haas, W, Gygi, SP, Spiegelman, BM & Puigserver, P 2005, 'Nutrient control of glucose homeostasis through a complex of PGC-1 α and SIRT1', *Nature*, vol. 434, no. 7029, pp. 113-8.

Roglic, G 2016, 'WHO Global report on diabetes: A summary', *International Journal of Noncommunicable Diseases*, vol. 1, no. 1, p. 3.

Sadi, G & Güray, T 2009, 'Gene expressions of Mn-SOD and GPx-1 in streptozotocin-induced diabetes: effect of antioxidants', *Molecular and Cellular Biochemistry*, vol. 327, no. 1-2, pp. 127-34.

Saliques, S, Zeller, M, Lorin, J, Lorgis, L, Teyssier, J-R, Cottin, Y, Rochette, L & Vergely, C 2010, 'Telomere length and cardiovascular disease', *Archives of Cardiovascular Diseases*, vol. 103, no. 8, pp. 454-9.

Salpea, KD, Talmud, PJ, Cooper, JA, Maubaret, CG, Stephens, JW, Abelak, K & Humphries, SE 2010, 'Association of telomere length with type 2 diabetes, oxidative stress and UCP2 gene variation', *Atherosclerosis*, vol. 209, no. 1, pp. 42-50.

Samani, NJ, Boulby, R, Butler, R, Thompson, JR & Goodall, AH 2001, 'Telomere shortening in atherosclerosis', *The Lancet*, vol. 358, no. 9280, pp. 472-3.

Sampson, MJ, Winterbone, MS, Hughes, JC, Dozio, N & Hughes, DA 2006, 'Monocyte telomere shortening and oxidative DNA damage in type 2 diabetes', *Diabetes Care*, vol. 29, no. 2, pp. 283-9.

Sandu, O, Song, K, Cai, W, Zheng, F, Uribarri, J & Vlassara, H 2005, 'Insulin resistance and type 2 diabetes in high-fat-fed mice are linked to high glycotoxin intake', *Diabetes*, vol. 54, no. 8, pp. 2314-9.

Schächinger, V, Britten, MB & Zeiher, AM 2000, 'Prognostic impact of coronary vasodilator dysfunction on adverse long-term outcome of coronary heart disease', *Circulation*, vol. 101, no. 16, pp. 1899-906.

Shao, D, Fry, JL, Han, J, Hou, X, Pimentel, DR, Matsui, R, Cohen, RA & Bachschmid, MM 2014, 'A redox-resistant sirtuin-1 mutant protects against hepatic metabolic and oxidant stress', *Journal of Biological Chemistry*, vol. 289, no. 11, pp. 7293-306.

Shaw, J 2012, *Diabetes: the silent pandemic and its impact on Australia*, Baker IDI Heart and Diabetes Institute, viewed 1/10/2016 2016, <<https://static.diabetesaustralia.com.au/s/fileassets/diabetes-australia/e7282521-472b-4313-b18e-be84c3d5d907.pdf>>.

Sivitz, WI, Walsh, S, Morgan, D, Donohoue, P, Haynes, W & Leibel, RL 1998, 'Plasma leptin in diabetic and insulin-treated diabetic and normal rats', *Metabolism*, vol. 47, no. 5, pp. 584-91.

Srinivasan, K & Ramarao, P 2007, 'Animal models in type 2 diabetes research: an overview', *Indian Journal of Medical Research*, vol. 125, no. 3, pp. 451-72.

Srinivasan, K, Viswanad, B, Asrat, L, Kaul, C & Ramarao, P 2005, 'Combination of high-fat diet-fed and low-dose streptozotocin-treated rat: a model for type 2 diabetes and pharmacological screening', *Pharmacological Research*, vol. 52, no. 4, pp. 313-20.

Tajbakhsh, N & Sokoya, EM 2012, 'Regulation of cerebral vascular function by sirtuin 1', *Microcirculation*, vol. 19, no. 4, pp. 336-42.

Tentolouris, N, Nzietchueng, R, Cattan, V, Poitevin, G, Lacolley, P, Papazafiropoulou, A, Perrea, D, Katsilambros, N & Benetos, A 2007, 'White blood cells telomere length is shorter in males with type 2 diabetes and microalbuminuria', *Diabetes Care*, vol. 30, no. 11, pp. 2909-15.

Testa, R, Olivieri, F, Sirolla, C, Spazzafumo, L, Rippo, M, Marra, M, Bonfigli, A, Ceriello, A, Antonicelli, R & Franceschi, C 2011, 'Leukocyte telomere length is associated with complications of type 2 diabetes mellitus', *Diabetic Medicine*, vol. 28, no. 11, pp. 1388-94.

Trachootham, D, Lu, W, Ogasawara, MA, Valle, NR-D & Huang, P 2008, 'Redox regulation of cell survival', *Antioxidants & Redox Signaling*, vol. 10, no. 8, pp. 1343-74.

Ungvari, Z, Labinskyy, N, Mukhopadhyay, P, Pinto, JT, Bagi, Z, Ballabh, P, Zhang, C, Pacher, P & Csizsar, A 2009, 'Resveratrol attenuates mitochondrial oxidative stress in coronary arterial endothelial cells', *American Journal of Physiology-Heart and Circulatory Physiology*, vol. 297, no. 5, pp. H1876-H81.

Valdes, AM, Andrew, T, Gardner, JP, Kimura, M, Oelsner, E, Cherkas, LF, Aviv, A & Spector, TD 2005, 'Obesity, cigarette smoking, and telomere length in women', *The Lancet*, vol. 366, no. 9486, pp. 662-4.

Vaziri, H, Dessain, SK, Eaton, EN, Imai, S-I, Frye, RA, Pandita, TK, Guarente, L & Weinberg, RA 2001, 'hSIR2SIRT1 functions as an NAD-dependent p53 deacetylase', *Cell*, vol. 107, no. 2, pp. 149-59.

Venugopal, SK, Devaraj, S, Yuhanna, I, Shaul, P & Jialal, I 2002, 'Demonstration that C-reactive protein decreases eNOS expression and bioactivity in human aortic endothelial cells', *Circulation*, vol. 106, no. 12, pp. 1439-41.

Wever, RM, van Dam, T, van Rijn, HJ, de Groot, F & Rabelink, TJ 1997, 'Tetrahydrobiopterin regulates superoxide and nitric oxide generation by recombinant endothelial nitric oxide synthase', *Biochemical and Biophysical Research Communications*, vol. 237, no. 2, pp. 340-4.

WHO 2015, *Diabetes*, WHO, viewed 13/07/2015 2015, <<http://www.who.int/mediacentre/factsheets/fs312/en/>>.

Wild, S, Roglic, G, Green, A, Sicree, R & King, H 2004, 'Global prevalence of diabetes estimates for the year 2000 and projections for 2030', *Diabetes Care*, vol. 27, no. 5, pp. 1047-53.

Wilson, WRW, Herbert, KE, Mistry, Y, Stevens, SE, Patel, HR, Hastings, RA, Thompson, MM & Williams, B 2008a, 'Blood leucocyte telomere DNA content predicts vascular telomere DNA content in humans with and without vascular disease', *European Heart Journal*, vol. 29, no. 21, pp. 2689-94.

Wilson, WRW 2008b, 'Blood leucocyte telomere DNA content predicts vascular telomere DNA content in humans with and without vascular disease', *European Heart Journal*, vol. 29, no. 21, pp. 2689-94.

Winer, N & Sowers, JR 2004, 'Epidemiology of diabetes', *The Journal of Clinical Pharmacology*, vol. 44, no. 4, pp. 397-405.

Winnik, S, Auwerx, J, Sinclair, DA & Matter, CM 2015, 'Protective effects of sirtuins in cardiovascular diseases: from bench to bedside', *European Heart Journal*, vol. 36, no. 48, pp. 3404-12.

Xu, X, Zhu, X, Ma, M, Han, Y, Hu, C, Yuan, S, Yang, Y, Xiao, L, Liu, F & Kanwar, YS 2016, 'p66Shc: A novel biomarker of tubular oxidative injury in patients with diabetic nephropathy', *Scientific Reports*, vol. 6, p.29302.

Yang, J, Wang, N, Zhu, Y & Feng, P 2011, 'Roles of SIRT1 in high glucose-induced endothelial impairment: association with diabetic atherosclerosis', *Archives of Medical Research*, vol. 42, no. 5, pp. 354-60.

Yao, H & Rahman, I 2012, 'Perspectives on translational and therapeutic aspects of SIRT1 in inflammaging and senescence', *Biochemical Pharmacology*, vol. 84, no. 10, pp. 1332-9.

Yeung, F, Hoberg, JE, Ramsey, CS, Keller, MD, Jones, DR, Frye, RA & Mayo, MW 2004, 'Modulation of NF- κ B-dependent transcription and cell survival by the SIRT1 deacetylase', *The EMBO Journal*, vol. 23, no. 12, pp. 2369-80.

You, Y-K, Huang, X-R, Chen, H-Y, Lyu, X-F, Liu, H-F & Lan, HY 2016, 'C-Reactive Protein Promotes Diabetic Kidney Disease in db/db Mice via the CD32b-Smad3-mTOR signaling Pathway', *Scientific Reports*, vol. 6, p. 26740.

Zee, RY, Castonguay, AJ, Barton, NS, Germer, S & Martin, M 2010, 'Mean leukocyte telomere length shortening and type 2 diabetes mellitus: a case-control study', *Translational Research*, vol. 155, no. 4, pp. 166-9.

Zhang, P, Zhang, X, Brown, J, Vistisen, D, Sicree, R, Shaw, J & Nichols, G 2010, 'Global healthcare expenditure on diabetes for 2010 and 2030', *Diabetes Research and Clinical Practice*, vol. 87, no. 3, pp. 293-301.

Zhang, QJ, Wang, Z, Chen, H-z, Zhou, S, Zheng, W, Liu, G, Wei, Y-s, Cai, H, Liu, D-p & Liang, C-c 2008, 'Endothelium-specific overexpression of class III deacetylase SIRT1 decreases atherosclerosis in apolipoprotein E-deficient mice', *Cardiovascular Research*, vol. 80, no. 2, pp. 191-9.

Zhang, QJ, Wang, Z, Chen, H-z, Zhou, S, Zheng, W, Liu, G, Wei, Y-s, Cai, H, Liu, D-p & Liang, C-c 2008, 'Endothelium-specific overexpression of class III deacetylase SIRT1 decreases atherosclerosis in apolipoprotein E-deficient mice', *Cardiovascular Research*, vol. 80, no. 2, pp. 191-9.

Zhu, N, Liu, B, Luo, W, Zhang, Y, Li, H, Li, S & Zhou, Y 2014, 'Vasoconstrictor role of cyclooxygenase-1-mediated prostacyclin synthesis in non-insulin-dependent diabetic mice induced by high-fat diet and streptozotocin', *American Journal of Physiology-Heart and Circulatory Physiology*, vol. 307, no. 3, pp. H319-27.

APPENDICES

Appendix 1: DNA Concentrations Measured by Using Thermo Scientific NanoDrop 2000 Spectrophotometer.

DNA sample	Concentration (µg/mL)	A260 (10 mm path)	A280 (10 mm path)	260/280	260/230
Rat 2	6.15	0.12	0.07	1.65	0.17
Rat 2	8.65	0.17	0.11	1.58	0.28
Rat 2	9.3	0.18	0.14	1.33	0.17
Rat 2	7.05	0.14	0.08	1.73	0.26
Rat 3	9.45	0.19	0.1	1.85	0.35
Rat 3	13.1	0.26	0.15	1.71	0.44
Rat 3	11.1	0.22	0.11	2.01	0.25
Rat 3	14.9	0.29	0.18	0.89	0.78
Rat 4	13.6	0.27	0.15	1.9	0.49
Rat 4	8.05	0.16	0.09	1.78	0.45
Rat 4	10.8	0.22	0.11	1.89	0.74
Rat 6	10	0.2	0.11	1.75	0.58
Rat 6	11.6	0.23	0.13	1.82	0.65
Rat 6	6.1	0.12	0.06	1.92	1.29
Rat 6	10.5	0.21	0.11	1.92	1.01
Rat 8	9	0.18	0.09	2.02	0.47
Rat 8	15.6	0.312	0.18	1.73	0.4
Rat 8	10.1	0.2	0.1	1.95	0.74
Rat 8	14.4	0.29	0.16	1.76	0.32
Rat 9	9	0.18	0.09	1.97	0.46
Rat 9	6.8	0.14	0.07	2.07	0.52
Rat 9	10.2	0.2	0.09	2.13	0.34
Rat 9	6.4	0.13	0.06	2.08	0.46
Rat 10	23.9	0.48	0.29	1.65	0.28
Rat 10	20.4	0.4	0.24	1.7	0.35
Rat 10	24.6	0.49	0.32	1.52	0.23
Rat 10	15.5	0.31	0.17	1.78	0.4

Rat 11	28.2	0.56	0.34	1.66	0.32
Rat 11	24.6	0.49	0.27	1.78	0.43
Rat 11	21.3	0.42	0.24	1.77	0.41
Rat 11	20.1	0.4	0.22	1.84	0.56
Rat 12	22.7	0.45	0.27	1.64	0.39
Rat 12	16.5	0.33	0.19	1.77	0.46
Rat 12	19.5	0.39	0.23	1.69	0.45
Rat 12	18.9	0.38	0.23	1.67	0.28
Rat 13	21.6	0.43	0.25	1.74	0.53
Rat 13	24.6	0.49	0.25	1.96	0.47
Rat 13	37.9	0.76	0.42	1.79	0.37
Rat 13	18.8	0.38	0.2	1.91	0.39
Rat 14	25.1	0.5	0.28	1.76	0.57
Rat 14	24.9	0.49	0.31	1.62	0.29
Rat 14	26.6	0.53	0.34	1.54	0.26
Rat 14	21.7	0.43	0.25	1.72	0.49
Rat 15	27.8	0.56	0.34	1.64	0.28
Rat 15	17	0.34	0.19	1.75	0.46
Rat 15	23.6	0.47	0.25	1.9	0.47
Rat 15	19.6	0.39	0.21	1.77	0.5
Rat 16	21.3	0.43	0.22	1.91	0.44
Rat 16	24.8	0.5	0.28	1.78	0.28
Rat 16	13.9	0.28	0.14	1.97	0.66
Rat 16	21.4	0.43	0.21	2.06	0.56
Rat 17	25.2	0.5	0.29	1.76	0.42
Rat 17	21.8	0.44	0.25	1.74	0.3